

Universalities of Defects in Quantum Field Theories

A Dissertation Presented

by

Siwei Zhong

to

The Graduate School

in Partial Fulfillment of the Requirements

for the Degree of

Doctor of Philosophy

in

Physics

Stony Brook University

May 2026

Abstract of the Dissertation

Universalities of Defects in Quantum Field Theories

by

Siwei Zhong

Doctor of Philosophy

in

Physics

Stony Brook University

2026

Defects are both physically rich objects and powerful tools in modern quantum field theory. They are extended operators, such as boundaries, impurities, and probe particles, embedded in many-body systems. In this dissertation, we study the universal aspects of defect dynamics from the perspective of symmetry principles. We bring together several themes, including defect renormalization group flows, effective string theory, and impurities in atomic quantum gases.

Contents

List of Publications	iv
List of Figures	v
List of Tables	vi
Conventions	vii
Acknowledgements	viii
1 Introduction and Summary	1
1.1 Outline	1
1.2 Future directions	2
2 Defect Renormalization Group Flows	4
2.1 Conformal defects	5
2.1.1 Bulk-to-defect OPE	6
2.1.2 Defect identity operator	7
2.1.3 Displacement and tilt operators	8
2.2 Constraints on DCFTs in Maxwell theory	10
2.2.1 Topological duality defect	10
2.2.2 Twist defects for electromagnetic duality	13
2.2.3 Bulk-defect two-point functions	14
2.2.4 Bulk-defect-defect three-point functions	15
2.2.5 Chiral current sector and anyonic branes	18
2.3 Defect RG flows in the $O(N)$ models	21
2.3.1 Bilinear defect deformation	22
2.3.2 Monotonicity and the defect central charge	25
2.3.3 Phases of defects in interacting theories	26
2.3.4 IR effective theory of defects	31
2.4 Matching UV and IR defects	33

2.4.1	UV and IR symmetries	34
2.4.2	Free-fermion lattice model example	36
2.4.3	Crystalline impurities and localized emanant fluxes	37
2.4.4	Observables in quantum critical lattice models	42
3	Defects and Effective String Theory	44
3.1	Confining strings	45
3.1.1	Nambu–Goto action	45
3.1.2	Open string boundary conditions	47
3.1.3	Open-closed duality	48
3.2	Effective theory of baryon junctions	50
3.2.1	Baryon junction condition	51
3.2.2	Free-field limit and junction stability	53
3.2.3	An accidental \mathbb{Z}_2 symmetry	57
3.3	Open-closed duality of baryon junctions	60
3.3.1	S -wave scattering and selection rules	61
3.3.2	Nonlinear corrections to the partition function	64
4	Defects in Atomic Quantum Gases	69
4.1	Galilean field theories	70
4.1.1	Schrödinger symmetry	71
4.1.2	Unitary Fermi gases	72
4.2	Conformal defects in Schrödinger field theories	74
4.2.1	Bulk-to-defect OPE	75
4.2.2	One-body operators and s -wave resonance	76
4.2.3	Defects in free and unitary Fermi gases	78
4.3	Giant superfluid vortices	80
4.3.1	Rapidly rotating superfluids	81
4.3.2	Giant vortices in a hard-wall trap	82
4.3.3	Giant vortices in smooth traps	84
	Bibliography	88

List of Publications

1. A. Raviv-Moshe and S. Zhong, *Phases of surface defects in Scalar Field Theories*, *JHEP* **08** (2023) 143, [[arXiv:2305.11370](#)].
2. G. Cuomo, Z. Komargodski, and S. Zhong, *Chiral modes of giant superfluid vortices*, *Phys. Rev. B* **110** (2024), no. 14 144514, [[arXiv:2312.06095](#)].
3. Z. Komargodski and S. Zhong, *Baryon junction and string interactions*, *Phys. Rev. D* **110** (2024), no. 5 056018, [[arXiv:2405.12005](#)].
4. A. Raviv-Moshe and S. Zhong, *Impurities in Schrödinger field theories and s-wave resonance*, *JHEP* **09** (2025) 134, [[arXiv:2411.04040](#)].
5. M. Barkeshli, C. Fechisin, Z. Komargodski, and S. Zhong, *Disclinations, Dislocations, and Emanant Flux at Dirac Criticality*, *Phys. Rev. X* **16** (2026), no. 1 011017, [[arXiv:2501.13866](#)].
6. S.-H. Shao and S. Zhong, *Where non-invertible symmetries end: twist defects for electromagnetic duality*, *JHEP* **01** (2026) 118, [[arXiv:2509.21279](#)].
7. X. Lou and S. Zhong, *Baryon Junction and String Interactions: Part II*, [arXiv:2602.17771](#).

List of Figures

2.1	The configuration of the conformal twist defect in \mathbb{R}^4	13
2.2	DCFT two-point and three-point functions.	16
2.3	The configuration of the anyonic brane $(\mathcal{A}_N)^k$ and the twist defect.	20
2.4	IR-stable fixed points in the free theory.	24
2.5	Perturbative phase diagram for surface defects in the Wilson–Fisher CFT.	30
2.6	Crystalline impurities in the square lattice.	37
2.7	Azimuthal current C_J and energy density C_T of the flat space defect.	40
2.8	Azimuthal current C_J and conformal weight C_T of conical defects.	41
2.9	Observables in Qi–Wu–Zhang model with crystalline impurities.	43
3.1	Confining strings in a probe baryon.	50
3.2	Topological defect line \mathcal{D} on the confining string worldsheet.	58
3.3	Merging the topological defect lines with the baryon junction worldline.	59
3.4	Tree-level scattering amplitudes of massive modes in the closed channel.	62
3.5	Worldsheet loop diagrams.	65
4.1	Ladder diagrams induced by the defect bilinear deformation.	78
4.2	Feynman diagrams of the defect two-body operator for $d \gtrsim 2$	79
4.3	Feynman diagrams of the defect two-body operator for $d \lesssim 4$	80
4.4	Particle density and eigenmode profiles of a giant vortex in a hard-wall trap.	83
4.5	Particle density and eigenmode profiles of a giant vortex in smooth traps.	84

List of Tables

2.1	$O(M) \times O(N - M)$ -symmetric defect RG fixed points for $2 \leq N \leq 6$	30
2.2	$O(N - 1) \times \mathbb{Z}_2$ -symmetric defect RG fixed points for $7 \leq N \leq 10$	30
2.3	Crystalline quantum numbers of Dirac cones in the Qi–Wu–Zhang model . . .	37

Conventions

δX	infinitesimal variation of X ;
$\delta_{\mu\nu}$, δ_{μ}^{ν}	Kronecker delta symbol;
$\delta^p(x)$	p -dimensional Dirac delta function;
$\star F$	Hodge dual of the differential form F ;
$(x)_n$	Pochhammer symbol, i.e., $(x)_n \equiv \Gamma(x+n)/\Gamma(x)$;
\mathbf{q} , \mathbf{q}_x , \dots	Modular parameters;
$\eta(\mathbf{q})$	Dedekind eta function;
$E_{2k}(\mathbf{q})$	Eisenstein series;
$K_{\alpha}(x)$	Modified Bessel function of the second type;
$\Theta(\tau)$	Heaviside step function;

Acknowledgements

This dissertation would not have been possible without the guidance and support of my advisor, Zohar Komargodski. To me, he has been an inspiring teacher, a generous collaborator, and an exceptionally visionary scientist. Beyond all the physics lessons, he has taught me by setting an example to always stay curious about nature, to always be kind to others, and to always pursue excellence in research. My appreciation is beyond words.

I am deeply grateful to Gabriel Cuomo, Leonardo Rastelli, and Shu-Heng Shao. I got to know Gabriel just as I was starting my first research project. His comments have always been kind, thoughtful, and full of physical insight. During my first years of graduate school, I benefited greatly from Leonardo's lectures on several advanced topics. They were among the most memorable lectures of my student years. As I began to find my footing in research, I learned a great deal from many discussions with Shu-Heng. His broad perspective and enthusiasm for physics have greatly influenced the way I think about my own research.

I would like to acknowledge my collaborators Avia Raviv-Moshe, Maissam Barkeshli, and Christopher Fechisin. I am especially thankful to Avia, who was my very first coauthor. Her kind support and stimulating ideas meant a lot to me as a beginning researcher.

I am grateful to Paul Goldbart, Yin-Chen He, Mengkun Liu, Martin Roček, George Sterman, Tzu-Chieh Wei, and the entire Physics Department. It has been quite a journey studying and working at Stony Brook. Special thanks go to Clark McGrew and Yifan Wang for kindly serving on my dissertation committee.

I would like to thank Mykola Dedushenko, Diego Delmastro, Justin Kulp, Fedor K. Popov, Brandon C. Rayhaun, Fei Yan, Yunqing Zheng, and the entire SCGP community. It has been a wonderful experience exploring research topics and developing new ideas together with them. I would also like to thank Jan Albert, Yichul Choi, and Ho Tat Lam for many productive discussions and enjoyable conversations.

I am grateful to Heidi Ciolfi, Dawn Huether, Brigid O'Connor, and Donald Sheehan for rescuing me from endless administrative paperwork. I would also like to thank the SCGP

café staff for their delicious and healthy food. Because of them, SCGP will always hold a special place in my heart.

I would like to thank Ling-Yan Hung, Yidun Wan, Xinan Zhou, and Yang Zhou for kindly hosting my visits and for their support since my undergraduate years. Before this list becomes infinitely long, I would also like to thank Jinwei Chu, Xuanjing Chu, Anirudh Deb, Wenhan Guo, Shenyang Shi, Xuejing Huang, Xinyi Sun, Jialun Wang, Meng Ye, Haolan Xu, and all my dear friends. My life would not have been the same without them.

Finally, I would like to thank my mom. She may not know much about physics, but she certainly knows how love can help a son go farther than he ever thought possible.

Chapter 1

Introduction and Summary

Quantum field theory provides a universal language for describing physical systems across vastly different scales. Prominent examples include the Landau–Ginzburg theory of phase transitions in ferromagnets and Quantum Chromodynamics (QCD), which describes the strong interactions between elementary particles. One of the central lessons of modern quantum field theory is that the long-distance, infrared (IR) properties of a system are often insensitive to its microscopic ultraviolet (UV) details. This idea underlies the concept of universality classes. Different systems can exhibit the same universal IR behavior, which is largely determined by their symmetries.

This paradigm is enriched by defects in a fundamental way. Defects arise naturally in a wide range of physical contexts, including boundaries and interfaces in statistical-mechanics models, Wilson lines and 't Hooft operators in gauge theories, crystalline impurities in lattice systems, and vortices in superfluids. Although the UV realizations of these defects can differ significantly from one model to another, one may ask whether they exhibit universal behavior in the IR. In this dissertation, we address this question using symmetry principles.

While defects are rich subjects of study in their own right, they also serve as powerful tools to understand the quantum field theories in which they are embedded. In particular, we note that certain defects can be continuously deformed without affecting any physical observables. These are topological defects, which generalize the very notion of symmetry in modern physics [1, 2]. This perspective has shed new light on many profound phenomena in quantum field theories, and we will apply it extensively throughout this dissertation.

1.1 Outline

The chapters of this dissertation are devoted to different themes. Below, we outline the main topics covered by each chapter and summarize the key results.

In Chapter 2, we discuss Renormalization Group (RG) flows governing the evolution of defect dynamics under changes of scale. Defects with enhanced conformal symmetry lie at

special fixed points of these RG flows. We show that the dynamics of conformal defects are subject to strong constraints. In certain cases [3], they are universally determined by conformal symmetry and the dynamics of the bulk theory, independent of microscopic details. We also examine how different fixed points are connected by defect RG flows. In particular, we investigate the phase diagram of defects embedded in the $O(N)$ Wilson–Fisher theory [4]. Finally, we identify impurities in microscopic lattice models with defects in the continuum field theory. The RG flows connecting these two descriptions are subject to novel symmetry constraints, which we explain through examples in [5].

In Chapter 3, we discuss defects that play important roles in understanding the strongly coupled regime of QCD. These include chromoelectric flux tubes and their junctions [6, 7]. In the long-distance limit, we show that the dynamics of these defects are universally fixed by the symmetry-breaking pattern. Using the open-closed duality, we further determine the leading contributions to the coupling constants governing the s -wave scattering of large glueball excitations. We comment on selection rules associated with a novel accidental symmetry of the defects.

In Chapter 4, we turn to defects immersed in atomic quantum gases. We develop a general framework for scale-invariant defects in nonrelativistic quantum field theories [8]. For point-like impurities, we show a correspondence between defect operators and many-body states in a harmonic trap with possible s -wave resonance. As a representative example, we apply this framework to impurities in dilute Fermi gases. We also analyze the giant vortex [9], a macroscopic defect that arises in rotating superfluids. We show that rapidly rotating superfluids confined to a two-dimensional trap exhibit new universal behavior, including chiral modes with emergent warped conformal symmetry.

Taken together, these chapters survey defects across a variety of physical settings. We aim to deepen our understanding of their universal properties and to demonstrate how defects offer new perspectives on exotic physical phenomena.

1.2 Future directions

We close this chapter with comments on several future directions and open questions.

Defects respond to both intrinsic and extrinsic geometry. For conformal defects, one class of universal responses is given by conformal anomalies. These anomalies have long played an important role in the study of defect RG flows, as they govern monotonicity theorems for defect RG flows in many cases [10–12]. This motivates the question of whether defect conformal anomalies can be extracted directly from physical observables. In particular, we would like to explore this question for parity-odd anomalies. An example is provided by the chiral edge modes of three-dimensional Chern-Simons theories [13–16], where the edge gravitational anomaly is encoded in the Casimir momentum. It would be interesting to understand whether an analogous statement can be made for gapless systems.

Another promising future direction is to develop effective field theories for special defect

configurations. For instance, the effective description of two parallel conformal boundaries was studied in [17]. More generally, defects can support global symmetries that are absent from the ambient quantum field theory. This perspective becomes particularly interesting in gauge theories. See [18, 19] for some recent works. By studying the symmetries, anomalies, and dynamics of defect effective field theories, we aim to sharpen our understanding of exotic quantum phases and the universal structures that organize them.

Finally, it is intriguing to realize and test defect models in experimental settings. Our analyses in [5, 9] were strongly motivated by experimental studies and led to testable predictions. It would be valuable to explore the phenomenological implications of other defect models.

Chapter 2

Defect Renormalization Group Flows

Historically, the idea of renormalization was introduced to address the divergences arising from loop corrections in quantum field theories. For early developments of RG flows, see [20–26], among many others.

From a modern perspective, the RG flow describes how a physical system evolves under scale transformations. A generic quantum field theory can be viewed as a point in the space of theories, interpolating between the fixed points of RG flows. In most cases¹, these fixed points are strongly constrained by the enhanced conformal symmetry, which renders their dynamics more tractable. In recent years, substantial effort has been devoted to understanding the dynamics of these Conformal Field Theories (CFTs) through their symmetries and consistency conditions. See [31, 32] for pedagogical reviews of the modern CFT framework, and [33–37] for a partial list of relevant studies. Throughout this dissertation, we make extensive use of standard concepts of CFT, such as state-operator correspondence, conformal primaries and descendants, and Operator Product Expansion (OPE).

The concept of RG flow extends naturally to defects in quantum field theory. A defect is usually characterized by a set of parameters describing its dynamics and its couplings to the ambient field theory, both of which evolve under scale transformations. As in ordinary quantum field theories, defect RG flows can also admit fixed points with enhanced conformal symmetry. Defect Conformal Field Theory (DCFT) [11, 38–47] provides a framework for analyzing universalities of defects at these fixed points.

In this chapter, we discuss defect RG flows through examples drawn from [3–5]. We first study general aspects of defects with extended conformal symmetry and introduce the basics of DCFT in Section 2.1. Conformal symmetry imposes strong constraints on defect dynamics. As an example, in Section 2.2 we show that a chiral conformal defect in Maxwell theory is universally determined by symmetry principles, regardless of the microscopic details. In Section 2.3, we examine how different fixed points are connected via defect RG flows. In

¹For Lorentz-invariant theories, examples of scale-invariant but not conformally invariant theories include [27–30]. In Chapter 4, we discuss Galilean-invariant theories, where scaling symmetry is enhanced to Schrödinger symmetry instead of the conformal symmetry.

particular, we explore the phase diagram of surface defects embedded in the $O(N)$ Wilson–Fisher conformal field theory. Finally, in Section 2.4, we identify impurities in UV discrete lattice models with defects in IR continuum field theory. The RG flows connecting these two descriptions are subject to novel symmetry constraints, which we discuss in detail.

2.1 Conformal defects

We begin by discussing the general properties of defects at the RG flow fixed points. To set the stage, we consider unitary CFTs defined in d -dimensional Euclidean space $x_\mu \in \mathbb{R}^d$. Local operators in the CFT furnish representations of the d -dimensional conformal algebra $\mathfrak{so}(d+1, 1)$, and are characterized by their scaling dimension $\Delta \geq 0$ and spin $j \geq 0$. Schematically, we denote local primaries in the CFT by \mathcal{O}_j . These operators transform as tensors for integer j and as spinors for half-integer j under $\mathfrak{so}(d) \subset \mathfrak{so}(d+1, 1)$.

We next consider a p -dimensional defect supported on the hyperplane $\mathbb{R}^p \subseteq \mathbb{R}^d$, with x_\parallel^i denoting the coordinates parallel to the defect plane and x_\perp^i denoting the coordinates perpendicular to it.² As noted in the preface, we focus on the cases where the translation symmetries along the perpendicular directions are explicitly broken by the defect. The maximal subalgebra of $\mathfrak{so}(d+1, 1)$ that can be preserved by the planar defect is therefore

$$\mathfrak{so}(p+1, 1) \times \mathfrak{so}(q) , \tag{2.1}$$

where $q = d - p$ is the codimension of the defect. In what follows, we assume that scaling invariance is enhanced to the residual conformal algebra $\mathfrak{so}(p+1, 1)$ at the fixed points of defect RG flows.³ We further assume the transverse rotation algebra $\mathfrak{so}(q)$ is also preserved, so that the defect is isotropic in the perpendicular directions when $q \geq 2$. The dynamics of defects preserving the symmetry (2.1) are encoded in the DCFT data, which we detail in the remainder of this section.

Local operators confined to the p -dimensional defect are characterized by their scaling dimension $\Delta \geq 0$, parallel spin $\ell \geq 0$, and transverse spin $s \geq 0$. In analogy with the bulk CFT, we denote local primaries in the DCFT by $\hat{\mathcal{O}}_\ell^s$. The parallel spin ℓ labels the tensor and spinor representations of $\mathfrak{so}(p) \subset \mathfrak{so}(p+1, 1)$ and takes either integer or half-integer values. The selection rule for the transverse spin s , on the other hand, depends on the possible topological volumes associated with the defect; see Sections 2.2 and 2.4.

²Point-like defects ($p = 0$) essentially coincide with local operators, which have been extensively studied in CFT. We will not discuss them further in this dissertation.

³This enhancement for CFT boundaries ($q = 1$) is discussed in [48]. In particular, there exist non-unitary boundary theories that are scale-invariant but not conformally invariant.

2.1.1 Bulk-to-defect OPE

DCFT concerns the relation between bulk operators \mathcal{O}_j and defect operators $\hat{\mathcal{O}}_\ell^s$. One possibility is that the correlation functions between bulk and defect operators completely factorize. For example, one can stack a decoupled p -dimensional CFT onto the given DCFT without affecting its dynamics, so that correlation functions of operators in the decoupled sector factorize from those of bulk operators. A non-trivial example of such factorization is discussed in Section 2.2 below.

More interestingly, we bring a bulk operator \mathcal{O}_j close to the defect at $x_\sigma^\perp = 0$. It follows from the branching rule of $\mathfrak{so}(d+1, 1) \rightarrow \mathfrak{so}(p+1, 1) \times \mathfrak{so}(q)$ that bulk operators can be expanded in an infinite sum of defect operators:

$$\mathcal{O}_j(x^\perp, x'') \rightarrow \sum C_{\mathcal{O}_j}^{\hat{\mathcal{O}}_\ell^s} (\hat{\mathcal{O}}_\ell^s(x'') + \text{descendants}) . \quad (2.2)$$

This is known as the bulk-to-defect OPE [38, 39, 41, 42], where $C_{\mathcal{O}_j}^{\hat{\mathcal{O}}_\ell^s}$ denote the corresponding OPE coefficients. At the level of representations, a spin- j representation of $\mathfrak{so}(d)$ can be decomposed into representations of $\mathfrak{so}(p) \times \mathfrak{so}(q)$ with spin (ℓ, s) satisfying $\ell + s \leq j$. Notably, one can use the transverse vector x_σ^\perp to construct tensors that carry the $\mathfrak{so}(q)$ spin on the right-hand side of (2.2), while tensors built from x_ν'' are forbidden by translation symmetry. We therefore find the selection rule for the OPE coefficients

$$C_{\mathcal{O}_j}^{\hat{\mathcal{O}}_\ell^s} = 0 , \quad \text{for } \ell > j . \quad (2.3)$$

For instance, a bulk scalar primary \mathcal{O} with $j = 0$ can be expanded in terms of defect scalar primaries $\hat{\mathcal{O}}^s$ with $\ell = 0$. The explicit bulk-to-defect OPE for \mathcal{O} is fixed by the algebra (2.1) and takes the form [41, 45]

$$\mathcal{O}(x^\perp, x'') = \sum_{\hat{\mathcal{O}}^s} \frac{Y_s(x_\sigma^\perp / |x^\perp|)}{|x^\perp|^{\Delta(\mathcal{O}) - \Delta(\hat{\mathcal{O}}^s)}} C_{\mathcal{O}}^{\hat{\mathcal{O}}^s} \sum_{n \geq 0} \frac{(-|x^\perp|^2 \partial^\nu \partial_\nu / 4)^n}{n! (\Delta(\hat{\mathcal{O}}^s) + 1 - \frac{p}{2})_n} \hat{\mathcal{O}}^s(x'') , \quad (2.4)$$

where Y_s denote the spin s spherical harmonic on S^{q-1} with its $\mathfrak{so}(q)$ indices suppressed, as those of $\hat{\mathcal{O}}^s$.

The OPE (2.2) encodes how the presence of the defect affects bulk observables. This can be seen by considering bulk-defect two-point functions. One can choose a normalization for the two-point function of the defect scalar primary $\hat{\mathcal{O}}^s$ as follows

$$\langle \hat{\mathcal{O}}^s(x'') \hat{\mathcal{O}}^s(\tilde{x}'') \rangle = |x'' - \tilde{x}''|^{-2\Delta(\hat{\mathcal{O}}^s)} , \quad (2.5)$$

such that it is non-degenerate and diagonal in the $\mathfrak{so}(q)$ indices. Using (2.4) and (2.5), one

finds the correlation function between the bulk scalar \mathcal{O} and the defect scalar $\hat{\mathcal{O}}^s$:

$$\langle \mathcal{O}(x^\perp, x'') \hat{\mathcal{O}}^s(\tilde{x}'') \rangle = \frac{Y_s(x_\sigma^\perp/|x^\perp|) C_{\mathcal{O}}^{\hat{\mathcal{O}}^s}}{|x^\perp|^{\Delta(\mathcal{O})-\Delta(\hat{\mathcal{O}}^s)} (|x^\perp|^2 + |x'' - \tilde{x}''|^2)^{\Delta(\hat{\mathcal{O}}^s)}} . \quad (2.6)$$

The two-point function (2.6) probes the location of the defect when $\Delta(\mathcal{O}) \neq \Delta(\hat{\mathcal{O}}^s)$ and $C_{\mathcal{O}}^{\hat{\mathcal{O}}^s} \neq 0$, indicating that the defect does not factorize from the bulk.

Our analysis extends to general bulk and defect operators, despite the more involved tensor structures in (2.2). See, e.g., [41, 43, 46] for a systematic enumeration of these tensors. In what follows, we discuss the defect operators that play a special role in the DCFT, in particular the identity operator, the displacement operator, and the tilt operator.

2.1.2 Defect identity operator

In this subsection, we consider the defect identity operator⁴ \hat{I} , for which $\ell = 0$, $s = 0$, and $\Delta(\hat{I}) = 0$. Given a bulk CFT operator \mathcal{O}_j , it is natural to ask whether \hat{I} appears on the right-hand side of the expansion (2.2) with a non-zero OPE coefficient. Such coefficients determine the one-point functions of bulk operators in the presence of the defect. We denote them by

$$C_{\mathcal{O}_j} \equiv C_{\mathcal{O}_j}^{\hat{I}} . \quad (2.7)$$

For example, the one-point function of a bulk scalar operator \mathcal{O} simply follows from the dimensional analysis, and is given by

$$\langle \mathcal{O}(x^\perp, x'') \rangle = \frac{C_{\mathcal{O}}}{|x^\perp|^{\Delta(\mathcal{O})}} , \quad (2.8)$$

which is also consistent with (2.6) upon taking the defect operator to be \hat{I} .

The OPE coefficients (2.7) depend on both the bulk and defect dynamics, while also being constrained by the conformal algebra (2.1). In the following discussion, we focus on bulk operators transforming in the symmetric traceless tensor representation of $\mathfrak{so}(d)$. For a spinning operator \mathcal{O}_j , it is convenient to define a degree- j polynomial [49]

$$\mathcal{P}_{\mathcal{O}_j} \equiv v^{\mu_1} \dots v^{\mu_j} (\mathcal{O}_j)_{\mu_1 \dots \mu_j} , \quad (2.9)$$

where v_μ is a null vector satisfying $v^\mu v_\mu = 0$. The operator $\mathcal{P}_{\mathcal{O}_j}$ transforms as a scalar under the conformal algebra (2.1). Moreover, the one-point function of $\mathcal{P}_{\mathcal{O}_j}$ must also be degree- j

⁴We have assumed that the defect identity operator is unique, which in turn implies that the CFT with the defect inserted has a unique vacuum.

polynomial in v_μ . We thereby find [41, 43]

$$\langle \mathcal{P}_{\mathcal{O}_j}(x^\perp, x'') \rangle = \frac{C_{\mathcal{O}_j}}{|x^\perp|^{\Delta(\mathcal{O}_j)}} \left(v^\sigma v_\sigma - \frac{(v^\sigma x_\sigma^\perp)^2}{|x^\perp|^2} \right)^{\frac{j}{2}} . \quad (2.10)$$

For conformal boundaries and interfaces, the one-point function (2.10) implies that [39]

$$C_{\mathcal{O}_j} = 0 , \quad \text{for integer } j \geq 1 \text{ when } q = 1 . \quad (2.11)$$

Meanwhile, the polynomial in parentheses in (2.10) only becomes a perfect square for defect codimension $q = 2$. We note that

$$C_{\mathcal{O}_j} = 0 , \quad \text{for odd integer } j \text{ when } q \geq 3 . \quad (2.12)$$

For example, the bulk conserved current J_μ admits a non-zero one-point function only for defects of codimension $q = 2$. The one-point function of bulk stress-energy tensor $T_{\mu_1\mu_2}$, by contrast, can take non-zero values for defects of any codimension $q \geq 2$. In Section 2.4, we study the OPE coefficients (2.7) associated with J_μ and $T_{\mu_1\mu_2}$ in concrete physical settings.

2.1.3 Displacement and tilt operators

In this subsection, we turn to other defect operators whose quantum numbers, like that of the identity operator \hat{I} , are fixed across different DCFTs. This includes the displacement operator \hat{D} [10, 38, 39, 50], which is a universal defect primary for local DCFTs.

To define the \hat{D} operator, it is helpful to generalize the background metric on the d -dimensional space to $(ds)^2 = g_{\mu_1\mu_2} dx^{\mu_1} dx^{\mu_2}$. We denote the embedding of the p -dimensional defect by $X_\mu(x'')$, and the induced metric on the defect is given by

$$\hat{g}_{\nu_1\nu_2} \equiv g_{\mu_1\mu_2} \frac{\partial X^{\mu_1}}{\partial x''_{\nu_1}} \frac{\partial X^{\mu_2}}{\partial x''_{\nu_2}} . \quad (2.13)$$

The defect dynamics depends both on the induced metric $\hat{g}_{\nu_1\nu_2}$ and on the embedding X_μ into the ambient space. In particular, the displacement operator \hat{D} is defined through the leading linear response of the DCFT action to variations of X_μ as follows

$$\begin{aligned} \delta S_{\text{DCFT}} = & -\frac{1}{2} \int d^d x \sqrt{g} \delta g_{\mu_1\mu_2} T^{\mu_1\mu_2} \\ & - \frac{1}{2} \int d^p x'' \sqrt{\hat{g}} \delta g_{\mu_1\mu_2} \hat{T}^{\mu_1\mu_2} - \int d^p x'' \sqrt{\hat{g}} \delta X_\mu (\hat{D})^\mu + \text{higher-order terms} , \end{aligned} \quad (2.14)$$

where $T_{\mu_1\mu_2}$ is the bulk stress-energy tensor. For planar defects embedded in the Euclidean

space \mathbb{R}^d , we have $g_{\mu_1\mu_2} = \delta_{\mu_1\mu_2}$ and $X_\mu = \delta_\mu^\nu x_\nu''$.⁵ Clearly, the embedding function X_μ in this case has the dimension -1 , which in turn fixes the scaling dimension of the displacement operator to be $\Delta(\hat{D}) = p + 1$.

The DCFT action is expected to be invariant under bulk and defect reparametrizations. Requiring $\delta S_{\text{DCFT}} = 0$ under the defect coordinate variation $\delta g_{\mu_1\mu_2} = 0$ and $\delta X_\mu = \delta_\mu^\nu \delta x_\nu''$, we find from (2.14) that the displacement operator has $\ell = 0$ and $s = 1$. We also consider the bulk coordinate variation:

$$\delta g_{\mu_1\mu_2} = \partial_{\mu_1} \delta x_{\mu_2} + \partial_{\mu_2} \delta x_{\mu_1} \ , \quad \delta X_\mu = -\delta x_\mu \ . \quad (2.15)$$

The Ward identities following from $\delta S_{\text{DCFT}} = 0$ are then given by

$$\partial_\mu T_{\text{tot}}^{\mu\sigma} = \delta^q(x^\perp) (\hat{D})^\sigma \ , \quad \text{and} \quad \partial_\mu T_{\text{tot}}^{\mu\nu} = 0 \ , \quad (2.16)$$

where $T_{\text{tot}}^{\mu_1\mu_2} \equiv T^{\mu_1\mu_2} + \delta^q(x^\perp) \hat{T}^{\mu_1\mu_2}$. In the x_ν'' -directions, (2.16) implies that momentum can flow between the bulk and the defect and remain conserved, while the explicit breaking of translation symmetries in the x_σ^\perp -directions leads to the displacement operator \hat{D} . Notably, the Ward identities fix the norm of the two-point function of the \hat{D} operator, which takes the form

$$\langle (\hat{D})_{\sigma_1}(x'') (\hat{D})_{\sigma_2}(\tilde{x}'') \rangle = \delta_{\sigma_1\sigma_2} C_{\hat{D}\hat{D}} |x'' - \tilde{x}''|^{-2(p+1)} \ . \quad (2.17)$$

The coefficient $C_{\hat{D}\hat{D}}$ encodes information about the defect Weyl anomaly; see [47] for details.

Each continuous global symmetry of the bulk CFT is associated with a conserved current operator. For simplicity, we consider a 0-form $U(1)$ symmetry and the corresponding bulk current J_μ in the following. Generalizations to non-abelian groups and higher-form symmetries are straightforward [51].

The Ward identity for J_μ is generally modified in the presence of the defect. As in (2.16), it takes the form

$$\partial_\mu J^\mu = \delta^q(x^\perp) \hat{\tau} \ . \quad (2.18)$$

This implies that the $\hat{\tau}$ operator has quantum numbers $\ell = 0$, $s = 0$, and $\Delta(\hat{\tau}) = p$.

The $\hat{\tau}$ operator encodes the DCFT response to the symmetry transformation. To see that, we consider the topological operator $\exp(i\alpha \int \star J)$ and sweep it across the defect at $x_\sigma^\perp = 0$. The Ward identity (2.18) indicates that

$$\delta S_{\text{DCFT}} = i\alpha \int d^p x'' \hat{\tau} \ . \quad (2.19)$$

We note that δS_{DCFT} becomes trivial when $\hat{\tau} = \partial_\nu \hat{J}^\nu$ is a total derivative. In such cases, the total $U(1)$ charge of the bulk and the defect remains conserved, and the defect is symmetric.

⁵The definition analogously applies to defects in curved spacetimes. However, the quantum numbers of the corresponding operator may depend on the background metric. We discuss such examples in Section 2.4.

By contrast, the $\hat{\tau}$ operator in (2.19) generates a non-trivial marginal deformation when the defect breaks the symmetry. The defect primary $\hat{\tau}$ associated with broken global symmetries is referred to as the tilt operator [51–54].

Deforming the DCFT with the tilt operator $\hat{\tau}$ as in (2.19) generates an exact defect conformal manifold, which is isomorphic to the coset space associated with the broken symmetries. The Zamolodchikov metric on this conformal manifold is determined by the two-point function of the $\hat{\tau}$ operator, which takes the form

$$\langle \hat{\tau}(x'') \hat{\tau}(\tilde{x}'') \rangle = C_{\hat{\tau}\hat{\tau}} |x'' - \tilde{x}''|^{-2p} . \quad (2.20)$$

Similar to (2.17), the local metric $C_{\hat{\tau}\hat{\tau}}$ is fixed by the Ward identity (2.18).

2.2 Constraints on DCFTs in Maxwell theory

What is the space of possible DCFTs, up to decoupled sectors, for a given bulk theory? This is a profound and challenging problem that, in general, can only be attacked using numerical bootstrap methods [39]. One may expect that the bulk-to-defect OPE (2.2) becomes stringent for certain representations of the bulk conformal algebra $\mathfrak{so}(d+1, 1)$, in particular for free theories. Indeed, the spaces of DCFTs in free scalar field theory [45, 55] and in free Maxwell theory [56, 57] are considerably more constrained.

In this section, we discuss the $p = 2$ chiral surface defects in the $d = 4$ Maxwell theory that are defined as the boundaries of topological duality defects. We show that the constraints from bulk dynamics in such cases completely determine the DCFT spectrum. Correlation functions of operators confined to these defects factorize into two sectors [3]: a universal generalized free-field sector, and a chiral current sector analogous to edge modes in Chern-Simons theory.

2.2.1 Topological duality defect

We first review Maxwell theory and its global symmetries. The Maxwell action for a $U(1)$ abelian gauge field A on a 4-dimensional Euclidean manifold \mathcal{M}_4 is

$$S_{\text{Maxwell}} = \frac{1}{2e^2} \int_{\mathcal{M}_4} F \wedge \star F , \quad (2.21)$$

where $e > 0$ denotes the gauge coupling, and $F = dA$ is the field strength⁶. The action (2.21) has an ordinary \mathbb{Z}_2 symmetry, which acts on the gauge field by charge conjugation $C : A \rightarrow -A$. Furthermore, it has a continuous 1-form global symmetry $U(1)_e^{(1)} \times U(1)_m^{(1)}$

⁶More generally, one can include a theta-angle term in the Maxwell action (2.21). Even though this topological term doesn't affect the equations of motion, it changes the global properties of the theory and leads to new non-invertible symmetries [58–60]. However, we will not study this generalization here.

generated by the electric current J_e and the magnetic current J_m [1]. Explicitly, the 1-form symmetry currents $J_{e/m}$ and their defects $\eta_{e/m}$ are defined as follows:

$$\begin{aligned} U(1)_e^{(1)} : \quad J_e &= \frac{i}{e^2} F, \quad \eta_e(\alpha) = \exp\left(i\alpha \int_{\mathcal{M}_2} \star J_e\right); \\ U(1)_m^{(1)} : \quad J_m &= \frac{1}{2\pi} \star F, \quad \eta_m(\alpha) = \exp\left(i\alpha \int_{\mathcal{M}_2} \star J_m\right), \end{aligned} \quad (2.22)$$

where $\mathcal{M}_2 \subset \mathcal{M}_4$ is a closed 2-dimensional surface in spacetime. They are genuine 2d surface defects in spacetime, and are special examples of the Gukov-Witten defects [61, 62]. These defects are topological, which follows from the equation of motion $d\star J_e = id\star F/e^2 = 0$ and the Bianchi identity $d\star J_m = dF/2\pi = 0$.

These two 1-form global symmetries in (2.22) have a mixed 't Hooft anomaly. We couple the symmetry currents to two 2-form background gauge fields, which we denote as B_e and B_m , respectively. The covariant Maxwell action reads

$$S_{\text{Maxwell}} = \frac{1}{2e^2} \int_{\mathcal{M}_4} (F - B_e) \wedge \star(F - B_e) + \frac{i}{2\pi} \int_{\mathcal{M}_4} B_m \wedge (F - B_e). \quad (2.23)$$

The background gauge transformations for $U(1)_e^{(1)} \times U(1)_m^{(1)}$ are:

$$A \rightarrow A + a_e, \quad B_e \rightarrow B_e + da_e, \quad B_m \rightarrow B_m + da_m, \quad (2.24)$$

where a_e and a_m are two 1-form gauge parameters. Under these gauge transformations, the Maxwell action (2.23) is not invariant and transforms as

$$S_{\text{Maxwell}} \rightarrow S_{\text{Maxwell}} - \frac{i}{2\pi} \int_{\mathcal{M}_4} a_m \wedge dB_e. \quad (2.25)$$

The variation term in (2.25) signals the mixed 't Hooft anomaly between $U(1)_e^{(1)}$ and $U(1)_m^{(1)}$, which can be canceled by a 5-dimensional anomaly inflow action.

For concreteness, we define the duality defect on the manifold $\mathcal{M}_4 = T^3 \times [0, 2\pi]$, with coordinates $x_i \sim x_i + 2\pi$ for $i = 1, 2, 3$, and $0 \leq x_4 \leq 2\pi$. We impose the Neumann boundary condition $F_{14} = F_{24} = F_{34} = 0$ on the two boundaries at $x_4 = 0$ and $x_4 = 2\pi$ for the Maxwell theory (2.21). Furthermore, we denote the 1-form gauge fields on the boundaries as

$$A^+(x_i) \equiv A(x_i, x_4 = 0), \quad \text{and} \quad A^-(x_i) \equiv A(x_i, x_4 = 2\pi). \quad (2.26)$$

The duality defect \mathcal{D}_N is defined by a gluing action that couples the gauge fields on the two

boundaries [60, 63–67]:

$$\mathcal{D}_N : S_{\text{duality}} = \frac{iN}{2\pi} \int_{T^3} A^- \wedge dA^+ . \quad (2.27)$$

Similar to the standard argument in Chern-Simons gauge theories, gauge invariance requires $N \in \mathbb{Z}$. For simplicity, we focus on the $N > 0$ case in the following, noting that $\mathcal{D}_{-N} = C \times \mathcal{D}_N = \mathcal{D}_N \times C$, where C is the charge conjugation defect.

It follows from the equation of motion that the stress-energy tensor is conserved across the duality defect (2.27) if

$$e^2 = \frac{2\pi}{N} . \quad (2.28)$$

We will always assume this condition from now on, so that \mathcal{D}_N is a topological defect⁷.

We note the variation of the Maxwell action (2.21) on the open manifold $\mathcal{M}_4 = T^3 \times [0, 2\pi]$ is given by

$$\delta S_{\text{Maxwell}} = \frac{N}{2\pi} \int_{T^3 \times [0, 2\pi]} \delta A \wedge d \star F - \frac{N}{2\pi} \int_{T^3} \delta A^+ \wedge \star F^+ + \frac{N}{2\pi} \int_{T^3} \delta A^- \wedge \star F^- . \quad (2.29)$$

Clearly, the first term vanishes when the equations of motion are imposed, while the second and the third terms have to be canceled against the variation of the defect action (2.27):

$$\delta S_{\text{duality}} = \frac{iN}{2\pi} \int_{T^3} (\delta A^- \wedge dA^+ + A^- \wedge d\delta A^+) \quad (2.30)$$

We therefore find

$$F^+ = i \star F^- . \quad (2.31)$$

This gluing condition across \mathcal{D}_N implements the electromagnetic duality (or S-duality). In particular, (2.31) implies the fusion rules

$$\begin{aligned} \eta_e(\alpha) \times \mathcal{D}_N &= \mathcal{D}_N \times \eta_m(N\alpha) , \\ \mathcal{D}_N \times \eta_e(\alpha) &= \eta_m(-N\alpha) \times \mathcal{D}_N . \end{aligned} \quad (2.32)$$

We note that the duality defect can absorb the electric 1-form symmetry defects associated with the subgroup $\mathbb{Z}_N^{(1)} \subset U(1)_e^{(1)}$:

$$\eta_e(\alpha) \times \mathcal{D}_N = \mathcal{D}_N \times \eta_e(\alpha) = \mathcal{D}_N , \quad \text{if } \alpha \in \frac{2\pi\mathbb{Z}}{N} . \quad (2.33)$$

This indicates that \mathcal{D}_N is non-invertible when $N > 1$. At $N = 1$, (2.28) reduces to the self-dual radius, and the duality defect $\mathcal{D}_{N=1}$ is invertible.

⁷More generally, the topological duality defect can be defined for $e^2/2\pi \in \mathbb{Q}^+$; See [3, 60, 66].

2.2.2 Twist defects for electromagnetic duality

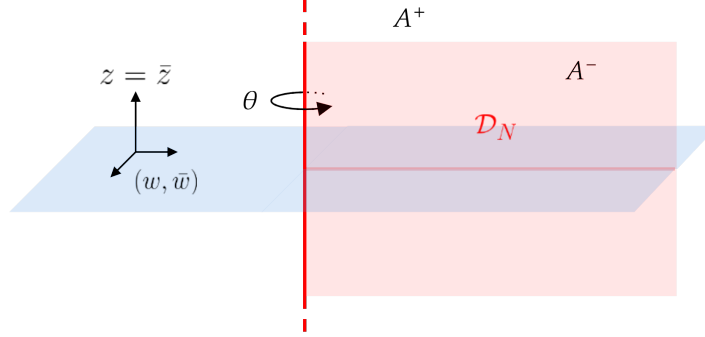


Figure 2.1: The configuration of the conformal twist defect and the topological duality defect in \mathbb{R}^4 . The vertical red line is the 2-dimensional twist defect, which is localized at $w = \bar{w} = 0$ and extends along the (z, \bar{z}) plane. The twist defect is attached to the 2-dimensional topological defect \mathcal{D}_N shown as the half-infinite red plane. This figure only displays the \mathbb{R}^3 slice defined by $z = \bar{z}$.

With preliminaries in place, we now introduce the setup for the $p = 2$ chiral surface defect. We consider the Euclidean spacetime $\mathcal{M}_4 = \mathbb{R}^4$, with complex coordinates $z, w \in \mathbb{C}$ and the metric

$$ds^2 = 2dzd\bar{z} + 2dw d\bar{w} . \quad (2.34)$$

We implement the topological duality defect \mathcal{D}_N so that it covers the complex z -plane and extends along the positive real axis $w > 0$ of the complex w -plane, terminating at the origin $w = \bar{w} = 0$. See Figure 2.1. More concretely, the action for the duality defect reads

$$\mathcal{D}_N : \quad S_{\text{duality}} = \frac{iN}{2\pi} \int_{w \in \mathbb{R}^+} A^- \wedge dA^+ . \quad (2.35)$$

where A_{\pm} are the gauge fields on the two sides of \mathcal{D}_N :

$$A^{\pm}(z, \bar{z}, |w|) = \lim_{\epsilon \rightarrow 0^{\pm}} A(z, \bar{z}, w = |w| + i\epsilon, \bar{w} = |w| - i\epsilon) . \quad (2.36)$$

Since the duality defect \mathcal{D}_N is topological, it preserves the $\mathfrak{so}(2)$ rotation symmetry of the complex w -plane. Denoting $w = |w|e^{i\theta}$, we find that the gluing condition (2.31) implies the following monodromy condition under $\theta \rightarrow \theta + 2\pi$:

$$F \longrightarrow -i \star F \longrightarrow -F \longrightarrow i \star F \longrightarrow F , \quad (2.37)$$

The $\theta \sim \theta + 2\pi$ periodicity is therefore lifted to $\theta \sim \theta + 8\pi$ in the presence of \mathcal{D}_N .

The twist defect [68–71] is defined by the $p = q = 2$ boundary of the topological defect \mathcal{D}_N as in Figure 2.1. The Maxwell theory in 4-dimensional spacetime has the conformal symmetry $\mathfrak{so}(5, 1)$. In what follows, we assume that the twist defect preserves a $\mathfrak{so}(3, 1) \times \mathfrak{so}(2)$ conformal subalgebra at the defect RG fixed point.

What are the possible twist defect CFTs compatible with the duality defect (2.35) and the bulk monodromy condition (2.37)? In the following subsections, we address this question using the techniques developed in [3, 46, 56].

2.2.3 Bulk-defect two-point functions

We first consider the two-point function $\langle F\hat{\mathcal{O}}_\ell^s \rangle$ between the bulk field strength operator $F_{\mu_1\mu_2}(x)$ and a defect primary $\hat{\mathcal{O}}_\ell^s$ at $z = \bar{z} = 0$. See Figure 2.2. With slight abuse of notation, we now allow the parallel spin ℓ and the transverse spin s to take both positive and negative values, corresponding to the doublet representations of $\mathfrak{so}(2)$. We also denote the conformal weights of $\mathfrak{so}(3, 1)$ by (h, \bar{h}) , such that $\Delta = h + \bar{h}$ and $\ell = h - \bar{h}$.

Our first hint follows from (2.37). For the two-point function to be nontrivial, the defect operator has to satisfy the spin selection rule

$$\langle F\hat{\mathcal{O}}_\ell^s \rangle \neq 0 \quad \Rightarrow \quad s \in \mathbb{Z} \pm \frac{1}{4}. \quad (2.38)$$

The form of the non-zero function $\langle F\hat{\mathcal{O}}_\ell^s \rangle$ is strongly constrained by the $so(3, 1) \times so(2)$ conformal symmetry. In particular, covariant tensor structures in the two-point function between a bulk primary and a defect primary are spanned by polynomials of the following basis tensors:

$$\begin{aligned} \mathcal{X}_\mu &= \frac{|w|}{|z|^2 + |w|^2} \left(\bar{z}, z, \frac{\bar{w}}{2}(1 - |z/w|^2), \frac{w}{2}(1 - |z/w|^2) \right) ; \\ \mathcal{Y}_\mu &= \frac{1}{2} \left(0, 0, \frac{\bar{w}}{|w|}, -\frac{w}{|w|} \right) ; \\ \mathcal{I}_{\mu z} &= -\frac{1}{2(|z|^2 + |w|^2)} (\bar{z}^2, -|w|^2, \bar{z}\bar{w}, \bar{z}w) ; \\ \mathcal{I}_{\mu \bar{z}} &= -\frac{1}{2(|z|^2 + |w|^2)} (-|w|^2, z^2, z\bar{w}, zw) . \end{aligned} \quad (2.39)$$

We have $\mathcal{X}^\mu \mathcal{X}_\mu = \frac{1}{2}$, $\mathcal{Y}^\mu \mathcal{Y}_\mu = -\frac{1}{2}$, and $\mathcal{I}^\mu{}_z \mathcal{I}_{\mu \bar{z}} = \frac{1}{4}$, while the index contractions between other pairs of these tensors yield zero. Since one cannot build a tensor out of (2.39) with a pair of anti-symmetrized indices $[\mu_1\mu_2]$ and parallel spin $|\ell| \geq 2$, the two-point function $\langle F\hat{\mathcal{O}}_\ell^s \rangle$ must vanish unless $|\ell| < 2$. To admit a non-zero two-point function, the defect primary $\hat{\mathcal{O}}_\ell^s$ is either a scalar ($\ell = 0$) or a vector ($\ell = \pm 1$). It is further shown in [56] that a defect scalar primary $\hat{\mathcal{O}}^s$ yields $\langle F\hat{\mathcal{O}}^s \rangle = 0$ unless $s = 0$ and $\Delta(\hat{\mathcal{O}}^s) = 2$, which is obviously incompatible

with the spin selection rule (2.38). We are therefore left with the vector primaries.

We denote the vector primary of parallel spin $\ell = 1$ and transverse spin s on the twist defect by \hat{V}_z^s . The two-point function $\langle F_{\mu_1\mu_2} \mathcal{V}_z^s \rangle$ admits two compatible tensor structures, namely $\mathcal{X}_{[\mu_1\mathcal{I}_{\mu_2]z}}$ and $\mathcal{Y}_{[\mu_1\mathcal{I}_{\mu_2]z}}$. Note that the linear combination $\mathcal{X}_{[\mu_1\mathcal{I}_{\mu_2]z}} + \mathcal{Y}_{[\mu_1\mathcal{I}_{\mu_2]z}}$ is self-dual under the Hodge star operation, while $\mathcal{X}_{[\mu_1\mathcal{I}_{\mu_2]z}} - \mathcal{Y}_{[\mu_1\mathcal{I}_{\mu_2]z}}$ is anti-self-dual. The conformal algebra $so(3,1) \times so(2)$ and the monodromy condition (2.37) fix the functional form of $\langle F_{\mu\nu} \mathcal{V}_z^s \rangle$ up to the OPE coefficient as follows

$$\langle F_{\mu_1\mu_2}(x) \hat{V}_z^s(0) \rangle \Big|_{s \in \mathbb{Z} \pm \frac{1}{4}} = \frac{C_F \hat{V}_z^s}{|w|^2} \left(\frac{|w|}{|w|^2 + |z|^2} \right)^{\Delta(\hat{V}_z^s)} (\mathcal{X}_{[\mu_1\mathcal{I}_{\mu_2]z}} \mp \mathcal{Y}_{[\mu_1\mathcal{I}_{\mu_2]z}}) \left(\frac{w}{|w|} \right)^s. \quad (2.40)$$

A similar analysis can be applied to the defect vector primary $\hat{V}_{\bar{z}}^s$ of parallel spin $\ell = -1$, and we find

$$\langle F_{\mu_1\mu_2}(x) \hat{V}_{\bar{z}}^s(0) \rangle \Big|_{s \in \mathbb{Z} \pm \frac{1}{4}} = \frac{C_F \hat{V}_{\bar{z}}^s}{|w|^2} \left(\frac{|w|}{|w|^2 + |z|^2} \right)^{\Delta(\hat{V}_{\bar{z}}^s)} (\mathcal{X}_{[\mu_1\mathcal{I}_{\mu_2]\bar{z}}} \pm \mathcal{Y}_{[\mu_2\mathcal{I}_{\mu_1]\bar{z}}]) \left(\frac{w}{|w|} \right)^s. \quad (2.41)$$

Imposing the Bianchi identity $dF = 0$ on (2.40) and (2.41), we find that non-zero OPE coefficients are only compatible with the following scaling dimensions

$$\Delta(\hat{V}_z^s) \Big|_{s \in \mathbb{Z} \pm \frac{1}{4}} = 1 \pm s, \quad \Delta(\hat{V}_{\bar{z}}^s) \Big|_{s \in \mathbb{Z} \pm \frac{1}{4}} = 1 \mp s. \quad (2.42)$$

Note that the unitarity bound for a defect vector is $\Delta \geq 1$, which is saturated by the conserved spin-1 currents. We therefore conclude that the primaries on the twist defect that appear in the OPE of the bulk field strength F are given by

$$\begin{aligned} \hat{V}_z^s &: (h, \bar{h}) = \left(1 + \frac{|s|}{2}, \frac{|s|}{2} \right), \quad \text{where } |s| \in \mathbb{N} + \frac{1}{4}; \\ \hat{V}_{\bar{z}}^s &: (h, \bar{h}) = \left(\frac{|s|}{2}, 1 + \frac{|s|}{2} \right), \quad \text{where } |s| \in \mathbb{N} + \frac{3}{4}. \end{aligned} \quad (2.43)$$

Notably, the conformal weights in (2.43) are completely determined by conformal symmetry and unitarity. They are universal and insensitive to the possible interactions localized on the twist defect. Moreover, the transverse spin s in (2.43) is subject to the selection rule that depends on the parallel spin ℓ . This manifests a spin-momentum lock of photons propagating along the defect.

2.2.4 Bulk-defect-defect three-point functions

Next, we consider the three-point function $\langle F \hat{\mathcal{O}}_{\ell_2}^{s_2} \hat{\mathcal{O}}_{\ell_3}^{s_3} \rangle$ between the bulk field strength operator F at $x = (z_1, \bar{z}_1, w, \bar{w})$ and defect primaries $\hat{\mathcal{O}}_{\ell_2}^{s_2}$ at (z_2, \bar{z}_2) and $\hat{\mathcal{O}}_{\ell_3}^{s_3}$ at (z_3, \bar{z}_3) . See

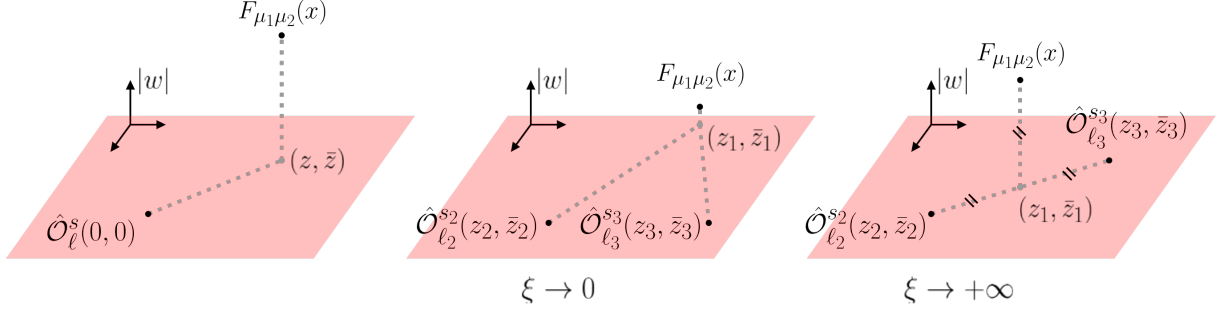


Figure 2.2: DCFT two-point and three-point functions. The red plane represents the twist defect at $w = \bar{w} = 0$. Left: the bulk-defect two-point function $\langle F\hat{\mathcal{O}}_\ell^s \rangle$. Middle: the bulk-defect-defect three-point function $\langle F\hat{\mathcal{O}}_{\ell_2}^{s_2}\hat{\mathcal{O}}_{\ell_3}^{s_3} \rangle$ in the limit $\xi \rightarrow 0$, where the bulk point x approaches the defect. Right: the three-point function $\langle F\hat{\mathcal{O}}_{\ell_2}^{s_2}\hat{\mathcal{O}}_{\ell_3}^{s_3} \rangle$ in the limit $\xi \rightarrow +\infty$, where the projection of the bulk point onto the defect plane coincides with the midpoint between (z_2, \bar{z}_2) and (z_3, \bar{z}_3) .

Figure 2.2.

It follows from the monodromy condition (2.37) that $\langle F\hat{\mathcal{O}}_{\ell_2}^{s_2}\hat{\mathcal{O}}_{\ell_3}^{s_3} \rangle = 0$ unless $s = s_2 + s_3 \in \mathbb{Z} \pm \frac{1}{4}$, while s_2 and s_3 themselves need not satisfy the spin selection rule (2.38). The form of the non-zero function $\langle F\hat{\mathcal{O}}_{\ell_2}^{s_2}\hat{\mathcal{O}}_{\ell_3}^{s_3} \rangle$ is fixed by the conformal algebra $so(3,1) \times so(2)$ up to functions of the cross ratio ξ , defined as:

$$\xi = \frac{|z_{23}|^2 |w|^2}{(|w|^2 + z_{12}\bar{z}_{13})(|w|^2 + \bar{z}_{12}z_{13})} > 0, \quad (2.44)$$

where $z_{ij} = z_i - z_j$.

Tensor structures in the three-point function $\langle F\hat{\mathcal{O}}_{\ell_2}^{s_2}\hat{\mathcal{O}}_{\ell_3}^{s_3} \rangle$ can be enumerated in a way similar to (2.40) and (2.41). They are spanned by polynomial combinations of four vector building blocks: $\mathcal{X}_{12,\mu}$, $\mathcal{X}_{13,\mu}$, \mathcal{Y}_μ , and \mathcal{I}_μ . The pseudo-vector \mathcal{Y}_μ follows the same definition as in (2.39), while the other vectors are given by

$$\begin{aligned} \mathcal{X}_{ij,\mu} &= \frac{|w|}{|z_{ij}|^2 + |w|^2} \left(\bar{z}_{ij}, z_{ij}, \frac{\bar{w}}{2}(1 - |z_{ij}/w|^2), \frac{w}{2}(1 - |z_{ij}/w|^2) \right); \\ \mathcal{I}_\mu &= \frac{z_{12}\bar{z}_{13} + |w|^2}{2|w|z_{23}(|z_{13}|^2 + |w|^2)} \left(-|w|^2, z_{13}^2, \bar{w}z_{13}, wz_{13} \right). \end{aligned} \quad (2.45)$$

We consider the following combinations of these building block vectors

$$\mathcal{X}_{12, [\mu_1} \mathcal{X}_{13, \mu_2]}, \quad \mathcal{X}_{12, [\mu_1} \mathcal{Y}_{\mu_2]}, \quad \mathcal{X}_{12, [\mu_1} \mathcal{I}_{\mu_2]}, \quad \mathcal{X}_{13, [\mu_1} \mathcal{Y}_{\mu_2]}, \quad \mathcal{X}_{13, [\mu_1} \mathcal{I}_{\mu_2]}, \quad \mathcal{Y}_{[\mu_1} \mathcal{I}_{\mu_2]}. \quad (2.46)$$

These six tensors are linearly independent, and they provide a complete basis for rank-2 anti-symmetric tensors. We organize the (2.46) into the combinations that are either self-dual (+) and anti-self-dual (-) under the Hodge star operation:

$$\begin{aligned}
\mathcal{Z}_{1,\mu_1\mu_2}^\pm &= \mathcal{X}_{13, [\mu_1 \mathcal{I}_{\mu_2}]} \mp \mathcal{Y}_{[\mu_1 \mathcal{I}_{\mu_2}]} ; \\
\mathcal{Z}_{2,\mu_1\mu_2}^\pm &= \mathcal{X}_{12, [\mu_1 \mathcal{X}_{13, \mu_2}]} - 2\mathcal{X}_{12, [\mu_1 \mathcal{I}_{\mu_2}]} + 2\mathcal{X}_{13, [\mu_1 \mathcal{I}_{\mu_2}]} \pm (\mathcal{X}_{12, [\mu_1 \mathcal{Y}_{\mu_2}]} + \mathcal{X}_{13, [\mu_1 \mathcal{Y}_{\mu_2}]}); \\
\mathcal{Z}_{3,\mu_1\mu_2}^\pm &= \xi^{-1}(\mathcal{X}_{12, [\mu_1 \mathcal{Y}_{\mu_2}]} - \mathcal{X}_{13, [\mu_1 \mathcal{Y}_{\mu_2}]} \\
&\quad \pm (2\mathcal{X}_{12, [\mu_1 \mathcal{I}_{\mu_2}]} + 2\mathcal{X}_{13, [\mu_1 \mathcal{I}_{\mu_2}]} + \xi^{-1}\mathcal{X}_{12, [\mu_1 \mathcal{X}_{13, \mu_2}]}) .
\end{aligned} \tag{2.47}$$

With (2.47) at hand, we find that a general three-point function $\langle F \hat{\mathcal{O}}_{\ell_2}^{s_2} \hat{\mathcal{O}}_{\ell_3}^{s_3} \rangle$ takes the form

$$\begin{aligned}
\langle F_{\mu_1\mu_2}(x) \hat{\mathcal{O}}_{\ell_2}^{s_2}(z_2, \bar{z}_2) \hat{\mathcal{O}}_{\ell_3}^{s_3}(z_3, \bar{z}_3) \rangle \Big|_{s \in \mathbb{Z} \pm \frac{1}{4}} &= \frac{(w/|w|)^s |w|^{\Delta(\hat{\mathcal{O}}_{\ell_2}^{s_2}) + \Delta(\hat{\mathcal{O}}_{\ell_3}^{s_3}) - 2}}{(|z_{12}|^2 + |w|^2)^{\Delta(\hat{\mathcal{O}}_{\ell_2}^{s_2})} (|z_{13}|^2 + |w|^2)^{\Delta(\hat{\mathcal{O}}_{\ell_3}^{s_3})}} \\
&\times \left(\frac{|w|^2 + \bar{z}_{12} z_{13}}{z_{23} |w|} \right)^{\ell_2} \left(\frac{|w|^2 + \bar{z}_{13} z_{12}}{z_{23} |w|} \right)^{\ell_3} \left(\sum_{a=1}^3 f_a^\mp(\xi) \mathcal{Z}_{a, \mu_1 \mu_2}^\mp \right) ,
\end{aligned} \tag{2.48}$$

where $f_a^\pm(\xi)$ are real-valued functions of the cross ratio (2.44). Imposing the Bianchi identity $dF = 0$ on (2.48), we obtain an algebraic relation among the functions f_a^\pm :

$$\left(\frac{s}{4} \pm (h_2 - h_3) \right) f_1^\pm + s f_2^\pm + (\ell_2 - \ell_3) f_3^\pm = 0 , \text{ for } s \in \mathbb{Z} \mp \frac{1}{4} . \tag{2.49}$$

This relation allows us to express f_2^\pm in terms of f_1^\pm and f_3^\pm . Furthermore, the Bianchi identity yields an ordinary differential equation:

$$\begin{aligned}
s\xi(1 + \xi)\partial_\xi f_1^\pm &= 2(s^2 + \xi(\ell_2 - \ell_3)^2) f_3^\pm \\
&\quad + \left[\left(\frac{s}{2}(2 + \ell_2 + \ell_3) \pm (h_2 - h_3)(\ell_2 - \ell_3) \right) \xi + s \left(1 \pm \frac{s}{2} - \bar{h}_2 - \bar{h}_3 \right) \right] f_1^\pm , \\
s\xi(1 + \xi)\partial_\xi f_3^\pm &= \frac{\xi}{8}(s^2 - 4(h_2 - h_3)^2) f_1^\pm \\
&\quad + \left[\left(\frac{s}{2}(2 + \ell_2 + \ell_3) \mp (h_2 - h_3)(\ell_2 - \ell_3) \right) \xi + s \left(1 \mp \frac{s}{2} - \bar{h}_2 - \bar{h}_3 \right) \right] f_3^\pm .
\end{aligned} \tag{2.50}$$

The two hypergeometric solutions to (2.50) are discussed in [3]. These solutions are subject to constraints from unitarity (at $\xi \rightarrow 0$) as well as convergence (at $\xi \rightarrow \infty$). Crucially, we

find that $\langle F\hat{\mathcal{O}}_{\ell_2}^{s_2}\hat{\mathcal{O}}_{\ell_3}^{s_3}\rangle = 0$ unless the following conditions are satisfied:

$$\begin{aligned}
&\text{if } |s| \in \mathbb{N} + \frac{1}{4}, \quad \text{either } (h_2, \bar{h}_2) - (h_3, \bar{h}_3) \in (1 + \frac{|s|}{2} + \mathbb{N}, \frac{|s|}{2} + \mathbb{N}) \\
&\qquad\qquad\qquad \text{or } (h_3, \bar{h}_3) - (h_2, \bar{h}_2) \in (1 + \frac{|s|}{2} + \mathbb{N}, \frac{|s|}{2} + \mathbb{N}) ; \\
&\text{if } |s| \in \mathbb{N} + \frac{3}{4}, \quad \text{either } (h_2, \bar{h}_2) - (h_3, \bar{h}_3) \in (\frac{|s|}{2} + \mathbb{N}, 1 + \frac{|s|}{2} + \mathbb{N}) \\
&\qquad\qquad\qquad \text{or } (h_3, \bar{h}_3) - (h_2, \bar{h}_2) \in (\frac{|s|}{2} + \mathbb{N}, 1 + \frac{|s|}{2} + \mathbb{N}) .
\end{aligned} \tag{2.51}$$

We see that the differences between the allowed values of (h_2, \bar{h}_2) and (h_3, \bar{h}_3) correspond to the conformal weights of \hat{V}_z^s and $\hat{V}_{\bar{z}}^s$ in (2.43), or their descendants.

The selection rule (2.51) implies that the operator spectrum in the OPE between $\hat{V}_z^s, \hat{V}_{\bar{z}}^s$, and a generic defect primary $\hat{\mathcal{O}}_\ell^s$ is of the double-twist type, with no anomalous dimension. The correlation functions of these defect operators therefore obey Wick's theorem [45, 56]. We thus conclude that $\hat{V}_z^s, \hat{V}_{\bar{z}}^s$, and their descendants form a universal sector of generalized free fields on the twist defect.

Notably, the generalized free field spectrum contains a unique operator doublet with $|s| = 1, \ell = 0$, and $\Delta = 3$. They are exactly the displacement operators (2.14), whose existence marks the mobility of the twist defect. Up to overall normalizations, we identify the displacement operators as

$$\hat{D}^{+1} = \hat{V}_z^{+\frac{1}{4}}\hat{V}_{\bar{z}}^{+\frac{3}{4}}, \quad \hat{D}^{-1} = \hat{V}_z^{-\frac{1}{4}}\hat{V}_{\bar{z}}^{-\frac{3}{4}}. \tag{2.52}$$

2.2.5 Chiral current sector and anyonic branes

We have determined a universal sector of the twist defect CFT using just conformal symmetry (2.1), the monodromy condition (2.37), and the unitarity. In this subsection, we argue that there has to be another sector, which we call the chiral current sector, enforced by anomaly inflow and the 1-form global symmetry (2.22). This is intuitively clear, since the action (2.35) for the 3d topological duality defect \mathcal{D}_N takes the form of a Chern-Simons action. Our discussion below follows closely the standard treatment of conformal boundary conditions of chiral 3d Chern-Simons theory in [13, 14].

Again, let us consider the defect configuration in Figure 2.1. Since the topological defect \mathcal{D}_N is supported on a three-dimensional manifold with a boundary, variation of its action yields an extra boundary contribution:

$$\delta S_{\text{duality}} = \frac{iN}{2\pi} \int_{w \in \mathbb{R}^+} (\delta A^- \wedge dA^+ + \delta A^+ \wedge dA^-) + \frac{iN}{2\pi} \int_{w=\bar{w}=0} A \wedge \delta A. \tag{2.53}$$

With the gluing condition (2.31), the first two terms are canceled by the variation of the bulk action in (2.29). Following [14], we pick a complex structure along the twist defect at $w = \bar{w} = 0$ and introduce a local counterterm:

$$S_{\text{counter}} = -\frac{N}{2\pi} \int_{w=\bar{w}=0} A_z A_{\bar{z}} dz d\bar{z} . \quad (2.54)$$

The variation of the total action is then

$$\delta(S_{\text{bulk}} + S_{\text{duality}} + S_{\text{counter}}) = -\frac{N}{\pi} \int_{w=\bar{w}=0} A_{\bar{z}} \delta A_z dz d\bar{z} . \quad (2.55)$$

To ensure a well-defined variational principle, we impose a Dirichlet condition on the holomorphic component of the gauge field:

$$A_z|_{w=\bar{w}=0} = 0 . \quad (2.56)$$

This is precisely the usual conformal boundary condition for the chiral WZW model in the chiral Chern-Simons theory [13, 14]. The standard analysis implies that there is a chiral compact boson $\hat{\varphi}$ living along the twist defect, which, on-shell, is related to the gauge field as $A_{\bar{z}}|_{w=\bar{w}=0} = \partial_{\bar{z}}\hat{\varphi}$. From (2.55), we define a current operator as:

$$\hat{J}_{\bar{z}} = -\frac{iN}{\pi} A_{\bar{z}} = -\frac{iN}{\pi} \partial_{\bar{z}}\hat{\varphi} . \quad (2.57)$$

It has conformal weights $(h, \bar{h}) = (0, 1)$ and zero transverse spin $s = 0$. From the spin selection rule in (2.38), the two-point function $\langle F \hat{J}_{\bar{z}} \rangle = 0$ vanishes. We have also shown in (2.51) that fusion of defect operators $\hat{V}_z^s, \hat{V}_{\bar{z}}^s$, and their descendants cannot produce current operators with either $h = 0$ or $\bar{h} = 0$. We therefore conclude that correlation functions associated with the chiral current sector and the generalized free field sector factorize.

How does the chiral current localized on the twist defect couple to the bulk Maxwell theory? To see this, we place the twist defect on a Lorentzian cylinder parameterized by (t, σ) and embed it in the $(3+1)$ -dimensional spacetime $\mathbb{R}^{3,1}$. See Figure 2.3. The effective action of the right-moving chiral current is given by⁸

$$S_{\text{chiral}} = -\frac{N}{2\pi} \int dt d\sigma [(\partial_{\sigma}\hat{\varphi})^2 + \partial_t\hat{\varphi}\partial_{\sigma}\hat{\varphi}] , \quad (2.58)$$

where the compact boson field $\hat{\varphi} \sim \hat{\varphi} + 2\pi$. This theory has a chiral $U(1)_{2N}$ global symmetry that shifts the chiral boson, which is generated by the current $\hat{J} = \frac{N}{\pi} \partial_{\sigma}\hat{\varphi}(dt - d\sigma)$.

Next, we discuss the charge quantization for this chiral $U(1)_{2N}$ symmetry. The total

⁸For manifestly Lorentz invariant formulations of the chiral boson action, see, e.g. [72–74].

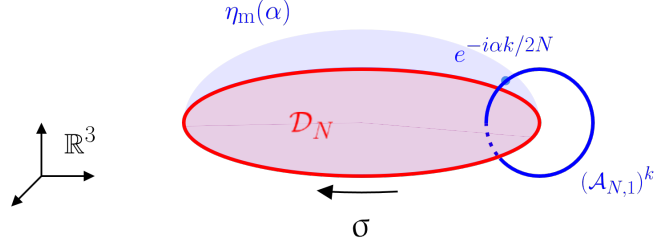


Figure 2.3: The configuration of the anyonic brane $(\mathcal{A}_N)^k$ and the twist defect. The red circle denotes the twist defect defined on a Lorentzian cylinder. The red disk denotes the topological duality defect \mathcal{D}_N . The anyonic brane is shown as a blue circle, which links with the twist defect. The magnetic 1-form symmetry operator $\eta_m(\alpha)$ is shown as the blue surface. This figure only shows the spatial \mathbb{R}^3 , and every defect except for $\eta_m(\alpha)$ extends in the time direction.

$U(1)_{2N}$ charge on the spatial circle of the twist defect is

$$Q_R = \int_{S^1} d\sigma \hat{J}_t = \frac{2N}{2\pi} \int_{S^1} d\sigma \partial_\sigma \hat{\varphi} = \frac{2N}{2\pi} \int_{S^1} d\sigma A_\sigma . \quad (2.59)$$

The charge Q_R can be understood in two complementary ways: In the second equation of (2.59), it is the winding number of $\hat{\varphi}$ multiplied by $2N$. In the third equation of (2.59), we interpret it as the gauge field holonomy, which equals the magnetic 1-form symmetry defect ending on the twist defect. See also figure 2.3. Note that a fractional winding number of $\hat{\varphi}$ would result in $Q_R \notin 2N\mathbb{Z}$. This signals a discontinuity in the chiral boson field and can be interpreted as the insertion of a 1-form symmetry defect, which we now explain.

Consider the following discrete $\mathbb{Z}_{2N}^{(1)}$ subgroup of the $U(1)_e^{(1)} \times U(1)_m^{(1)}$ 1-form global symmetry (2.22) generated by the operator \mathcal{A}_N supported on a 2d surface \mathcal{M}_2 :

$$\mathcal{A}_N = \eta_e\left(\frac{\pi}{N}\right)\eta_m(\pi) = \exp\left(\frac{i}{2} \int_{\mathcal{M}_2} (F - \star F)\right) . \quad (2.60)$$

It is a certain linear combination of the electric and magnetic fluxes and is of order $2N$, i.e., $(\mathcal{A}_N)^{2N} = 1$. It follows from the fusion rule (2.32) that \mathcal{A}_N commutes with \mathcal{D}_N :

$$\mathcal{A}_N \times \mathcal{D}_N = \mathcal{D}_N \times \mathcal{A}_N . \quad (2.61)$$

In other words, $\mathbb{Z}_{2N}^{(1)}$ is the 1-form symmetry subgroup preserved by the duality symmetry defect \mathcal{D}_N . We can therefore consider the defect configuration of \mathcal{D}_N intersects topologically

with the k -th power of \mathcal{A}_N at a point.

Let us consider the magnetic 1-form symmetry operator $\eta_m(\alpha)$, defined on an open surface that terminates on the twist defect as in figure 2.3. The mixed 't Hooft anomaly between \mathcal{A}_N and $\eta_m(\alpha)$, which follows from (2.25), modifies the latter operator from its original form in (2.22) to:

$$\eta_m(\alpha) = \exp\left(\frac{i\alpha}{2\pi} \int F - \frac{i\alpha k}{2N}\right) = \exp\left(\frac{i\alpha}{2N}(Q_R - k)\right). \quad (2.62)$$

Since the $\eta_m(2\pi)$ surface can be annihilated with \mathcal{D}_N , we demand $\eta_m(2\pi) = 1$, leading to the charge quantization condition $Q_R \in 2N\mathbb{Z} + k$. The insertions of $(\mathcal{A}_{N,1})^k$ correspond to the $2N$ primaries of the compact chiral boson (2.58), whose conformal weights are

$$(h, \bar{h}) = \left(0, \frac{Q_R^2}{4N}\right), \quad \text{where } Q_R \in 2N\mathbb{Z} + k. \quad (2.63)$$

In the context of 3d chiral Chern-Simons theories, these primaries of the chiral boson correspond to the insertions of the bulk anyon lines in a similar way. For this reason, we will refer to \mathcal{A}_N as an anyonic brane.

Finally, we note that the twist defect CFT is stable against perturbations from the generalized free field sector and the chiral current sector. The lowest-lying primary operator that preserves both the defect Lorentz symmetry and the transverse rotation symmetry is $\hat{J}_{\bar{z}} \hat{J}_z \hat{V}_z^{+1/4} \hat{V}_z^{-1/4}$, which has scaling dimension $\Delta = 4.5 > 2$ and is therefore irrelevant. Even if we relax constraints from the transverse rotation symmetry, the lowest-lying primaries $\hat{J}_{\bar{z}} \hat{V}_z^{+1/4}$ and $\hat{J}_z \hat{V}_z^{-1/4}$ have $\Delta = 2.25 > 2$, and the twist defect CFT remains stable against anisotropic perturbations.

2.3 Defect RG flows in the $O(N)$ models

In Sections 2.1 and 2.2, we have discussed the fixed points of the defect RG flows. In particular, we show that the surface defect attached to the topological duality operator in Maxwell theory admits a universal chiral DCFT.

Away from the fixed points, the parameters governing the defect dynamics generally evolve under scale transformations. In this section, we study the defect RG flow itself, with particular emphasis on the monotonicity theorem and defect phase diagrams. For concreteness, we discuss surface defects embedded in a free scalar field theory and in the $O(N)$ Wilson–Fisher theory [4, 75, 76]. These models are closely related to boundary and defect criticalities in the 3-dimensional Ising model and Heisenberg model. See, e.g., [40, 52, 77–80] for both theoretical and numerical studies of this subject.

2.3.1 Bilinear defect deformation

We begin with a Gaussian defect model, defined by adding a localized mass term to a free scalar field $\phi \in \mathbb{R}$ in d -dimensional Euclidean spacetime \mathbb{R}^d . We consider the bilinear mass deformation ϕ^2 on a 2-dimensional plane $\mathbb{R}^2 \subset \mathbb{R}^d$, such that the action reads

$$S_{\text{free}} = \frac{1}{2} \int_{\mathbb{R}^d} d^d x (\partial_\mu \phi)^2 + \frac{\gamma_b}{2} \int_{\mathbb{R}^2} d^2 x' \phi^2, \quad (2.64)$$

where γ_b is the bare defect coupling constant. The free theory Hamiltonian is unbounded from below when $\gamma_b < 0$ ⁹, and we therefore restrict to unitary defects with $\gamma_b \geq 0$. A simple power-counting also shows that the defect deformation is irrelevant when $d > 4$, classically marginal when $d = 4$, and relevant when $d < 4$. In this and the following subsections, we will also denote $d = 4 - \epsilon$ with $\epsilon \geq 0$.

The defect RG flow of the model (2.64) is exactly solvable. Following the Wilsonian analysis [21, 22, 83], we introduce a UV momentum cutoff Λ to the model (2.64). In terms of Fourier modes, the scalar field ϕ can be written as

$$\phi(x) = \int_{k^2 \leq \Lambda^2} \frac{d^d k}{(2\pi)^d} e^{ikx} \phi_k. \quad (2.65)$$

Correspondingly, the Gaussian action (2.64) takes the form

$$S_{\text{free}}(\Lambda) = \frac{1}{2} \int_{k_1^2 \leq \Lambda^2} \frac{d^d k_1}{(2\pi)^d} \int_{k_2^2 \leq \Lambda^2} \frac{d^d k_2}{(2\pi)^d} (k_1^2 \delta^{d-2}(k_1^\perp + k_2^\perp) + \gamma_b) \delta^2(k_1'' + k_2'') \phi_{k_1} \phi_{k_2}. \quad (2.66)$$

We consider the coarse-graining procedure by lowering the cutoff from Λ to $\tilde{\Lambda}$ and integrating the Fourier modes between Λ and $\tilde{\Lambda}$. Clearly, the UV modes with $\tilde{\Lambda} \leq |k| \leq \Lambda$ couple the IR modes with $|k| \leq \tilde{\Lambda}$ due to the explicit breaking of translation symmetry along the x_σ^\perp -directions. This coarse-graining procedure gives the following correction term:

$$S_{\text{free}}(\tilde{\Lambda}) + \delta S_{\text{free}}(\tilde{\Lambda}, \Lambda) = -\ln \left(\int (d\phi_k) |_{\tilde{\Lambda} \leq |k| \leq \Lambda} e^{-S_{\text{free}}(\Lambda)} \right). \quad (2.67)$$

A straightforward linear algebra computation yields

$$\delta S_{\text{free}}(\tilde{\Lambda}, \Lambda) = -\frac{\gamma_b}{2} \int_{k_1^2 \leq \tilde{\Lambda}^2} \frac{d^d k_1}{(2\pi)^d} \int_{k_2^2 \leq \tilde{\Lambda}^2} \frac{d^d k_2}{(2\pi)^d} \frac{\gamma_b W(k_1''; \tilde{\Lambda}, \Lambda)}{1 + \gamma_b W(k_1''; \tilde{\Lambda}, \Lambda)} \delta^2(k_1'' + k_2'') \phi_{k_1} \phi_{k_2}, \quad (2.68)$$

⁹The defect RG flows associated with $\gamma_b < 0$ are conjectured to exhibit runaway behavior [4, 11, 81, 82].

where we have introduced the shorthand

$$\begin{aligned}
W(k''; \tilde{\Lambda}, \Lambda) &\equiv \int_{\tilde{\Lambda}^2 - (k'')^2 \leq (k^\perp)^2 \leq \Lambda^2 - (k'')^2} \frac{d^{2-\epsilon} k^\perp}{(2\pi)^{2-\epsilon}} \frac{1}{(k'')^2 + (k^\perp)^2} \\
&= \frac{(4\pi)^{\frac{\epsilon}{2}}}{\pi \epsilon^2 \Gamma(-\frac{\epsilon}{2})} (\Lambda^{-\epsilon} - \tilde{\Lambda}^{-\epsilon}) + O((k'')^2) .
\end{aligned} \tag{2.69}$$

Next, we define the renormalized defect coupling γ and the coordinate τ along the RG flow as follows

$$\gamma \equiv \Lambda^{-\epsilon} \gamma_b , \quad \text{and} \quad \tau \equiv -\ln(\tilde{\Lambda}/\Lambda) \geq 0 . \tag{2.70}$$

Using the Wilsonian term (2.68), we find the exact RG running of the dimensionless defect coupling γ , which reads

$$\frac{1}{\gamma(\tau)} = \frac{(4\pi)^{\frac{\epsilon}{2}}(1 - e^{-\epsilon\tau})}{2\pi\Gamma(1 - \frac{\epsilon}{2})} + \frac{e^{-\epsilon\tau}}{\gamma(0)} . \tag{2.71}$$

Let us first consider two special cases of (2.71):

$$\begin{aligned}
\gamma(\tau) &= \frac{2\pi\gamma(0)}{2\pi + \tau\gamma(0)} , \quad \text{for } d = 4 ; \\
\gamma(\tau) &= e^{2\tau}\gamma(0) , \quad \text{for } d = 2 .
\end{aligned} \tag{2.72}$$

In both cases, the defect RG flow admits only the trivial fixed point at $\gamma = 0$. When $d = 4$, one-loop effects render the bilinear defect deformation in (2.64) marginally irrelevant. The surface defect fills the entire spacetime when $d = 2$, in which case (2.71) simply describes the trivial scaling of the free field mass term.

When $2 < d < 4$, the defect RG flow (2.71) admits a non-trivial IR-stable fixed point at

$$\gamma_{\text{fixed}} = \frac{2\pi\epsilon}{(4\pi)^{\frac{\epsilon}{2}}}\Gamma(1 - \frac{\epsilon}{2}) . \tag{2.73}$$

In particular, we find that $\gamma_{\text{fixed}} = \pi$ when $d = 3$. To see the physical meaning of this fixed point, we examine the propagator derived from (2.66):

$$\langle \phi_{k_1} \phi_{k_2} \rangle|_{\gamma_b = \pi\Lambda} = \frac{1}{(k_1)^2} \left[\delta(k_1^\perp + k_2^\perp) - \frac{2|k_2''|}{(k_2)''^2} + O(\Lambda^{-3}) \right] \delta^2(k_1'' + k_2'') , \tag{2.74}$$

where the subleading terms are suppressed by the cutoff Λ and are scheme-dependent. It is

useful to evaluate the layer susceptibility [84, 85], given by

$$\begin{aligned} \chi(x_1^\perp, x_2^\perp) &\equiv \lim_{|k'^\perp| \rightarrow 0} \int \frac{dk_1^\perp}{2\pi} \int \frac{dk_2^\perp}{2\pi} \frac{e^{i(k_1^\perp x_1^\perp + k_2^\perp x_2^\perp)}}{(k'^\perp)^2 + (k_1^\perp)^2} \left[\delta(k_1^\perp + k_2^\perp) - \frac{2|k'^\perp|}{(k'^\perp)^2 + (k_2^\perp)^2} \right] \\ &= \frac{1}{2} (|x_1^\perp| + |x_2^\perp| - |x_1^\perp - x_2^\perp|). \end{aligned} \quad (2.75)$$

The susceptibility vanishes when x_1^\perp and x_2^\perp are on different sides of the defect plane, so that the defect effectively splits \mathbb{R}^3 into two decoupled half-spaces in the IR. We conclude that, when $d = 3$, the fixed point (2.73) corresponds to two Dirichlet boundaries of the free field. Another perspective follows from the defect central charge, as we discuss in Section 2.3.2.

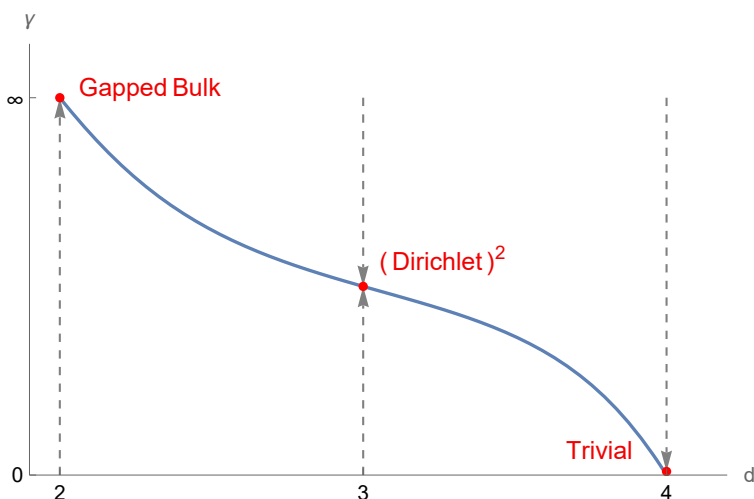


Figure 2.4: IR-stable fixed points associated with bilinear defect deformations in the free theory. The blue curve shows how the fixed point depends on the spacetime dimension d , while the grey dashed arrow indicates the defect RG flow from the UV to the IR. Fixed points with physical interpretations in integer dimensions are marked in red.

The fixed point (2.73) interpolates between the trivial defect at $d = 4$, the Dirichlet boundaries at $d = 3$, and the gapped bulk theory at $d = 2$. See Figure 2.4. The DCFT at this fixed point is governed by the conformal algebra $\mathfrak{so}(3, 1) \times \mathfrak{so}(d - 2)$. As a technical side note, the spin- s representation of $\mathfrak{so}(q)$ is of dimension

$$\deg(q, s) \equiv (2s + q - 2) \frac{\Gamma(s + q - 3)}{\Gamma(s + 1)\Gamma(q - 1)}, \quad (2.76)$$

which is non-integer for $s > 0$ and generic q . Nevertheless, the spin-0 representation is unambiguous, as $\deg(q, 0) = 1$. We denote by $\hat{\phi}$ the defect primary with $s = 0$ and $\ell = 0$ that appears in the bulk-to-defect OPE of the scalar field ϕ . At the trivial fixed point

$\gamma = 0$, the defect operator $\hat{\phi}$ coincides with the bulk operator ϕ . Once the bilinear defect deformation is turned on, $\hat{\phi}$ deviates from ϕ and becomes distinct. It follows from the RG equation (2.71) that the $\hat{\phi}$ operator at the fixed point $\gamma = \gamma_{\text{fixed}}$ has scaling dimension

$$\Delta(\hat{\phi}) = 3 - \frac{d}{2}, \quad (2.77)$$

while the bulk free scalar field has $\Delta(\phi) = \frac{d}{2} - 1$.

The same conclusion can also be reached by studying a free scalar field conformally coupled to the curved spacetime $\text{AdS}_3 \times S^{d-3}$, whose isometry is precisely $\mathfrak{so}(3, 1) \times \mathfrak{so}(d-2)$. We focus on the Kaluza-Klein mode that is independent of the coordinates on S^{d-3} , which transforms in the spin-0 representation of $\mathfrak{so}(d-2)$. In this setup, the two defect RG fixed points $\gamma = 0$ and $\gamma = \gamma_{\text{fixed}}$ correspond to the different conformal boundary conditions of the scalar field on AdS_3 , namely the alternative and standard quantizations [70, 86, 87].

2.3.2 Monotonicity and the defect central charge

The monotonicity of the surface defect RG flow is associated with the defect central charge, also known as the b -coefficient [10, 12]. To facilitate the definition, we consider a spherical surface defect supported on $S^2 \subset \mathbb{R}^d$ with radius R . At RG fixed points, the defect contribution to the free energy is given by

$$\mathcal{F} \equiv -\ln \frac{Z_{\text{DCFT}}}{Z_{\text{CFT}}}, \quad (2.78)$$

where Z_{CFT} is the partition function of the ambient CFT on \mathbb{R}^d , and Z_{DCFT} is the corresponding partition function in the presence of the spherical defect.

Next, we consider the large-size limit of the spherical defect. By locality, the leading terms of the free energy \mathcal{F} in this limit take the form

$$\mathcal{F} = a^{(-2)}(\Lambda'R)^2 + a^{(0)} + \frac{b}{3} \log(\Lambda'R) + O((\Lambda'R)^{-2}), \quad (2.79)$$

where Λ' is the UV cutoff scale. The scale Λ' is clearly scheme-dependent, and so are the coefficients $a^{(-2)}$ and $a^{(0)}$ appearing in the expansion (2.79). By contrast, the coefficient b extracted from the logarithmic divergence of (2.79) is scheme-independent and corresponds to the defect Weyl anomaly.

The monotonicity theorem [10, 12] for surface defects states that if a UV DCFT and an IR DCFT are connected by a defect RG flow, then their defect central charges satisfy

$$b_{\text{UV}} \geq b_{\text{IR}}. \quad (2.80)$$

Conversely, if $b_{\text{UV}} < b_{\text{IR}}$, then the UV DCFT cannot admit a deformation that takes it back

to the IR DCFT. This establishes the irreversibility of defect RG flows.

Let us now examine the theorem (2.80) for the defect RG fixed point (2.73). Since the spherical surface defect preserves the rotational symmetry $\mathfrak{so}(3)$, the problem reduces to finding the Laplacian eigenvalues associated with spin- l spherical harmonics. We find

$$\mathcal{F} = \frac{1}{2} \sum_{l \in \mathbb{N}} (2l + 1) \ln \left(1 + \frac{\pi \epsilon (\Lambda R)^\epsilon}{2 \sin(\pi \epsilon / 2)} \frac{\Gamma(l - \frac{\epsilon}{2} + 1)}{\Gamma(l + \frac{\epsilon}{2} + 1)} \right). \quad (2.81)$$

To extract the defect central charge from (2.81), we apply the dimensional regularization to the defect dimension p and then take the limit $R \rightarrow +\infty$. In this limit, (2.81) can be simplified as

$$\mathcal{F} = -\frac{1}{2} \lim_{p \rightarrow 2} \sum_{l \in \mathbb{N}} \text{deg}(p + 1, l) \ln \frac{\Gamma(l + \frac{p}{2} + \frac{\epsilon}{2})}{\Gamma(l + \frac{p}{2} - \frac{\epsilon}{2})}. \quad (2.82)$$

We identify the $1/(p-2)$ -pole term in (2.82) with the logarithmic IR-divergence in the cutoff regularization scheme [88, 89]. For the free scalar field theory in $d = 4 - \epsilon$ dimensions, we obtain

$$b_{\text{IR}} = -\frac{\epsilon^3}{8}. \quad (2.83)$$

For the trivial fixed point $\gamma = 0$, it follows directly from the definition (2.78) that $b_{\text{UV}} = 0$. The first consistency check for (2.83) is $b_{\text{IR}} < b_{\text{UV}} = 0$ when $d < 4$, hence the inequality (2.80) is indeed satisfied. We also observe that

$$b_{\text{IR}}|_{d=3} = 2b_{\text{D}} = -\frac{1}{8}, \quad (2.84)$$

so that the defect central charge agrees with that of two free field Dirichlet boundaries [10]. Finally, when $d=2$, one can no longer perform a Weyl transformation on the defect independently, since the defect is then indistinguishable from the ambient theory. It is well known that a two-dimensional free scalar has central charge $c = 1$. Therefore, the physical Weyl anomaly coefficient is $b_{\text{IR}} + c = 0$. This is consistent with (2.71) and the phase diagram in Figure 2.4, according to which the theory flows to a trivially gapped phase.

2.3.3 Phases of defects in interacting theories

In this section, we study bilinear defect deformations in the $O(N)$ model at the Wilson–Fisher fixed point [83]. This bulk theory consists of N scalar fields ϕ_i , with $1 \leq i \leq N$, interacting through quartic couplings in Euclidean spacetime \mathbb{R}^d . We denote the dimensionless, fully symmetric coupling tensor by $\lambda_{i_1 i_2 i_3 i_4}$, so that the bulk action takes the form

$$S_{\text{WF}} = \int_{\mathbb{R}^d} d^d x \left(\frac{1}{2} (\partial \phi^i)^2 + \frac{\Lambda^{4-d}}{4!} \lambda_{i_1 i_2 i_3 i_4} \phi^{i_1} \phi^{i_2} \phi^{i_3} \phi^{i_4} \right), \quad (2.85)$$

where Λ is the UV cutoff scale. This theory admits perturbative interacting fixed points when $\epsilon = 4 - d \ll 1$. At the one-loop level, the $O(N)$ symmetric fixed point is given by

$$(\lambda_{\text{fixed}})_{i_1 i_2 i_3 i_4} = \frac{16\pi^2 \epsilon}{N + 8} (\delta_{i_1 i_2} \delta_{i_3 i_4} + \delta_{i_1 i_3} \delta_{i_2 i_4} + \delta_{i_1 i_4} \delta_{i_2 i_3}) + O(\epsilon^2) , \quad (2.86)$$

which we adopt in the remainder of this section.

There are two types of bilinear operators in this weakly-interacting CFT, distinguished by their transformation properties under $O(N)$. We introduce the singlet operator [90, 91]:

$$O \equiv \frac{1}{2N} (\phi_i)^2 , \quad \Delta(O) = 2 - \frac{6}{N + 8} \epsilon + O(\epsilon^2) , \quad (2.87)$$

and the symmetric traceless operator

$$\Upsilon_{i_1 i_2} \equiv \phi_{i_1} \phi_{i_2} - \frac{\delta_{i_1 i_2}}{N} (\phi_i)^2 , \quad \Delta(\Upsilon) = 2 - \frac{N + 6}{N + 8} \epsilon + O(\epsilon^2) . \quad (2.88)$$

Both operators are even under the $\mathbb{Z}_2 \subset O(N)$: $\phi_i \rightarrow -\phi_i$. In analogy with the defect model (2.64), we consider the bilinear deformations localized on a 2-dimensional plane:

$$S_{\text{dWF}} = S_{\text{WF}} + \int_{\mathbb{R}^2} d^2 x'' (\Lambda^{2-\Delta(O)} \gamma^O O + \Lambda^{2-\Delta(\Upsilon)} \gamma_{i_1 i_2}^{\Upsilon} \Upsilon^{i_1 i_2}) , \quad (2.89)$$

where γ^O and γ^{Υ} denotes the dimensionless defect coupling constants. The defect RG flow of the model (2.89) can be analyzed perturbatively in $\epsilon = 4 - d \ll 1$, assuming that both γ^O and γ^{Υ} are of order $O(\epsilon)$.

In what follows, we compute the beta functions for γ^O and γ^{Υ} and determine the associated defect RG fixed points at one-loop order. Using the conformal perturbation theory [92], we find the bulk one-point function of the singlet operator as follows

$$\begin{aligned} \langle O(x^\perp, 0) \rangle &= -\Lambda^{\frac{6\epsilon}{N+8}} \gamma^O \int d^2 x'' \langle O(x^\perp, 0) O(0, x'') \rangle \\ &\quad + \frac{1}{2} \Lambda^{2\frac{N+6}{N+8}\epsilon} \gamma_{i_1 i_2}^{\Upsilon} \gamma_{i_3 i_4}^{\Upsilon} \int d^2 z_1 d^2 z_2 \langle O(x^\perp, 0) \Upsilon^{i_1 i_2}(0, x'_1) \Upsilon^{i_3 i_4}(0, x'_2) \rangle \\ &\quad + \frac{1}{2} \Lambda^{\frac{12\epsilon}{N+8}} (\gamma^O)^2 \int d^2 x''_1 d^2 x''_2 \langle O(x^\perp, 0) O(0, x''_1) O(0, x''_2) \rangle + O(\epsilon^3) \quad (2.90) \\ &= -\frac{|x^\perp|^{-\Delta(O)}}{32\pi^3 N} \left(\gamma^O - \frac{N + 8}{12\pi N \epsilon} (\gamma^O)^2 - \frac{(N + 8)}{\pi(N + 3)\epsilon} \text{Tr}((\gamma^{\Upsilon})^2) + O(\epsilon^2) \right) . \end{aligned}$$

It then follows from the minimal subtraction scheme that the beta function for γ^O reads

$$-\beta(\gamma^O) = \frac{6\epsilon}{N+8}\gamma^O - \frac{1}{2\pi N}(\gamma^O)^2 - \frac{2}{\pi}\text{Tr}((\gamma^\Upsilon)^2) + O(\epsilon^3) . \quad (2.91)$$

Similarly, we consider the bulk one-point function of the symmetric traceless operator

$$\begin{aligned} \langle \Upsilon_{i_1 i_2}(x^\perp, 0) \rangle &= -\Lambda^{\frac{N+6}{N+8}\epsilon} \gamma_{i_3 i_4}^\Upsilon \int d^2 z \langle \Upsilon_{i_1 i_2}(x^\perp, 0) \Upsilon^{i_3 i_4}(0, x'') \rangle \\ &\quad + \frac{1}{2} \Lambda^{2\frac{N+6}{N+8}\epsilon} \gamma_{i_3 i_4}^\Upsilon \gamma_{i_5 i_6}^\Upsilon \int d^2 x_1'' d^2 x_2'' \langle \Upsilon_{i_1 i_2}(x^\perp, 0) \Upsilon^{i_3 i_4}(0, x_1'') \Upsilon^{i_5 i_6}(0, x_2'') \rangle \\ &\quad + \Lambda^{\frac{N+12}{N+8}\epsilon} \gamma^O \gamma_{i_3 i_4}^\Upsilon \int d^2 x_1'' d^2 x_2'' \langle \Upsilon_{i_1 i_2}(x^\perp, 0) O(0, x_1'') \Upsilon^{i_3 i_4}(0, x_2'') \rangle + O(\epsilon^3) \\ &= -\frac{|x^\perp|^{-\Delta(\Upsilon)}}{8\pi^3} \left(\gamma_{i_1 i_2}^\Upsilon - \frac{N+8}{6\pi N \epsilon} \gamma_{i_1 i_2}^\Upsilon \gamma^O - \frac{N+8}{\pi(N+6)\epsilon} ((\gamma^\Upsilon)^2)_{i_1 i_2} \right. \\ &\quad \left. + \frac{N+8}{\pi N(N+6)\epsilon} \delta_{i_1 i_2} \text{Tr}((\gamma^\Upsilon)^2) \right) . \end{aligned} \quad (2.92)$$

With the minimal subtraction scheme, we find

$$-\beta(\gamma_{i_1 i_2}^\Upsilon) = \frac{N+6}{N+8} \epsilon \gamma_{i_1 i_2}^\Upsilon - \frac{1}{\pi N} \gamma_{i_1 i_2}^\Upsilon \gamma^O - \frac{1}{\pi} ((\gamma^\Upsilon)^2)_{i_1 i_2} + \frac{\delta_{i_1 i_2}}{\pi N} \text{Tr}((\gamma^\Upsilon)^2) + O(\epsilon^3) . \quad (2.93)$$

The beta functions (2.91) and (2.93) govern the defect RG flows near the trivial fixed point $\gamma^O = \gamma_{i_1 i_2}^\Upsilon = 0$. For every N , there is also a nontrivial $O(N)$ -symmetric fixed point:

$$(\gamma^O)_{\text{fixed}} \equiv \frac{12\pi N}{N+8} \epsilon + O(\epsilon^2) ; \quad (\gamma_{i_1 i_2}^\Upsilon)_{\text{fixed}} = 0 . \quad (2.94)$$

At this fixed point, the lowest-lying defect primaries with $s = 0$ and $\ell = 0$ include the $O(N)$ vector $\hat{\phi}_i$, the singlet \hat{O} , and the symmetric traceless tensor $\hat{\Upsilon}_{i_1 i_2}$. Their scaling dimensions are given by [4]:

$$\begin{aligned} \Delta(\hat{\phi}) &= 1 - \frac{N-4}{2N+16} \epsilon + O(\epsilon^2) , \\ \Delta(\hat{O}) &= 2 + \frac{6}{N+8} \epsilon + O(\epsilon^2) , \\ \Delta(\hat{\Upsilon}) &= 2 - \frac{N-6}{N+8} \epsilon + O(\epsilon^2) . \end{aligned} \quad (2.95)$$

The defect RG fixed point (2.94) is clearly stable against the $O(N)$ symmetric deformations. By contrast, the deformations triggered by the $\hat{\Upsilon}_{i_1 i_2}$ operators break $O(N)$ down to subgroups containing the \mathbb{Z}_2 symmetry. These deformations are relevant for $N > 6$ and irrelevant for

$N < 6$. When $N = 6$, the relevance of these deformations depends on the subgroup they preserve, as we explain below.

We consider the bilinear defect deformations that preserve the $O(M) \times O(N - M)$ subgroup of the $O(N)$ symmetry. In particular, we take $\gamma_{i_1 i_2}^{\Upsilon} \Upsilon^{i_1 i_2} = \gamma_M^{\Upsilon} \Upsilon_M$, where the projection onto the symmetric traceless tensor, up to field redefinitions, is given by

$$\Upsilon_M \equiv -\frac{1}{M} \sum_{1 \leq i \leq M} (\phi_i)^2 + \frac{1}{N - M} \sum_{M < i \leq N} (\phi_i)^2 . \quad (2.96)$$

Since Υ_M and Υ_{N-M} preserve the same subgroup symmetry, the analyses for $\gamma_M^{\Upsilon} \geq 0$ proceed in the same way as that of $\gamma_{N-M}^{\Upsilon} \leq 0$. To avoid overcounting of equivalent cases, we adopt the convention $\gamma_M^{\Upsilon} \geq 0$.

The beta function for the defect coupling constant γ_M^{Υ} follows directly from (2.93):

$$-\beta(\gamma_M^{\Upsilon}) = \frac{N + 6}{N + 8} \epsilon \gamma_M^{\Upsilon} - \frac{1}{\pi N} \gamma_M^{\Upsilon} \gamma^O - \frac{2M - N}{\pi M(N - M)} (\gamma_M^{\Upsilon})^2 + O(\epsilon^3) . \quad (2.97)$$

Using (2.91) and (2.97), we identify new defect RG fixed points that preserve the $O(M) \times O(N - M)$ subgroup. We find that when the $\hat{\Upsilon}_M$ operators are irrelevant at (2.94), they connect the $O(N)$ -symmetric stable fixed point to metastable fixed points. When $N < 6$, each choice of $1 \leq M \leq N - 1$ admits a single perturbative fixed point with $(\gamma_M^{\Upsilon})_{\text{fixed}} > 0$. When $N = 6$, we find the beta function at the $O(N)$ -symmetric fixed point (2.94) as follows

$$-\beta(\gamma_M^{\Upsilon}) \Big|_{\gamma^O = (\gamma^O)_{\text{fixed}}, N=6} = \frac{2(M - 3)}{\pi M(M - 6)} (\gamma_M^{\Upsilon})^2 + O(\epsilon^3) . \quad (2.98)$$

We conclude that, for $N = 6$, the defect bilinear operators $\hat{\Upsilon}_{M=1,2}$ are marginally relevant, whereas $\hat{\Upsilon}_{M=4,5}$ are marginally irrelevant, and $\hat{\Upsilon}_{M=3}$ remains marginal at the one-loop level. See Table 2.1 for the fixed point solutions and the left panel in Figure 2.5 for schematic defect RG flows.

When $N > 6$, most values of N and M admit no perturbative fixed point other than the trivial fixed point and the $O(N)$ -symmetric fixed point (2.94). See also the right panel of Figure 2.5. The exceptions arise for $M = N - 1$ and $7 \leq N \leq 9$, in which case the beta function admits two $O(N - 1) \times \mathbb{Z}_2$ -symmetric fixed points. For convenience, we denote the metastable one by fixed point 1 and the stable one by fixed point 2. When $N = 10$, fixed point 1 and fixed point 2 collide at the one-loop order, and higher-loop calculations are needed to determine the existence of the $O(N - 1) \times \mathbb{Z}_2$ fixed points. See Table 2.2 for these fixed-point solutions and the middle panel of Figure 2.5 for the corresponding defect RG flows.

	$N = 2$	$N = 3$	$N = 4$	$N = 5$	$N = 6$
$M = 1$	$\left(\frac{\sqrt{2}}{5}, \frac{8}{5}\right)$	$\left(\frac{4\sqrt{7}-2}{33}, \frac{26+2\sqrt{7}}{11}\right)$	$\left(\frac{\sqrt{6}-1}{8}, \frac{9+\sqrt{6}}{3}\right)$	$\left(\frac{8\sqrt{5}-12}{65}, \frac{46+6\sqrt{5}}{13}\right)$	no fixed point
$M = 2$		$\left(\frac{4\sqrt{7}+2}{33}, \frac{26-2\sqrt{7}}{11}\right)$	$\left(\frac{\sqrt{5}}{6}, \frac{10}{3}\right)$	$\left(\frac{12\sqrt{3}-6}{65}, \frac{54+2\sqrt{3}}{13}\right)$	no fixed point
$M = 3$			$\left(\frac{\sqrt{6}+1}{8}, \frac{9-\sqrt{6}}{3}\right)$	$\left(\frac{12\sqrt{3}+6}{65}, \frac{54-2\sqrt{3}}{13}\right)$	undetermined
$M = 4$				$\left(\frac{8\sqrt{5}+12}{65}, \frac{46-6\sqrt{5}}{13}\right)$	$\left(\frac{8}{21}, \frac{32}{7}\right)$
$M = 5$					$\left(\frac{10}{21}, \frac{20}{7}\right)$

Table 2.1: $O(M) \times O(N - M)$ -symmetric defect RG fixed points for $2 \leq N \leq 6$. This table presents $((\gamma_M^Y)_{\text{fixed}}, (\gamma^O)_{\text{fixed}})$ in units of $\pi\epsilon$, with terms of order $O(\epsilon^2)$ omitted. For $N = 6$ and $M = 3$, the existence of the fixed point needs to be examined at higher loop orders.

	$N = 7$	$N = 8$	$N = 9$	$N = 10$
fixed point 1	$\left(\frac{10+4\sqrt{3}}{35}, \frac{66-10\sqrt{3}}{15}\right)$	$\left(\frac{21+7\sqrt{2}}{64}, \frac{19-3\sqrt{2}}{4}\right)$	$\left(\frac{8}{17}, \frac{72}{17}\right)$	undetermined
fixed point 2	$\left(\frac{10-4\sqrt{3}}{35}, \frac{66+10\sqrt{3}}{15}\right)$	$\left(\frac{21-7\sqrt{2}}{64}, \frac{19+3\sqrt{2}}{4}\right)$	$\left(\frac{40}{153}, \frac{100}{17}\right)$	undetermined

Table 2.2: $O(N - 1) \times \mathbb{Z}_2$ -symmetric defect RG fixed points for $7 \leq N \leq 10$. This table presents $((\gamma_M^Y)_{\text{fixed}}, (\gamma^O)_{\text{fixed}})$ in units of $\pi\epsilon$, with terms of order $O(\epsilon^2)$ omitted. For $N = 10$ and $M = 9$, the two defect RG fixed points collide at the one-loop level, and higher loop corrections are needed to distinguish them.

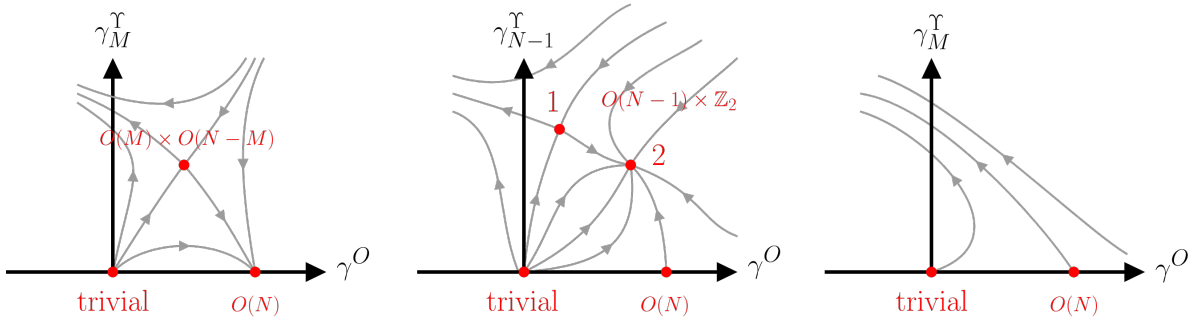


Figure 2.5: Perturbative phase diagram for $O(M) \times O(N - M)$ surface defects in the Wilson–Fisher CFT. Left: cases listed in table 2.1. Middle: cases listed in table 2.2. Right: cases of no fixed point other than the trivial one and the $O(N)$ -symmetric one.

2.3.4 IR effective theory of defects

In addition to the perturbative fixed points, the beta functions (2.91) and (2.97) also admit regimes in which both γ^O and γ_M^Υ flow to large values. See also Figure 2.5. What is the IR theory governing the field dynamics near the surface defect in these regimes? In this section, we follow the approach in [4, 52, 93] and analyze the effective theory of such defects.

Classically, the defect tends to acquire localized degrees of freedom for large negative γ^O and large positive γ_M^Υ ¹⁰. We adopt the assumption that the IR effective action of the defect consists of three parts: a DCFT governing the dynamics of bulk scalar fields near the defect, the action of the effective degrees of freedom localized on the defect, and weak interactions between the DCFT and the effective degrees of freedom. In what follows, we first identify this DCFT and then examine the stability of the proposed effective action in the IR.

We begin by considering a DCFT in which the bulk order parameter ϕ_i develops a vacuum expectation value near the defect, thereby breaking the $O(N)$ symmetry down to the $O(N-1)$ subgroup. This is analogous to the pinning defect in the Wilson–Fisher fixed point [53]. Specifically, we consider the bulk one-point functions:

$$\langle \phi_i(x) \rangle = \frac{\delta_{i1} C_{\phi_1}}{|x^\perp|^{\Delta(\phi)}} , \quad \text{where } \Delta(\phi) = 1 - \frac{\epsilon}{2} + O(\epsilon^2) . \quad (2.99)$$

At leading order, the OPE coefficient C_{ϕ_1} can be determined by a mean-field calculation. Let us consider a classical field profile $\phi_1^{\text{cl}}(x)$ obeying the equation of motion from (2.85) as follows

$$-\partial_\mu^2 \phi_1^{\text{cl}} + \Lambda^\epsilon \left(\frac{8\pi^2 \epsilon}{N+8} + O(\epsilon) \right) (\phi_1^{\text{cl}})^3 = 0 . \quad (2.100)$$

In addition to the trivial solution $\phi_1^{\text{cl}}(x) = 0$, equation (2.100) also admits a solution that is singular near the defect at $x^\perp = 0$:

$$\phi_1^{\text{cl}}(x) = \frac{1}{\Lambda^{\frac{\epsilon}{2}} |x^\perp|} \sqrt{\frac{N+8}{8\pi^2 \epsilon}} (1 + O(\epsilon)) . \quad (2.101)$$

By matching (2.99) with (2.101) to the leading order in ϵ , we obtain

$$C_{\phi_1} = \sqrt{\frac{N+8}{8\pi^2 \epsilon}} + O(\epsilon^{1/2}) . \quad (2.102)$$

The symmetry-breaking DCFT associated with (2.99) contains tilt operators $\hat{\tau}_j$ with $2 \leq j \leq N$. In general, the two-point function between the bulk scalar ϕ_j and the tilt

¹⁰For studies on the subject of spontaneous symmetry breaking on surface defects, see [94].

operator $\hat{\tau}_j$ takes the form

$$\langle \phi_{j_1}(x) \hat{\tau}_{j_2}(\tilde{x}'') \rangle = \delta_{j_1 j_2} \frac{C_{\phi_j}^{\hat{\tau}} C_{\hat{\tau}\hat{\tau}}}{|x^\perp|^{\Delta(\phi)}} \left(\frac{|x^\perp|}{|x^\perp|^2 + |x'' - \tilde{x}''|^2} \right)^2, \quad (2.103)$$

where $C_{\phi_j}^{\hat{\tau}}$ is the OPE coefficient and $C_{\hat{\tau}\hat{\tau}}$ is fixed by (2.20). While computing $C_{\phi_j}^{\hat{\tau}}$ and $C_{\hat{\tau}\hat{\tau}}$ separately is rather involved, we can determine the product $(C_{\phi_j}^{\hat{\tau}})^2 C_{\hat{\tau}\hat{\tau}}$ at leading order in ϵ by mapping the system (2.85) onto $\text{AdS}_3 \times S^{1-\epsilon}$ through a Weyl transformation [4, 70]. The key observation is that the tilt operator is the lowest-lying defect primary appearing on the right-hand side of the OPE of ϕ_j , with scaling dimension $\Delta(\hat{\tau}) = 2$. We consider the two-point function $\langle \phi_{j_1} \phi_{j_2} \rangle$ on $\text{AdS}_3 \times S^{1-\epsilon}$, with the leading order result in ϵ dominated by the free field propagator. See appendix in [5] for a compact review of these propagators. Notably, the product $(C_{\phi_j}^{\hat{\tau}})^2 C_{\hat{\tau}\hat{\tau}}$ can be extracted by taking the two points close to the AdS_3 boundary, and it is given by

$$(C_{\phi_j}^{\hat{\tau}})^2 C_{\hat{\tau}\hat{\tau}} = \frac{1}{2\pi} + O(\epsilon). \quad (2.104)$$

Next, we turn to the effective degrees of freedom localized on the defect and their couplings to the DCFT. We consider a Non-Linear Sigma Model (NL Σ M) whose target space is the M -dimensional unit sphere S^M . The kinetic action of this model is given by

$$S_{\text{NL}\Sigma\text{M}} = \frac{1}{2g_\Sigma} \sum_{i=1}^M \int_{\mathbb{R}^2} d^2 x'' (\partial_\sigma \Omega_i)^2, \quad (2.105)$$

where $\sum_{i=1}^M (\Omega_i)^2 = 1$ and $g_\Sigma > 0$ is the coupling constant. It is convenient to parametrize S^M by Ω_j , with $2 \leq j \leq M$, so that

$$\Omega_1 = \left(1 - \sum_{j=2}^M (\Omega_j)^2 \right)^{\frac{1}{2}}. \quad (2.106)$$

The interactions between these Ω_j fields are governed by the NL Σ M coupling constant g_Σ . As implied by Coleman's theorem [95], for a standalone two-dimensional NL Σ M (2.105), the coupling g_Σ flows to large values at long distances, and the Ω_j fields become unstable. Nevertheless, we will take $g_\Sigma \ll 1$ and show that the coupling between the NL Σ M and the DCFT indeed stabilizes the Ω_j fields.

As in [52], we take the complete IR effective action for the surface defect in the regime of large negative γ^O and large positive γ_M^T to be

$$S_{\text{IR}} = S_{\text{DCFT}} + S_{\text{NL}\Sigma\text{M}} - \frac{\gamma_\Sigma}{\sqrt{C_{\hat{\tau}\hat{\tau}}}} \sum_{j=2}^M \int_{\mathbb{R}^2} d^2 x'' \Omega_j \hat{\tau}_j, \quad (2.107)$$

where γ_Σ couples the Ω_j fields with the tilt operators in the DCFT. The coupling constant γ_Σ is uniquely fixed by requiring that the effective action (2.107) preserves the symmetry $O(M) \times O(N - M)$. To see that, we consider an infinitesimal rotation in the NL Σ M target space, generated by $\Omega_2 \rightarrow \Omega_2 + \delta\Omega_2$. In the limit $g_\Sigma \ll 1$, we find that the ϕ_2 scalar field acquires a vacuum expectation value under this rotation:

$$\delta\langle\phi_2(x)\rangle = \frac{\delta\Omega_2\gamma_\Sigma}{\sqrt{C_{\hat{\tau}\hat{\tau}}}} \int d^2\tilde{x}'' \langle\phi_2(x)\hat{\tau}_2(\tilde{x}'')\rangle = \delta\Omega_2\pi\gamma_\Sigma C_{\phi_j}^{\hat{\tau}} \sqrt{C_{\hat{\tau}\hat{\tau}}} |x^\perp|^{-\Delta(\phi)}. \quad (2.108)$$

For the $O(M)$ subgroup not explicitly broken, we require that the result be reproduced by rotating the vacuum expectation value of the ϕ_1 by the same angle:

$$\delta\langle\phi_2(x)\rangle = \delta\Omega_2\langle\phi_1(x)\rangle = \delta\Omega_2 C_{\phi_1} |x^\perp|^{-\Delta(\phi)}. \quad (2.109)$$

From (2.108) and (2.109), we find

$$\gamma_\Sigma = \frac{C_{\phi_1}}{\pi C_{\phi_j}^{\hat{\tau}} \sqrt{C_{\hat{\tau}\hat{\tau}}}} = \sqrt{\frac{N+8}{4\pi^3\epsilon}} + O(\epsilon^{1/2}). \quad (2.110)$$

Crucially, the coupling constant γ_Σ does not run under the defect RG and is parametrically large when $\epsilon \ll 1$.

At the one-loop level, we obtain the beta function for the defect RG flow of the NL Σ M coupling constant g_Σ as follows [4]

$$\begin{aligned} -\beta(g_\Sigma) &= (M-2 - (\pi\gamma_\Sigma)^2) \frac{(g_\Sigma)^2}{2\pi} + O((g_\Sigma)^3) \\ &= -\frac{N+8}{8\pi^2\epsilon} (g_\Sigma)^2 + O((g_\Sigma)^3, \epsilon^0). \end{aligned} \quad (2.111)$$

When $\epsilon \ll 1$, interactions from the DCFT drive g_Σ to small values at long distances, thereby stabilizing the Ω_j fields. We have thus established the self-consistency of the IR effective action (2.107). This completes the phase diagrams shown in Figure 2.5.

2.4 Matching UV and IR defects

So far, we have discussed defect RG flows within the framework of continuum quantum field theory. In many cases, however, the UV description of a physical system is given by a discrete lattice model. The RG flow connecting a UV lattice model to an IR field theory is often subtle. For example, one needs to carefully distinguish accidental symmetries and emanant global symmetries [96–98].

In this section, we match the crystalline impurities in UV lattice models with defects in

IR field theories [5]. Our analysis is motivated by two considerations. First, these crystalline impurities flow to DCFTs that, on their own, exhibit intriguing physical properties. Second, such defects serve as probes of exotic topological invariants that constrain the RG flow from the UV to the IR, as we elaborate below.

2.4.1 UV and IR symmetries

We first discuss how UV symmetries are matched to IR symmetries. We denote the spatial and internal symmetry groups of the UV lattice model by G_{UV} , and those of the IR field theory by G_{IR} . In general, there exists a group homomorphism

$$\rho : G_{\text{UV}} \rightarrow G_{\text{IR}} . \quad (2.112)$$

Let us comment on a few basic properties of the homomorphism ρ . When ρ has a non-trivial kernel, some UV internal symmetries become trivial in the IR. This can happen when massive degrees of freedom decouple from the spectrum, whose associated symmetries become invisible to the field theory at long distances. When ρ has a non-trivial cokernel, the IR field theory is endowed with accidental symmetries, whose corresponding symmetry-breaking operators are irrelevant and therefore suppressed at low energies.

In particular, emanant symmetries arise when elements $g_{\text{UV}} \in G_{\text{UV}}$ and their images $\rho(g_{\text{UV}}) \in G_{\text{IR}}$ generate distinct symmetry groups [97]. The symmetry generated by $\rho(g_{\text{UV}})$ is said to emanate from the group generated by g_{UV} ; such symmetries are exact in the IR field theory, even though they may not be a subgroup of the G_{UV} . Such examples are common when g_{UV} generates a lattice translation.

In this section, we primarily focus on cases where the UV free-fermion lattice models are defined in $(2+1)$ -dimensional spacetime, and the IR field theory consists of N free massless Dirac fermions¹¹. The symmetry group G_{UV} that acts faithfully on fermionic lattice operators takes the form

$$G_{\text{UV}} = U(1)^f \times (\mathbb{Z}^2 \rtimes \mathbb{Z}_M) , \quad (2.113)$$

where \mathbb{Z}^2 is the lattice translation group, and \mathbb{Z}_M is the M -fold lattice rotation group. Here, $U(1)^f$ denotes a central extension of the bosonic particle-number symmetry $U(1)$ by the fermion parity \mathbb{Z}_2^f . We also assume that the particle-number symmetry $U(1)$ in the UV acts as a $U(1)$ symmetry in the IR, where each Dirac fermion field carries charge $+1$. If the UV model is a free-fermion lattice model, this is the only possibility. If the model includes interactions, then each IR Dirac fermion in principle could carry any odd integer charge. For simplicity, we have omitted the lattice reflection group from (2.113). The action of lattice reflection symmetries in the IR field theory involves several subtleties that lie beyond the scope of this section. See, e.g., [99, 100] for further discussion of lattice reflections.

¹¹We apologize for repeatedly using M and N to denote integers with different physical meanings across sections.

The IR CFT of N massless Dirac fermions in $(2 + 1)$ -dimensional spacetime is endowed with the symmetry

$$G_{\text{IR}} = (U(N)^{\text{f}} \times Spin(3, 2)) / \mathbb{Z}_2 , \quad (2.114)$$

where $U(N)^{\text{f}}$ denotes the $U(N)$ flavor symmetry group, with the -1 element corresponding to the fermion parity. Note that the IR theory also may contain charge conjugation, reflection, and time-reversal symmetries, which we ignore in this discussion.

We denote the Dirac fermion fields by $\Phi_i(t, \vec{x})$, where $1 \leq i \leq N$ labels the fermion species, t denotes time, and \vec{x} is the 2-dimensional spatial coordinate. For a given lattice model, the fermion fields describe the excitations near the Dirac cones located at momenta \vec{k}_i in the Brillouin zone. We thus expect a UV translation $P_{\delta\vec{x}}$ by the lattice vector $\delta\vec{x}$ to act on the IR fields as follows

$$\rho(P_{\delta\vec{x}}) : \Psi_i(t, \vec{x}) \rightarrow e^{i\vec{k}_i \cdot \vec{v}} \Psi_i(t, \vec{x} + \delta\vec{x}) . \quad (2.115)$$

The dislocation defect is defined by a locus in 2-dimensional space such that, upon encircling it, the fermion fields transform according to (2.115). The vector $\delta\vec{x}$ is of order the lattice spacing and is negligible in the continuum limit, whereas the phase $\vec{k}_i \cdot \delta\vec{x}$ remains finite and determines the long-distance physical properties of the dislocation defect.

The action of UV rotations on the IR fields is more intricate. Let us consider the rotation in the 2-dimensional lattice plane around a high symmetry point $\vec{\sigma}$ by the angle $2\pi/M$. We denote the operator implementing this rotation by $R_{M;\vec{\sigma}}$, with $(R_{M;\vec{\sigma}})^M = 1$ ¹². In general, the $R_{M;\vec{\sigma}}$ operator acts the fermion field as follows

$$\rho(R_{M;\vec{\sigma}}) : \Psi_i(t, \vec{x}) \rightarrow (U_{M;\vec{\sigma}})_{ii'} R_{\text{IR}}(2\pi/M) \Psi_{i'}(t, \vec{x}') , \quad (2.116)$$

where \vec{x}' is obtained from \vec{x} by a $2\pi/M$ rotation around the fixed point $\vec{\sigma}$. Here R_{IR} is the Lorentzian rotation matrix acting on the Dirac spinor indices, and $U_{M;\vec{\sigma}}$ denotes a flavor symmetry transformation. Since the Dirac fermion falls in the spin-1/2 representation of the Lorentz group, we have $(R_{\text{IR}}(2\pi/M))^M = -1$. It then follows from $(R_{M;\vec{\sigma}})^M = 1$ that $(U_{M;\vec{\sigma}})^M = -1$. Since the lattice translation generally does not commute with the lattice rotation, the unitary matrix $U_{M;\vec{\sigma}}$ need not be diagonal in the flavor basis set by (2.115). We denote the eigenvalues of $U_{M;\vec{\sigma}}$ by

$$U_{M;\vec{\sigma}} \sim \text{diag}(e^{\frac{2\pi i}{M} \mathbf{s}_{1;\vec{\sigma}}}, e^{\frac{2\pi i}{M} \mathbf{s}_{2;\vec{\sigma}}}, \dots, e^{\frac{2\pi i}{M} \mathbf{s}_{N;\vec{\sigma}}}) . \quad (2.117)$$

where the quantum numbers $\mathbf{s}_{i;\vec{\sigma}}$ are defined modulo M . For a UV lattice rotation symmetry

¹²For fermionic lattice models, we can also consider a possible lattice rotation operators that act as $(R_{M;\vec{\sigma}})^M = -1$ on states with odd fermion parity.

operator satisfying $(R_{M;\vec{\sigma}})^M = 1$, we find the selection rule

$$\mathbf{s}_{i;\vec{\sigma}} \in \mathbb{Z} + \frac{1}{2}. \quad (2.118)$$

Such $U_{M;\vec{\sigma}}$ matrices exist only when the IR global symmetry group contains an exact \mathbb{Z}_{2M}^f subgroup. Conversely, the IR field theories without such a \mathbb{Z}_{2M}^f symmetry are incompatible with a lattice rotation operator satisfying $(R_{M;\vec{\sigma}})^M = 1$.

Similar to the dislocation, the disclination defect is defined by a locus in the 2-dimensional space, around which the fermion fields transform according to (2.116). Clearly, both the rotation angle and the phase $2\pi\mathbf{s}_{i;\vec{\sigma}}/M$ remain finite in the continuum limit, and together they determine the long-distance response of the IR fields to the disclination defect.

2.4.2 Free-fermion lattice model example

For concreteness, we now turn to the Qi–Wu–Zhang model [101] as an example of free-fermion lattice models. This model describes fermions hopping on a 2-dimensional square lattice with sites labeled by $(n_1, n_2) \in \mathbb{Z}^2$. We denote the fermion creation operator at the site (n_1, n_2) by

$$c_{(n_1, n_2)}^\dagger = (c_{(n_1, n_2), \uparrow}^\dagger, c_{(n_1, n_2), \downarrow}^\dagger). \quad (2.119)$$

The Hamiltonian of the Qi–Wu–Zhang model is controlled by the on-site potential m and takes the form

$$H = m \sum_{(n_1, n_2) \in \mathbb{Z}^2} c_{(n_1, n_2)}^\dagger \sigma_z c_{(n_1, n_2)} + \frac{1}{2} \sum_{(n_1, n_2) \in \mathbb{Z}^2} \left(c_{(n_1+1, n_2)}^\dagger (\sigma_z + i\sigma_x) c_{(n_1, n_2)} + c_{(n_1, n_2+1)}^\dagger (\sigma_z + i\sigma_y) c_{(n_1, n_2)} + \text{h.c.} \right), \quad (2.120)$$

where σ_x , σ_y , and σ_z are the Pauli matrices. This Hamiltonian can be readily diagonalized by the Fourier transformation. Let $\vec{k} = (\mathbf{k}_1, \mathbf{k}_2)$ denote a vector in the Brillouin zone, with $-\pi < \mathbf{k}_1, \mathbf{k}_2 \leq \pi$. The corresponding momentum-space Hamiltonian is

$$H(\vec{k}) = (\sin \mathbf{k}_1) \sigma_x + (\sin \mathbf{k}_2) \sigma_y + (m + \cos \mathbf{k}_1 + \cos \mathbf{k}_2) \sigma_z. \quad (2.121)$$

In particular, the Qi–Wu–Zhang model is gapless at $m = 0$ and $m = \pm 1$, with the corresponding IR field theory described by free Dirac fermions.

The lattice translation operator acts on local fermion operators as follows

$$P_{(\delta n_1, \delta n_2)} c_{(n_1, n_2)} P_{(\delta n_1, \delta n_2)}^\dagger = c_{(n_1 + \delta n_1, n_2 + \delta n_2)}. \quad (2.122)$$

For lattice rotations, we need to distinguish between the vertex center $\vec{\sigma}_v = (0, 0)$ and the

plaquette center $\vec{\sigma}_p = (\frac{1}{2}, \frac{1}{2})$. Their actions on the local fermion operators are correspondingly

$$\begin{aligned} R_{4;\vec{\sigma}_v} c_{(n_1, n_2)} R_{4;\vec{\sigma}_v}^\dagger &= (i c_{(-n_2, n_1), \uparrow}, c_{(-n_2, n_1), \downarrow}) ; \\ R_{4;\vec{\sigma}_p} c_{(n_1, n_2)} R_{4;\vec{\sigma}_p}^\dagger &= (i c_{(1-n_2, n_1), \uparrow}, c_{(1-n_2, n_1), \downarrow}) . \end{aligned} \quad (2.123)$$

The crystalline quantum numbers (2.117) of the Qi–Wu–Zhang model can be determined by diagonalizing (2.123) near the Dirac cones when $m = 0, \pm 1$. For a more detailed treatment, see [5]. We summarize the quantum numbers associated with each Dirac cone in Table 2.3.

	Dirac cone \vec{k}	$\mathbf{s}_{\vec{\sigma}_v}$ (vertex)	$\mathbf{s}_{\vec{\sigma}_p}$ (plaquette)
$m = -1$	$(0, 0)$	$\frac{1}{2}$	$\frac{1}{2}$
$m = 0$, fermion 1	$(\pi, 0)$	$\frac{3}{2}$	$\frac{1}{2}$
$m = 0$, fermion 2	$(0, \pi)$	$\frac{7}{2}$	$\frac{5}{2}$
$m = +1$	(π, π)	$\frac{1}{2}$	$\frac{5}{2}$

Table 2.3: Crystalline quantum numbers of Dirac cones in the Qi–Wu–Zhang model. We note that the band structure contains a single Dirac cone at $m = \pm 1$, whereas it contains two Dirac cones at $m = 0$.

2.4.3 Crystalline impurities and localized emanant fluxes

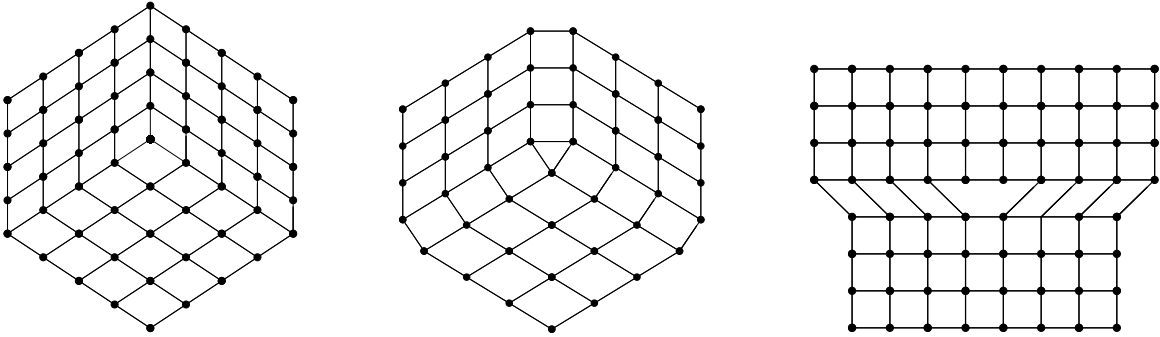


Figure 2.6: Crystalline impurities in the square lattice. Left: vertex-centered disclination with $\beta = 3/4$; Middle: plaquette-centered disclination with $\beta = 3/4$; Right: dislocation with unit Burgers vector.

How can one measure the quantum numbers listed in Table 2.3 at long distances? We

propose that these topological data are encoded in the DCFT one-point functions that are associated with crystalline impurities, including the disclinations and dislocations shown in Figure 2.6.¹³ In this and the following section, we carry out the DCFT analysis and present results from numerical simulations.

Intuitively, disclinations and dislocations can be viewed as localized fluxes of the lattice symmetry group. The operators (2.115) and (2.116) act on the IR fermion fields through a combination of Lorentz and global-symmetry transformations. We therefore assume that the IR description of these crystalline impurities is given by conical defects carrying magnetic fluxes of the flavor symmetry. We refer to such global-symmetry fluxes localized at crystalline impurities as emanant fluxes.

In general, a conical singularity on the two-dimensional lattice plane is characterized by the Riemann curvature

$$R = 4\pi(1 - \beta)\delta^2(x) + (\vec{b} \cdot \partial)\delta^2(x) + O(\partial^2) . \quad (2.124)$$

Here, the first term with $\beta > 0$ represents the angle deficit or excess arising from lattice disclinations. The second term, proportional to the Burgers vector \vec{b} , could arise from lattice dislocations [102].¹⁴ At long distances, the IR fermion fields respond only to the angle deficit or excess. It therefore suffices to consider the effective metric of the Lorentzian spacetime

$$(ds)^2 = -(dt)^2 + (dr)^2 + \beta^2 r^2 (d\theta)^2 , \quad (2.125)$$

where t denotes the time, $r \geq 0$ is the distance to the defect location and $\theta \sim \theta + 2\pi$ is the angular polar coordinate. Crucially, the metric (2.125) admits Killing vectors leading to the conformal symmetry algebra $so(1, 2) \times so(2) \subset so(3, 2)$. This is precisely the symmetry algebra (2.1) of conformal line defects in $(2 + 1)$ -dimensional spacetime. We can thus apply the DCFT formalism introduced in Section 2.1 to this problem.

Let us now focus on a single Dirac cone in the effective metric (2.125):

$$S_{\text{Dirac}} = \int \beta r dt dr d\theta \bar{\Psi} \not{\nabla} \Psi , \quad (2.126)$$

where $\not{\nabla}$ is the covariant Dirac operator. We also activate a static connection $A_\mu = \alpha \delta_{\mu\theta}$, with $0 \leq \alpha < 1$ that corresponds to the emanant Aharonov-Bohm flux at $r = 0$. As the fermion field is parallel transported around the defect, the emanant flux induces the phase

¹³We thank C. Fechisin for preparing Figures 2.6 and 2.9, as well as for carrying out the numerical simulation.

¹⁴We note that having two opposite disclinations next to each other can also lead to the $(\vec{b} \cdot \partial)\delta^2(x)$ term in the IR description of metric.

$\Psi \rightarrow e^{2\pi\alpha i}\Psi$. The explicit form of the Dirac operator is given by¹⁵

$$\not{D} = \begin{pmatrix} -i\partial_t & e^{-i\theta}(\partial_r + \frac{-i\partial_\theta + \alpha - \frac{\beta}{2}}{r\beta}) \\ e^{i\theta}(\partial_r + \frac{i\partial_\theta - \alpha - \frac{\beta}{2}}{r\beta}) & i\partial_t \end{pmatrix}. \quad (2.127)$$

This DCFT can be solved by mapping the system to $\text{AdS}_2 \times S^1$. See [5] for a detailed treatment. Schematically, the bulk-to-defect OPE (2.2) of the Dirac fermion field Ψ takes the form

$$\Psi(t, r, \theta) = \sum_s \frac{e^{i(s - \frac{\sigma_z}{2})\theta}}{r^{1-\Delta(\hat{\Psi}^s)}} e^{\frac{i\pi}{4}\sigma_y} C_\Psi^{\hat{\Psi}^s} (\hat{\Psi}^s(t) + \text{descendants}), \quad (2.128)$$

where $\hat{\Psi}^s$ are the defect spinor primaries with parallel spin $\ell = 1/2$. Here, s denotes the orbital angular momentum of the fermion harmonic waves, and is also identified with the transverse spin of the defect operators. With the presence of the emanant flux, the spin selection rule reads

$$s \in \mathbb{Z} + \alpha + \frac{1}{2}. \quad (2.129)$$

In the conical space (2.125), the allowed scaling dimensions of the defect spinor primaries are $\Delta(\hat{\Psi}^s) = \frac{1}{2} \pm \frac{|s|}{\beta}$, whereas the unitarity of the DCFT requires $\Delta(\hat{\Psi}^s) \geq 0$. Therefore, for sufficiently large $|s|$, the defect spinors must have $\Delta(\hat{\Psi}^s) = \frac{1}{2} + \frac{|s|}{\beta}$. This analysis parallels that of Section 2.2. More generally, we denote

$$\begin{aligned} \text{standard fixed point} &: \quad \forall s \in \mathbb{Z} + \alpha + \frac{1}{2}, \quad \Delta(\hat{\Psi}^s) = \frac{1}{2} + \frac{|s|}{\beta}, \\ \text{alternative fixed points} &: \quad \exists s \in \mathbb{Z} + \alpha + \frac{1}{2}, \quad \Delta(\hat{\Psi}^s) = \frac{1}{2} - \frac{|s|}{\beta} \geq 0. \end{aligned} \quad (2.130)$$

Let us first consider the particularly simple case $\beta = 1$, for which the background metric (2.125) is flat. In this case, there is a single alternative fixed point with $\Delta(\hat{\Psi}^{\alpha - \frac{1}{2}}) = \frac{1}{2} - |\frac{1}{2} - \alpha|$. We can perturb the unstable alternative fixed point with the bilinear operator

$$\delta S_{\text{DCFT}} = \hat{m} \int_{r=0} dt \bar{\hat{\Psi}}^{\frac{1}{2}-\alpha} \hat{\Psi}^{\alpha-\frac{1}{2}}, \quad \text{where} \quad \Delta(\bar{\hat{\Psi}}^{\frac{1}{2}-\alpha} \hat{\Psi}^{\alpha-\frac{1}{2}}) = 2\Delta(\hat{\Psi}^{\alpha-\frac{1}{2}}). \quad (2.131)$$

This deformation is relevant for $\alpha \neq \frac{1}{2}$, and it triggers a defect RG flow to the standard fixed point, where $\Delta(\hat{\Psi}^{\alpha-\frac{1}{2}}) = \frac{1}{2} + |\frac{1}{2} - \alpha|$. Notably, the defect deformation (2.131) approaches marginality as $\alpha \rightarrow \frac{1}{2}$, indicating large finite-size corrections. As we show below, the deformation (2.131) becomes exactly marginal when $\alpha = \frac{1}{2}$, giving rise to a defect conformal

¹⁵Our convention for gamma matrices is $\gamma_t = i\sigma_z$, $\gamma_r = \cos(\theta)\sigma_x + \sin(\theta)\sigma_y$, and $\gamma_\theta = \beta r(-\sin(\theta)\sigma_x + \cos(\theta)\sigma_y)$.

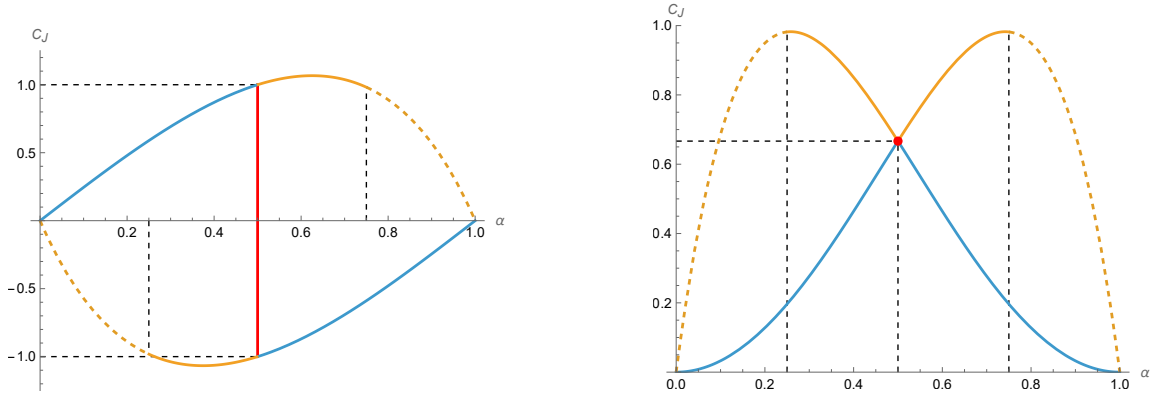


Figure 2.7: Azimuthal current C_J and energy density C_T of the defect without conical singularity (i.e., $\beta = 1$). We use blue curves to denote values at the standard fixed point, while orange curves denote those at the alternative fixed points. The dashed part of the orange curve represents where the defect quartic interaction becomes relevant. The red line and point mark the values at the defect conformal manifold.

manifold.

The bulk one-point functions of the $U(1)$ current J_μ and the stress-energy tensor $T_{\mu_1\mu_2}$ are particularly useful for understanding the structure of the defect fixed points. They also encode imprints of the crystalline quantum numbers, which we discuss in the next section. The functional forms of $\langle J_\mu \rangle$ and $\langle T_{\mu_1\mu_2} \rangle$ are fixed by the conformal algebra $\mathfrak{so}(1,2) \times \mathfrak{so}(2)$ up to overall OPE coefficients:

$$\begin{aligned} \langle J_\mu \rangle &= \langle i\bar{\Psi}\gamma_\mu\Psi \rangle = \frac{\delta_{\mu\theta}}{r} C_J ; \\ \langle T_{\mu_1\mu_2} \rangle &= \langle \bar{\Psi}\gamma_{\mu_1}\partial_{\mu_2}\Psi \rangle = \text{diag}(1, -1, 2\beta^2 r^2) \frac{C_T}{r^3} . \end{aligned} \quad (2.132)$$

See also (2.10). Physically, C_J represents the amplitude of the azimuthal current, whereas C_T denotes the local energy density induced by the defect. At a given defect fixed point, C_J and C_T are determined by the emanant flux α and the conical parameter β . When $\beta = 1$, the standard and alternative fixed points in the range $0 \leq \alpha < \frac{1}{2}$ yield

$$\begin{aligned} C_J^{\text{std}}(\alpha) &= \frac{\pi}{4} (1 - 4\alpha^2) \tan(\pi\alpha) , & C_J^{\text{alt}}(\alpha) &= C_J^{\text{std}}(\alpha) + \pi(2\alpha - 1) \tan(\pi\alpha) ; \\ C_T^{\text{std}}(\alpha) &= \frac{\pi}{3} \alpha (1 - 4\alpha^2) \tan(\pi\alpha) , & C_T^{\text{alt}}(\alpha) &= C_T^{\text{std}}(\alpha) + \pi(2\alpha - 1)^2 \tan(\pi\alpha) . \end{aligned} \quad (2.133)$$

Time-reversal symmetry implies $C_J(\alpha) = -C_J(1-\alpha)$ and $C_T(\alpha) = C_T(1-\alpha)$, thereby fixing the coefficients for $\frac{1}{2} < \alpha < 1$. See Figure 2.7. At the special point $\alpha = \frac{1}{2}$, we note there is a continuous family of DCFTs for which the azimuthal current takes values in the range

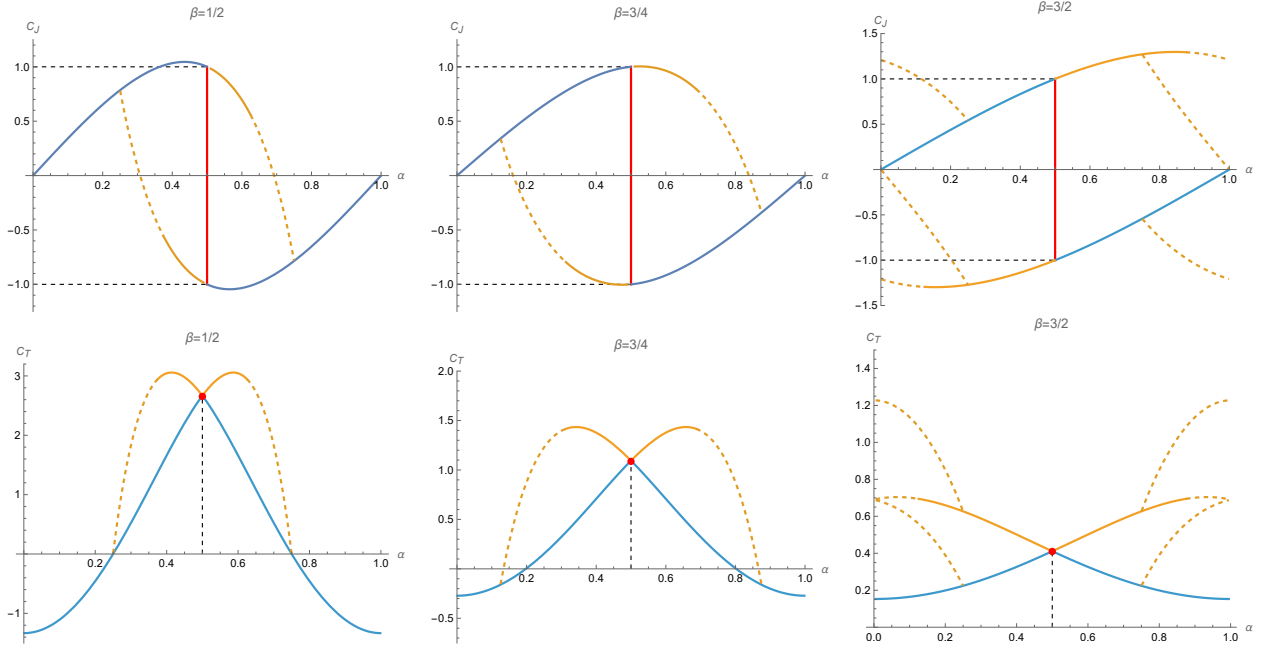


Figure 2.8: Azimuthal current C_J and conformal weight C_T of the defects with conical singularity. From left to right: defects with a conical deficit ($\beta = \frac{1}{2}$ and $\beta = \frac{3}{4}$) and defects with a conical excess ($\beta = \frac{3}{2}$).

$-1 \leq C_J \leq 1$. This is precisely the defect conformal manifold associated with the marginal deformation (2.131). We also note that the Zamolodchikov distance from a generic point on this manifold to the point $C_J = 0$ is given by $\arcsin |C_J|$.

Next, we turn to the fixed points of conical defects and their associated current and energy density. At the standard fixed point, C_J as a function of α and β admits an integral representation

$$C_J^{\text{std}} = -2 \lim_{v \rightarrow 2} \int_0^1 \left(\frac{u^{\frac{\alpha}{\beta}} - u^{-\frac{\alpha}{\beta}}}{u^{\frac{1}{2\beta}} - u^{-\frac{1}{2\beta}}} \right) \frac{u^{\frac{v}{2}-1} du}{(1-u)^v}, \quad (2.134)$$

where we take the analytical continuation of the index $v \rightarrow 2$. Similarly, C_T at the standard fixed point can be written as

$$C_T^{\text{std}} = \frac{4}{\beta^2} \lim_{v \rightarrow 2} \int_0^1 \left(\frac{(\frac{1}{2} - \alpha)(u^{\frac{2\alpha+2}{2\beta}} + u^{-\frac{2\alpha+1}{2\beta}})}{(u^{\frac{1}{2\beta}} - u^{-\frac{1}{2\beta}})^2} + \frac{(\frac{1}{2} + \alpha)(u^{\frac{2\alpha-1}{2\beta}} + u^{\frac{1-2\alpha}{2\beta}})}{(u^{\frac{1}{2\beta}} - u^{-\frac{1}{2\beta}})^2} \right) \frac{u^{\frac{v}{2}-1} du}{(1-u)^v}. \quad (2.135)$$

Denoting the spins $s' \in \mathbb{Z} + \alpha + \frac{1}{2}$ that are associated with alternative fixed points in (2.130),

we also find

$$\begin{aligned}
C_J^{\text{alt}} &= C_J^{\text{std}} + \frac{2\pi}{\beta} \sum_{s'} s' \cot(\pi|s' + \alpha|/\beta) , \\
C_T^{\text{alt}} &= C_T^{\text{std}} + \frac{4\pi}{\beta^3} \sum_{s'} (s')^2 \cot(\pi|s' + \alpha|/\beta) .
\end{aligned}
\tag{2.136}$$

Interestingly, the azimuthal current takes values in the range $-1 \leq C_J \leq 1$ at the special point $\alpha = \frac{1}{2}$, regardless of the parameter β . It follows that the Zamolodchikov volume of the defect conformal manifold is also independent of the cone angle.

Finally, we comment that the time-reversal symmetry can be realized at $\alpha = 0$ and $\alpha = \frac{1}{2}$, imposing $C_J = 0$. In this case, the current alone cannot distinguish the half emanant flux from zero flux, but we can still measure the energy density:

$$C_T^{\text{std}}(\alpha = \frac{1}{2}) - C_T^{\text{std}}(\alpha = 0) = \frac{1}{\beta^2} \left[2 + \int_0^1 \left(\frac{u^{\frac{1}{2\beta}} - 1}{u^{\frac{1}{2\beta}} + 1} \right)^2 \frac{du}{(u-1)^2} \right] > 0 ,
\tag{2.137}$$

which, among many other observables, distinguishes the time-reversal symmetric defects.

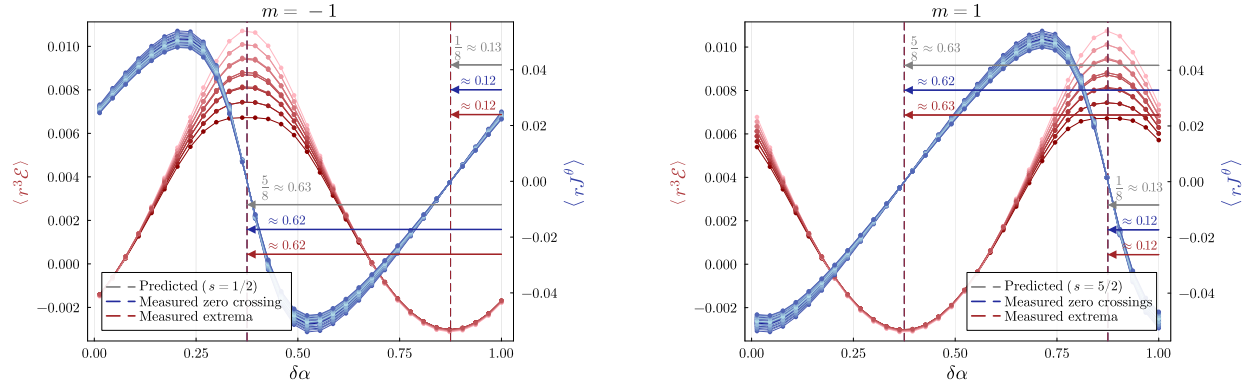
2.4.4 Observables in quantum critical lattice models

In this section, we compare the azimuthal current and energy density obtained from numerical simulations with the DCFT predictions. We focus on the $m = \pm 1$ quantum critical points of the Qi–Wu–Zhang model (2.120), both of which are described in the IR by a single Dirac fermion field. See [5] for other critical lattice models and further numerical results.

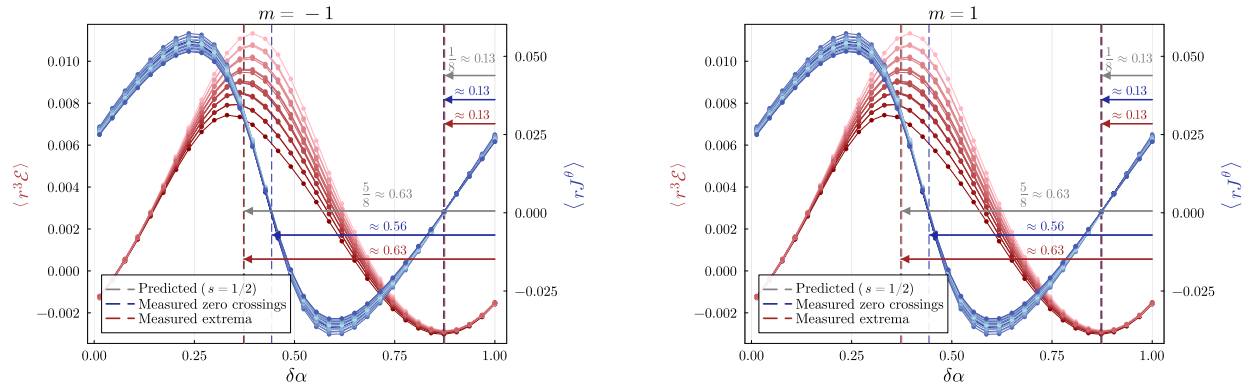
We impose an external $U(1)$ magnetic flux, parametrized by $\delta\alpha$, at the crystalline impurities. By scanning over $0 \leq \delta\alpha < 1$, we obtain the azimuthal current and energy density plots as in Figures 2.7 and 2.8. In the presence of emanant fluxes α_{em} induced by the crystalline impurities, the total flux seen by the IR fermion fields becomes $\alpha = \alpha_{\text{em}} + \delta\alpha$. For example, consider a disclination impurity with cone angle $2\pi\beta$, for which

$$\alpha_{\text{em}} = (\beta - 1)\mathbf{s}_{\vec{\sigma}} ,
\tag{2.138}$$

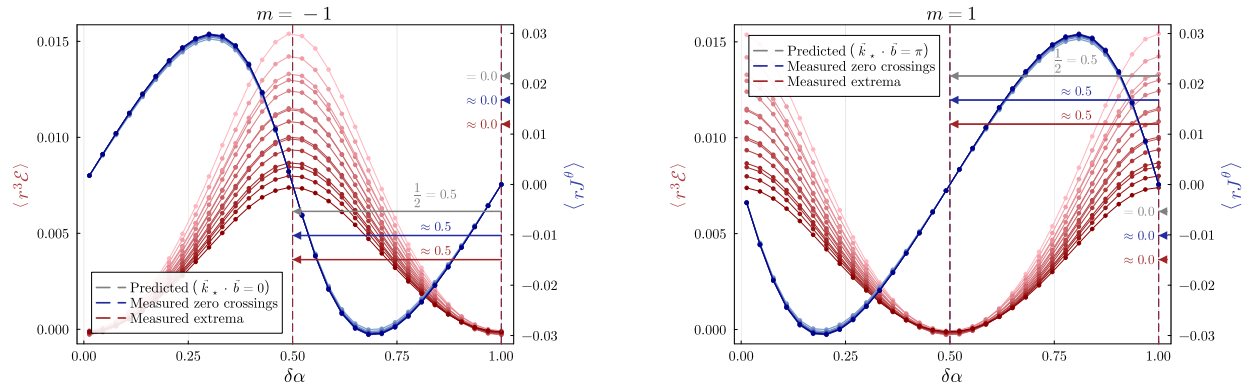
where $\mathbf{s}_{\vec{\sigma}}$ is the crystalline quantum number associated with the lattice rotation operator. The curves for C_J and C_T are accordingly shifted horizontally by α_{em} . This is indeed what we observe in Figure 2.9. The same method can be applied to other lattice models to extract the crystalline quantum numbers $\mathbf{s}_{i;\vec{\sigma}}$ and the Dirac cone momenta by fitting the horizontal shift induced by the emanant flux.



(a) Lattice with 5766 sites and a vertex-centered disclination impurity ($\beta = 3/4$).



(b) Lattice with 5582 sites and a plaquette-centered disclination impurity ($\beta = 3/4$).



(c) Lattice with 5460 sites and a dislocation impurity (unit Burgers vector)

Figure 2.9: Observables in Qi-Wu-Zhang model with crystalline impurities. In this figure, the shading of each curve indicates the distance from the measurement point to the defect, with lighter curves corresponding to lattice sites closer to the defect.

Chapter 3

Defects and Effective String Theory

In the previous chapter, we have seen that defects exhibit rich physics, and themselves probe aspects of the ambient quantum field theory that are often invisible to local operators. We now turn to a special class of defects that are central to understanding the strong forces in the Standard Model, namely confining strings.

Evidence from lattice simulations [103, 104] and simplified theoretical models [105, 106] of QCD indicates that the chromoelectric flux between quarks forms string-like excitations with nonzero tension, known as the QCD flux tubes. This provides a basic explanation for the mechanism that confines quarks inside hadrons at long distances. A similar phenomenon also occurs in type-II superconductors, where magnetic monopoles are confined by the Abrikosov vortices [107]. See [108–112] for a partial collection of other models exhibiting similar confining strings.

Unlike the examples discussed in Sections 2.2, 2.3, and 2.4, confining strings are typically realized in strongly coupled systems. When local excitations are fully gapped, these string-like excitations are stable against breaking and can only end on external defects or other strings. Studying the dynamics of these defects from a top-down perspective is challenging. Nevertheless, we can classify and study the possible low-energy effective theories of the confining strings. This is the effective string theory [6, 7, 113–132], which we will use extensively throughout this chapter.

The rest of this chapter is organized as follows. Section 3.1 provides a brief review of effective string theory, with an emphasis on the open-closed duality [133, 134]. In Section 3.2, we introduce baryon junctions in effective string theory. These junctions are important structures that connect multiple confining strings.¹ We establish the open-closed duality of the baryon junction in Section 3.3. Importantly, we map junctions with nonlinear corrections to the s -wave scattering amplitudes between confining string loops.

¹The baryon junctions are directly observed inside baryonic states in lattice simulations of $(3 + 1)$ -dimensional QCD [135–138].

3.1 Confining strings

We first review the effective field theory of long confining strings in d -dimensional spacetime. From a modern perspective, an infinitely long confining string is a vacuum of the underlying UV theory that spontaneously breaks the Poincaré symmetry $ISO(d)$ down to

$$ISO(2) \times SO(d-2) . \tag{3.1}$$

Here, the group $ISO(2)$ denotes the residual Poincaré symmetry along the string direction, whereas $SO(d-2)$ is the transverse rotation group. Despite the apparent resemblance to (2.1), we emphasize that the symmetry breaking in (3.1) is spontaneous, and it gives rise to exactly $(d-2)$ Nambu–Goldstone Bosons (NGBs) [139], which describe the transverse fluctuations of the string. Throughout this chapter, we assume that there are no other degrees of freedom in the low-energy effective theory of the string other than these NGBs.² This assumption applies to a wide class of gapped confining gauge theories, including the pure $SU(N)$ Yang–Mills theory in $(2+1)$ and $(3+1)$ dimensions [144–147].

For later convenience, we adopt the following EFT power-counting convention: an action term is of order n if it scales as (worldsheet size) $^{-n}$. In particular, an order n term in the worldsheet Lagrangian density scales as $O(\partial^{n+2})$, while an order n term localized on a one-dimensional submanifold of the worldsheet scales as $O(\partial^{n+1})$. In the low-energy limit, we retain the effective string action only up to a certain order.

3.1.1 Nambu–Goto action

The dynamics of the confining strings are elusive at first sight, since the underlying field theory is often strongly coupled at long distances. For sufficiently long strings, however, it was shown under mild assumptions that their low-energy dynamics are uniquely determined by the Nambu–Goto action [115, 118, 122, 124]. This action describes the shape fluctuations of a string with tension l_s^{-2} and is given by [148, 149]

$$S_{\text{string}} = -l_s^{-2} \int dt d\sigma \sqrt{-\det(\partial_\alpha X^\mu \partial_\beta X_\mu)} + O(\partial^4) , \tag{3.2}$$

where $X^\mu(t, \sigma)$ is the embedding of the string worldsheet in d -dimensional spacetime. Here, we have also included higher-order corrections starting at order 4. Such corrections include the Polyakov–Kleinert rigidity term [150, 151].

Taking advantage of the diffeomorphism invariance, we can choose the static gauge of

²Confining strings in supersymmetric gauge theories often support massless fermionic modes [140–143], as dictated by the preserved and spontaneously broken supercharges. These cases are beyond the scope of our discussion.

the worldsheet embedding $X_\mu(t, \sigma)$ as

$$X_1 = t, \quad X_2 = \sigma, \quad \text{and} \quad X_i = l_s x_i(t, \sigma) \text{ for } 3 \leq i \leq d. \quad (3.3)$$

In Lorentzian signature, the effective string action (3.2) under the ghost-free gauge (3.3) takes the expansion form

$$S_{\text{string}} = \int dt d\sigma \left[-\frac{1}{l_s^2} + \frac{1}{2} \left((\partial_t x_i)^2 - (\partial_\sigma x_i)^2 \right) + \frac{l_s^2}{8} (\partial_t x_i - \partial_\sigma x_i)^2 (\partial_t x_{i'} + \partial_\sigma x_{i'})^2 + O(\partial^6) \right], \quad (3.4)$$

where both the order 0 quadratic term and the order 2 quartic term follow from the Nambu-Goto action.

The action (3.4) can be used to compute the spectrum of a long, closed confining string with high precision. We consider a string that wraps along the periodic X_2 -direction of circumference $2\pi R$, such that in the static gauge (3.3) we have $\sigma \sim \sigma + 2\pi R$. The energy of a generic closed string state takes the following form [115, 119, 124, 152]

$$E_a^{\text{closed}} = \frac{2\pi R}{l_s^2} + \frac{2}{R} \left(n_a - \frac{d-2}{24} \right) - \frac{l_s^2}{\pi R^3} \left(n_a - \frac{d-2}{24} \right)^2 + O(R^{-5}), \quad (3.5)$$

where the subscript a (and similarly b and c below) labels weakly coupled multi-particle states on the closed string. In equation (3.5), n_a denotes the average of the left- and right-moving excitation levels, following from the order 0 free kinetic term in the action (3.4)³. For states with vanishing momentum along the X_2 -direction, we have $n_a \in \mathbb{N}$.

We note from (3.5) that there exists a large degeneracy between closed string excited states at the precision of $O(R^{-3})$, which is a consequence of the Poincaré symmetry and the integrability of the quartic deformation in (3.4). In the following sections, we will be interested in states that transform in the scalar representation of the transverse rotation group $SO(d-2)$ and carry zero longitudinal momentum. The two lowest-lying states satisfying these conditions are the ground state $\mathbf{0}$ (with $n_0 = 0$) and an excited state $\mathbf{1}$ (with $n_1 = 1$), while states with excitation levels $n_a \geq 2$ are degenerate.

³In the free theory approximation of (3.5), the worldsheet Hamiltonian of the closed string reads

$$H_{\text{free}} = \sum_{i=3}^d \sum_{n \in \mathbb{N}^+} \frac{n}{R} \left((\alpha_{L,n}^i)^\dagger \alpha_{L,n}^i + (\alpha_{R,n}^i)^\dagger \alpha_{R,n}^i \right) - \frac{d-2}{12R},$$

where $\alpha_{L,n}^i$ and $\alpha_{R,n}^i$ are the n -th annihilation operator left- and right-moving oscillator modes, respectively. Eigenvalues of H_{free} take the form of $\frac{2}{R} \left(n_a - \frac{d-2}{24} \right)$, as explained below equation (3.5).

3.1.2 Open string boundary conditions

In this subsection, we review the Dirichlet and the Neumann boundary effective theories of open confining strings. See, e.g., [115, 118, 120] for a systematic and detailed analysis.

Let us consider a semi-infinite string with longitudinal coordinate $X_2 = \sigma \geq 0$, whose worldsheet action is given by (3.4). The variational principle of the order 0 kinetic term in (3.4) leads to two canonical choices of boundary conditions at $\sigma = 0$, namely Dirichlet and Neumann. The Dirichlet boundary condition that preserves $SO(d-2)$ rotation symmetry reads

$$\text{Dirichlet : } \quad \partial_t x_i = 0 \text{ , for } 3 \leq i \leq d \text{ .} \quad (3.6)$$

It is also convenient to set the NGBs $x_i = 0$ at the Dirichlet boundary $\sigma = 0$. Higher-order corrections of the Dirichlet boundary are constrained by Poincaré symmetry, and the leading boundary deformation takes the following form:

$$S_{\text{Dirichlet}} = \int_{\sigma=0} dt \left[-m_D + \kappa_D (\partial_t \partial_\sigma x_i)^2 + O(\partial^6) \right] \text{ .} \quad (3.7)$$

The m_D term in (3.7) is of order -1 according to our EFT counting convention, whereas the κ_D term is of order 3. The constant m_D simply shifts the zero-point energy associated with the Dirichlet boundary. In lattice simulations, m_D represents the scheme-dependent mass of the static quarks. For convenience, we set $m_D = 0$ throughout this paper, i.e., we subtract the quark mass contributions.

On the other hand, the $SO(d-2)$ symmetric Neumann boundary condition reads

$$\text{Neumann : } \quad \partial_\sigma x_i = 0 \text{ , for } 3 \leq i \leq d \text{ .} \quad (3.8)$$

Similarly, we can consider higher-order corrections to the Neumann boundary condition that are compatible with the Poincaré symmetry. The leading deformations are as follows

$$\begin{aligned} S_{\text{Neumann}} &= \int_{\sigma=0} dt \left[-m_N \sqrt{-(\partial_t X_\mu)^2} + \kappa_N (\partial_t^2 x_i)^2 + O(\partial^6) \right] \\ &= \int_{\sigma=0} dt \left[-m_N + \frac{m_N l_s^2}{2} (\partial_t x_i)^2 - \frac{m_N l_s^4}{8} (\partial_t x_i)^4 + \kappa_N (\partial_t^2 x_i)^2 + O(\partial^6) \right] \text{ .} \end{aligned} \quad (3.9)$$

The first term in (3.9) denotes the worldline length of the dynamical string endpoint, where the parameter m_N is interpreted as the endpoint mass. We note that both the order -1 and order 1 terms in (3.9) are fixed by the mass m_N , whereas at order 3 an additional parameter κ_N can be introduced. Unlike m_D in (3.7), m_N perturbs the spectrum associated with the Neumann boundary.

3.1.3 Open-closed duality

We now follow [115, 117, 120, 153] and discuss the duality that associates the open string spectrum with an effective theory of closed string fields. For simplicity, we consider a finite string extending from $X_2 = \sigma = 0$ to $X_2 = \sigma = L$, with the Dirichlet boundary condition (3.6) at both ends. This confining string configuration describes a probe meson.

The partition function of the finite open string, denoted by Z_{meson} , can be computed and interpreted in several equivalent ways. In the open channel, the partition function is given by the Boltzmann sum

$$\text{open channel : } Z_{\text{meson}} = \sum_{E_{\text{open}}} e^{-\beta E_{\text{open}}} , \quad (3.10)$$

where E_{open} denotes the energy eigenvalues of open string states defined on $0 \leq \sigma \leq L$, and β is the inverse temperature. The partition function can be obtained by Wick rotating $t \rightarrow -i\tau$ and compactifying $\tau \sim \tau + \beta$ in the path-integral of the effective string action (3.4). In particular, we take the circumference of the Euclidean time circle to be $\beta = 2\pi R$. The open string partition function takes the following form

$$Z_{\text{meson}} = \frac{e^{-2\pi RL/l_s^2}}{[\eta(\mathbf{q})]^{(d-2)}} \left[1 - \frac{(d-2)\pi l_s^2}{1152L^2} \ln q (2E_4(\mathbf{q}) + (d-4)(E_2(\mathbf{q}))^2) + O(\partial^3) \right] , \quad (3.11)$$

where the modular parameter $\mathbf{q} \equiv \exp(-2\pi^2 R/L)$, $\eta(\mathbf{q})$ denotes the Dedekind eta function, and $E_2(\mathbf{q})$, $E_4(\mathbf{q})$ are the Eisenstein series. In the expansion (3.11), terms that scale as $O(L^{-n}R^{-n'})$ have been collectively denoted by $O(\partial^{n+n'})$. We note that order n terms in the effective action give leading contributions to the partition function that scale as $O(\partial^n)$. For example, corrections to the string endpoints, parametrized by κ_D (3.7) at $\sigma = 0$ and $\sigma = L$, are grouped into $O(\partial^3)$ terms in the expansion (3.11).

In the closed channel, the partition function is interpreted as the two-point function of the Polyakov loop operators wrapped along the X_1 -direction. A wrapped Polyakov loop preserves the Lorentz symmetry in the $(d-1)$ -dimensional space spanned by the coordinates $X^\perp = (X_2, X_{3 \leq i \leq d})$, and it defines a scalar point operator $\Omega(X^\perp)$. In general, the reducible operator Ω admits a decomposition into massive particle fields in the gapped effective theory as follows:

$$\Omega(X^\perp) = (\pi l_s^2)^{\frac{d-1}{4}} \sum_a v_a \sqrt{E_a^{\text{closed}}} \Phi_a(X^\perp) , \quad (3.12)$$

where $v_a \in \mathbb{C}$ denote decomposition coefficients, and Φ_a are d -dimensional complex scalar fields with definite masses. In equation (3.12) (and similarly below), the summation runs over Dirichlet boundary states of a confining closed string with circumference $2\pi R$. These boundary states reduce to Ishibashi states in the free theory limit, and are perturbed by higher-order corrections in the action (3.4) and (3.7). These closed string states satisfy the

following properties: (i) they carry zero longitudinal momentum, as required by the Cardy condition [134]; and (ii) they transform in the scalar representation of the transverse rotation group $SO(d-2)$, which is preserved by the Dirichlet condition (3.6). As we noted previously, the two lowest-lying boundary states are the ground state $\mathbf{0}$ and the excited state $\mathbf{1}$. We have also chosen the normalization in the decomposition (3.12) such that the coefficients v_a are dimensionless.

We adopt the following effective action ansatz for the dynamics of the closed-string fields Φ_a in d -dimensional space:

$$S_{\text{loops}} = \int d^{d-1} X^\perp \left[\frac{1}{2} \sum_a (|\partial_\nu \Phi_a|^2 + (E_a^{\text{closed}})^2 |\Phi_a|^2) + V(\Phi_a, \Phi_b, \dots) \right], \quad (3.13)$$

where $V(\Phi_a, \Phi_b, \dots)$ denotes interaction terms. The functional $V(\Phi_a, \Phi_b, \dots)$ is constrained by 1-form symmetries of the confining strings, whether IR emergent or UV exact. We will investigate the structure of $V(\Phi_a, \Phi_b, \dots)$ in Section 3.3. Notably, the mass of the field Φ_a corresponding to the closed-string state a is given by (3.5). From a d -dimensional viewpoint, E_a^{closed} plays the role of the internal mass of a particle at rest.

Following the decomposition (3.12) and the effective action (3.13), we find that the closed channel partition function takes the form

$$\begin{aligned} \text{closed channel : } Z_{\text{meson}} &= \langle \Omega^\dagger(X^\perp) \Omega(Y^\perp) \rangle \\ &= \sum_a |v_a|^2 \frac{(E_a^{\text{closed}})^{\frac{d-1}{2}} l_s^{d-2}}{\sqrt{\pi} (2L)^{\frac{d-3}{2}}} K_{\frac{d-3}{2}}(E_a^{\text{closed}} L), \end{aligned} \quad (3.14)$$

where $|X^\perp - Y^\perp| = L$, and $K_\alpha(x)$ denotes the modified Bessel function of the second type. In equation (3.14), we have used the tree-level propagator of massive particles in d -dimensional space and omitted possible loop corrections from the interaction terms. Such loop corrections are exponentially suppressed by the mass scale $O(E_a^{\text{closed}}) = O(R/l_s^2)$, and the partition function is therefore heavily dominated by the contribution in (3.14). With the dual modular parameter given by $\tilde{\mathbf{q}} \equiv \exp(-2L/R)$, the partition function (3.14) admits the expansion

$$\begin{aligned} Z_{\text{meson}} &= \left(\frac{\pi R}{L} \right)^{\frac{d-2}{2}} \frac{e^{-2\pi R L / l_s^2}}{\tilde{\mathbf{q}}^{\frac{d-2}{24}}} \sum_a |v_a|^2 \tilde{\mathbf{q}}^{n_a} \left[1 - \frac{(d-2)l_s^2}{2\pi R^2} \right. \\ &\quad \left. \times \left(\frac{\ln \tilde{\mathbf{q}}}{d-2} \left(n_a - \frac{d-2}{24} \right)^2 - \left(n_a - \frac{d-2}{24} \right) + \frac{d-4}{4 \ln \tilde{\mathbf{q}}} \right) + O(\partial^3) \right]. \end{aligned} \quad (3.15)$$

The open-closed duality identifies the partition functions evaluated in the open channel (3.10) and in the closed channel (3.14). Consequently, each term in the expansion (3.11) is matched to the corresponding term in (3.15) by a modular transformation. This leads

to strong constraints on the decomposition coefficients v_a . By locality, the coefficients $v_a = v_a(l_s, R, \kappa_D, \dots)$ are fixed solely by the local parameters of the Dirichlet boundaries, which are implemented by the Polyakov loops. From (3.10) and (3.15), we find that

$$\begin{aligned} v_0 &= 1 + \frac{(d-2)l_s^2}{48\pi R^2} + O(R^{-3}) , \\ v_1 &= \sqrt{d-2} \left(1 + \frac{(d-26)l_s^2}{48\pi R^2} + O(R^{-3}) \right) , \end{aligned} \tag{3.16}$$

to which we will return in Sections 3.3.

3.2 Effective theory of baryon junctions

In this section, we review the effective field theory of the trivalent baryon junctions introduced in [6]. We consider the confining string configurations as in Figure 3.1, which describe probe baryons composed of three identical quarks. Our analysis applies, for example, to baryonic states in $SU(3N)$ pure Yang-Mills theories in $(2+1)$ and $(3+1)$ dimensions.

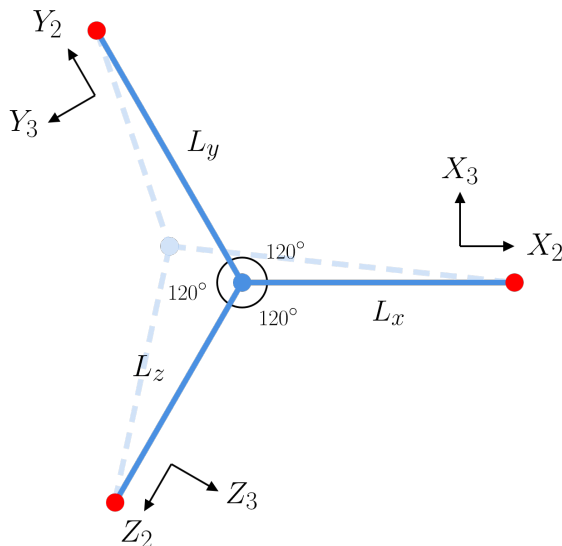


Figure 3.1: Confining strings in a probe baryon. The figure shows the spatial plane determined by the insertions of three static quarks (red points). The confining strings (blue lines) are tied at the dynamical baryon junction (blue point) and terminate on the quarks at their other ends.

Classically, the junction position in the space is determined by balancing the tensions l_s^{-2} of the three confining strings. It therefore coincides with the Fermat–Weber point of the

triangle whose vertices are set by the quarks. Throughout this chapter, we focus on baryon configurations where the Fermat–Weber point lies within the triangle.

We denote the coordinates of three strings by X_μ , Y_μ , and Z_μ , with their lengths L_x , L_y , and L_z . See also Figure 3.1. In the static gauge (3.3), we take $X_2 = Y_2 = Z_2 = \sigma = 0$ to be the joint baryon junction where three strings are connected, while $X_2 = \sigma = L_x$, $Y_2 = \sigma = L_y$, and $Z_2 = \sigma = L_z$ are the string endpoints on the quarks. Furthermore, we use x_i , y_i , and z_i for the NGBs on the corresponding worldsheet. In work [6, 7], we argued that the effective action of the probe baryon takes the following form:

$$S_{\text{baryon}} = \left(S_{\text{strings}}^{(-2)} + S_{\text{strings}}^{(0)} + S_{\text{strings}}^{(2)} \right) + \left(S_{\text{junction}}^{(-1)} + S_{\text{junction}}^{(1)} \right) + \left(S_{\text{displacement}}^{(1)} + S_{\text{displacement}}^{(2)} \right) + O(\partial^3) , \quad (3.17)$$

which we now unpack term by term.

3.2.1 Baryon junction condition

In the action (3.17), the terms $S_{\text{strings}}^{(-2)}$, $S_{\text{strings}}^{(0)}$, and $S_{\text{strings}}^{(2)}$ collect effective actions of the three strings up to order 2. As in the single string case (3.4), the order -2 classical term of three strings is as follows:

$$S_{\text{strings}}^{(-2)} = -l_s^{-2} \int dt \left(\int_0^{L_x} d\sigma + \int_0^{L_y} d\sigma + \int_0^{L_z} d\sigma \right) . \quad (3.18)$$

The order 0 term $S_{\text{strings}}^{(0)}$ is the quadratic kinetic action that governs the leading quantum fluctuations on the worldsheets:

$$S_{\text{strings}}^{(0)} = \frac{1}{2} \int dt \int_0^{L_x} d\sigma \left[(\partial_t x_i)^2 - (\partial_\sigma x_i)^2 \right] + (x \rightarrow y) + (x \rightarrow z) . \quad (3.19)$$

At the quark endpoints, the NGBs x_i , y_i , and z_i are subject to the Dirichlet boundary condition (3.6). On the other hand, the rigid geometry of confining strings at the baryon junction leads to the constraints:

$$x_3 + y_3 + z_3 = 0 , \quad \text{and} \quad x_j = y_j = z_j \quad \text{for} \quad 4 \leq j \leq d . \quad (3.20)$$

It is convenient to introduce the linear combinations $\xi_i^{[1]} = x_i + y_i + z_i$, $\xi_i^{[2]} = x_i - y_i$, and $\xi_i^{[3]} = x_i + y_i - 2z_i$ for $3 \leq i \leq d$. In these new variables, the geometry constraints (3.20) and the variational principle of (3.19) determine the following boundary condition at $\sigma = 0$:

$$\partial_t \xi_2^{[1]} = \partial_t \xi_2^{[2]} = \partial_t \xi_2^{[3]} = 0 , \quad \text{and} \quad \partial_\sigma \xi_2^{[2]} = \partial_\sigma \xi_2^{[3]} = \partial_\sigma \xi_j^{[1]} = 0 \quad \text{for} \quad 4 \leq j \leq d . \quad (3.21)$$

Higher-order corrections to the baryon junction boundary condition (3.21) arise from interaction terms localized at $\sigma = 0$. As we will show in Section 3.3, these interactions are strongly constrained by Poincaré symmetry and open-closed duality. Finally, the order 2 term $S_{\text{strings}}^{(2)}$ contains the quartic interactions on the worldsheets:

$$S_{\text{strings}}^{(2)} = \frac{l_s^2}{8} \int dt \int_0^{L_x} d\sigma (\partial_t x_i - \partial_\sigma x_i)^2 (\partial_t x_{i'} + \partial_\sigma x_{i'})^2 + (x \rightarrow y) + (x \rightarrow z) , \quad (3.22)$$

which follows from the Nambu–Goto action, as in equation (3.4).

The terms $S_{\text{junction}}^{(-1)}$ and $S_{\text{junction}}^{(1)}$ in equation (3.17) describe the worldline dynamics of the baryon junction. Let W_μ denote the spacetime coordinates of the baryon junction point. The leading worldline action compatible with Poincaré symmetry then takes the form:

$$S_{\text{junction}} = -m_j \int_{\sigma=0} dt \sqrt{-(\partial_t W_\mu)^2} = S_{\text{junction}}^{(-1)} + S_{\text{junction}}^{(1)} + O(\partial^3) . \quad (3.23)$$

We have introduced a new EFT parameter m_j in the action (3.23), which is interpreted as the classical mass of the baryon junction. Expanding the worldline action (3.23) in the NGBs x_i , y_i , and z_i , we find the order -1 term

$$S_{\text{junction}}^{(-1)} = -m_j \int_{\sigma=0} dt , \quad (3.24)$$

together with the order 1 term

$$S_{\text{junction}}^{(1)} = \frac{m_j l_s^2}{18} \int_{\sigma=0} dt [(\partial_t x_j + \partial_t y_j + \partial_t z_j)^2 + (\partial_t x_3 + \partial_t y_3 - 2\partial_t z_3)^2 + 3(\partial_t x_3 - \partial_t y_3)^2] . \quad (3.25)$$

In equation (3.25), we have chosen the linear combinations of x_i , y_i , and z_i that survive the geometry constraint (3.20).

Unlike the open string boundaries reviewed in Section 3.1, the baryon junction is allowed to fluctuate in the longitudinal directions of the confining strings. The longitudinal displacements of the three strings at $\sigma = 0$ are determined by the geometry in Figure 3.1, and are given by

$$\delta X_2 = \frac{l_s}{\sqrt{3}}(z_3 - y_3) , \quad \delta Y_2 = \frac{l_s}{\sqrt{3}}(x_3 - z_3) , \quad \text{and} \quad \delta Z_2 = \frac{l_s}{\sqrt{3}}(y_3 - x_3) . \quad (3.26)$$

These displacements couple to EFT operators that generate infinitesimal deformations of the worldsheet boundary, analogous to the DCFT displacement operators (2.14). For example, let us consider a single confining string whose endpoint fluctuates infinitesimally in the

longitudinal direction with $\sigma \geq \delta X_2(t)$. Expanding the worldsheet action (3.4) in powers of δX_2 , we identify the following effective coupling at the boundary:

$$S_{\text{displacement}} = \sum_{n \in \mathbb{N}} \int_{\sigma=0} dt (-\delta X_2)^{n+1} \partial_\sigma^n \left(-\frac{1}{l_s^2} + \frac{1}{2} ((\partial_t x_i)^2 - (\partial_\sigma x_i)^2) + O(\partial^4) \right) . \quad (3.27)$$

In the baryon junction case, the longitudinal displacements are promoted to dynamical fields as in equation (3.26), while the worldsheet action up to order 2 is dictated by (3.18), (3.19), and (3.22). The geometric constraint $\delta X_2 + \delta Y_2 + \delta Z_2 = 0$ ensures that the order -1 coupling of the longitudinal fluctuations is trivial. The leading order 1 coupling is therefore

$$S_{\text{displacement}}^{(1)} = \frac{l_s}{2\sqrt{3}} \int_{\sigma=0} dt \left[(y_3 - z_3) ((\partial_t x_i)^2 - (\partial_\sigma x_i)^2) + (z_3 - x_3) ((\partial_t y_i)^2 - (\partial_\sigma y_i)^2) + (x_3 - y_3) ((\partial_t z_i)^2 - (\partial_\sigma z_i)^2) \right] , \quad (3.28)$$

followed by the subleading order 2 term,

$$S_{\text{displacement}}^{(2)} = \frac{l_s^2}{12} \int_{\sigma=0} dt \left[(y_3 - z_3)^2 \partial_\sigma ((\partial_t x_i)^2 - (\partial_\sigma x_i)^2) + (z_3 - x_3)^2 \partial_\sigma ((\partial_t y_i)^2 - (\partial_\sigma y_i)^2) + (x_3 - y_3)^2 \partial_\sigma ((\partial_t z_i)^2 - (\partial_\sigma z_i)^2) \right] , \quad (3.29)$$

For simplicity, we have combined the longitudinal contributions from the three worldsheets in equations (3.28) and (3.29).

To summarize, we have classified terms in the effective action of the probe baryon up to order 2. We find that the effective action (3.17) is determined by two EFT parameters, namely the classical string tension l_s^{-2} and the classical baryon junction mass m_j . New EFT parameters may appear at higher orders; for example, the κ_D term in (3.7) at the quark endpoints is of order 3. The quantum fluctuations of the probe baryon are fully controlled by l_s^{-2} and m_j up to order 2, whose physical implications we will discuss in the upcoming sections.

3.2.2 Free-field limit and junction stability

We now analyze the spectrum of the probe baryon system in Figure 3.1 by considering the Euclidean path-integral of the effective action (3.17). As in Section 3.1.3, we compute this partition function by Wick rotating $t \rightarrow -i\tau$ and compactifying $\tau \sim \tau + 2\pi R$. The result

admits the following perturbative expansion:

$$Z_{\text{baryon}} = e^{-S_{\text{strings}}^{(-2)} - S_{\text{junction}}^{(-1)}} Z_{\text{baryon}}^{(0)} \left[1 - \langle S_{\text{junction}}^{(1)} \rangle - \langle S_{\text{strings}}^{(2)} \rangle - \langle S_{\text{displacement}}^{(2)} \rangle + \frac{1}{2} \langle (S_{\text{junction}}^{(1)})^2 \rangle + \frac{1}{2} \langle (S_{\text{displacement}}^{(1)})^2 \rangle + O(\partial^3) \right], \quad (3.30)$$

where we have defined

$$Z_{\text{baryon}}^{(0)} \equiv \int dx_i dy_i dz_i e^{-S_{\text{strings}}^{(0)}}, \quad \text{and} \quad \langle \dots \rangle \equiv \frac{1}{Z_{\text{baryon}}^{(0)}} \int dx_i dy_i dz_i (\dots) e^{-S_{\text{strings}}^{(0)}}. \quad (3.31)$$

The classical contributions to the path-integral are given by $S_{\text{strings}}^{(-2)}$ in equation (3.18) and $S_{\text{junction}}^{(-1)}$ in equation (3.24). We readily find that

$$S_{\text{strings}}^{(-2)} = \frac{2\pi R}{l_s^2} (L_x + L_y + L_z), \quad \text{and} \quad S_{\text{junction}}^{(-1)} = 2\pi R m_j. \quad (3.32)$$

We have organized the quantum fluctuations in the path-integral (3.30) according to their EFT order, where $Z_{\text{baryon}}^{(0)}$ is the leading order 0 contribution. Among the higher-order corrections, we note that the expectation values of parity-odd terms vanish. For example, $\langle S_{\text{displacement}}^{(1)} \rangle = 0$ and $\langle S_{\text{junction}}^{(1)} S_{\text{displacement}}^{(1)} \rangle = 0$.

In the rest of this section, we compute $Z_{\text{baryon}}^{(0)}$ and $\langle S_{\text{junction}}^{(1)} \rangle$, thereby fixing the partition function up to order 1. This amounts to treating the NGBs x_i , y_i , and z_i as free fields.

The order 0 effective action (3.19) is simply the free kinetic action for the NGBs x_i , y_i , and z_i . The partition function $Z^{(0)}$ with the baryon junction condition (3.20) and (3.21) can be evaluated as follows: we first fix the spacetime trajectory of the point-like junction, then integrate over the NGB fluctuations around the saddle point determined by this trajectory, and finally perform the quantum-mechanical path-integral over the junction worldline. See [7, 154–156] for a detailed treatment. For convenience, we define the modular parameters

$$\mathbf{q}_x \equiv e^{-\frac{2\pi^2 R}{L_x}}, \quad \mathbf{q}_y \equiv e^{-\frac{2\pi^2 R}{L_y}}, \quad \mathbf{q}_z \equiv e^{-\frac{2\pi^2 R}{L_z}}, \quad (3.33)$$

and the Gaussian path-integral in (3.31) yields

$$Z_{\text{baryon}}^{(0)} = \frac{(L_x^{-1} + L_y^{-1} + L_z^{-1})^{\frac{3-d}{2}}}{(2\pi R)^{\frac{d-1}{2}} (\eta(\mathbf{q}_x) \eta(\mathbf{q}_y) \eta(\mathbf{q}_z))^{d-2}} \sqrt{\frac{L_x L_y L_z}{L_x + L_y + L_z}} \prod_{n \in \mathbb{N}^+} \left[\tanh\left(\frac{nL_x}{R}\right) \times \tanh\left(\frac{nL_y}{R}\right) \tanh\left(\frac{nL_z}{R}\right) \frac{\left(\coth\left(\frac{nL_x}{R}\right) + \coth\left(\frac{nL_y}{R}\right) + \coth\left(\frac{nL_z}{R}\right)\right)^{3-d}}{\tanh\left(\frac{nL_x}{R}\right) + \tanh\left(\frac{nL_y}{R}\right) + \tanh\left(\frac{nL_z}{R}\right)} \right]. \quad (3.34)$$

To the best of our knowledge, the partition function (3.34) with generic L_x , L_y , and L_z does not admit a closed form. There are, however, special cases where the ratios of the three confining string lengths are rational:

$$\begin{aligned} \text{rational baryon} : \quad & L_x = N_x L, \quad L_y = N_y L, \quad L_z = N_z L, \\ & \text{s.t. } N_x, N_y, N_z \in \mathbb{N}^+ \quad \text{and} \quad \gcd(N_x, N_y, N_z) = 1. \end{aligned} \quad (3.35)$$

Let us first note several useful mathematical facts concerning N_x , N_y , and N_z . In particular, consider the following two polynomials:

$$\begin{aligned} P_1(z) &\equiv 1 + \frac{1}{3}(z^{N_x} + z^{N_y} + z^{N_z}) - \frac{1}{3}(z^{N_x+N_y} + z^{N_y+N_z} + z^{N_z+N_x}) - z^{N_x+N_y+N_z}, \\ P_2(z) &\equiv 1 - \frac{1}{3}(z^{N_x} + z^{N_y} + z^{N_z}) - \frac{1}{3}(z^{N_x+N_y} + z^{N_y+N_z} + z^{N_z+N_x}) + z^{N_x+N_y+N_z}. \end{aligned} \quad (3.36)$$

Both $P_1(r)$ and $P_2(r)$ have all of their roots on the unit circle $|z| = 1$ [157]. We can therefore write the factorization

$$P_1(z) = (1 - z) \prod_u (e^{2\pi i u} - z), \quad P_2(z) = (1 - z)^2 \prod_v (e^{2\pi i v} - z), \quad (3.37)$$

where $0 < u < 1$ denotes the phases of the $(N_x + N_y + N_z - 1)$ non-identity roots of P_1 , and $0 < v < 1$ denotes the phases of the $(N_x + N_y + N_z - 2)$ non-identity roots of P_2 . In terms of these roots, we find that the baryon partition function (3.34) takes the form

$$Z_{\text{baryon}}^{(0)} = \frac{1}{(\eta(\mathbf{q}))^{2d-5}} \left(\prod_u \frac{\mathbf{q}^{\frac{1}{48} - \frac{(u-\frac{1}{2})^2}{4}}}{(\mathbf{q}^u; \mathbf{q})_\infty} \right) \left(\prod_v \frac{\mathbf{q}^{\frac{1}{48} - \frac{(v-\frac{1}{2})^2}{4}}}{(\mathbf{q}^v; \mathbf{q})_\infty} \right)^{d-3}, \quad (3.38)$$

where $\mathbf{q} \equiv \exp(-2\pi^2 R/L)$. Equation (3.38) indicates that the probe baryon system (3.17) has a unique ground state. Moreover, we find the ground state energy

$$\begin{aligned} E_{\text{GS}} &= (N_x + N_y + N_z) \frac{L}{l_s^2} + m_j - \frac{(2d-5)\pi}{24L} \\ &\quad - \frac{\pi}{4L} \sum_u \left(\left(u - \frac{1}{2}\right)^2 - \frac{1}{12} \right) - \frac{(d-3)\pi}{4L} \sum_v \left(\left(v - \frac{1}{2}\right)^2 - \frac{1}{12} \right) + O(L^{-2}). \end{aligned} \quad (3.39)$$

When the three confining strings have equal length, their fluctuation modes within the string plane decouple from those perpendicular to the plane in the free-field limit. We refer to this particularly simple configuration as

$$\text{equilateral baryon} : \quad L_x = L_y = L_z = L. \quad (3.40)$$

The partition function (3.34) in such cases can be written in terms of (quasi-)modular forms of the parameters \mathbf{q} and $\sqrt{\mathbf{q}}$ as follows:

$$Z_{\text{baryon}}^{(0)} = \frac{1}{(\eta(\sqrt{\mathbf{q}}))^{d-1}(\eta(\mathbf{q}))^{d-4}} . \quad (3.41)$$

We now examine the stability of the baryon junction with the worldline kinetic term (3.25). For equilateral baryons, the equations of motion can be solved separately for modes within the string plane and for modes perpendicular to it. We denote the corresponding mode frequencies by $\omega_{//}$ and ω_{\perp} , respectively. The dispersion relation then follows from the quadratic actions (3.25) and (3.19) :

$$\cos(\omega_{//}L) = \frac{2}{3}m_j l_s^2 \omega_{//} \sin(\omega_{//}L) , \quad \cos(\omega_{\perp}L) = \frac{1}{3}m_j l_s^2 \omega_{\perp} \sin(\omega_{\perp}L) . \quad (3.42)$$

Depending on the scale and sign of m_j , there are essential differences in solutions to (3.42):

- $m_j < 0$: The dispersion relation (3.42) admits imaginary solutions with $\omega_{//}, \omega_{\perp} \sim i l_s^2 / |m_j|$ when $|m_j| \ll L/l_s^2$. These tachyonic modes do not immediately imply that the junction is unstable. In particular, when $|m_j| \lesssim 1/l_s$, the wavelengths of these tachyonic modes exceed the EFT cutoff, and junction stability must be examined with higher-order corrections taken into account. Interestingly, a junction mass satisfying $-1/l_s \lesssim m_j < 0$ is reported in certain large- N gauge theories [158].

When the junction mass is negative and parametrically large $|m_j| \gg 1/l_s$, we find perturbative tachyonic modes in the EFT. In this regime, the junction is clearly unstable, while the endpoints of these tachyonic directions are beyond the scope of our discussion.

- $0 \leq m_j \lesssim 1/l_s$: The solutions to the dispersion relation (3.42) satisfy $\omega_{//}, \omega_{\perp} \sim 1/L$. These solutions are positive half-integers in units of π/L with small corrections. This is the most relevant regime to Yang-Mills theory, where $m_j \sim l_s \sim \Lambda_{\text{YM}}$ [135, 136, 154, 159, 160].
- $1/l_s \ll m_j \ll L/l_s^2$: The solutions to the dispersion relation (3.42) separate into two regimes: low energy modes with $\omega_{//}, \omega_{\perp} \ll 1/m_j l_s^2$ remain positive half-integers in units of π/L , up to small corrections. By contrast, high energy modes with $1/m_j l_s^2 \ll \omega_{//}, \omega_{\perp} \ll 1/l_s$ become positive integers in units of π/L , again up to small corrections.
- $m_j \gg L/l_s^2$: The solutions to the dispersion relation (3.42) are positive integers in units of π/L , up to small corrections. In addition, there are semiclassical modes with $\omega_{//}, \omega_{\perp} \sim 1/l_s \sqrt{m_j L}$. These modes correspond to a heavy vertex oscillating in the classical potential without creating waves on the string.

In the low-energy limit, we assume that the worldsheet scales L , R are larger than any power combination of the intrinsic effective string scales l_s , m_j . We thereby find that our perturbative analysis applies as long as the baryon junction is stable with $m_j \gtrsim -1/l_s$.

Analogous to (3.34), the order 1 correction to the partition function also has an infinite-sum representation [7]

$$\langle S_{\text{junction}}^{(1)} \rangle = \frac{m_j l_s^2}{R} \sum_{n \in \mathbb{N}^+} \left[\frac{(d-3)n}{\coth\left(\frac{nL_x}{R}\right) + \coth\left(\frac{nL_y}{R}\right) + \coth\left(\frac{nL_z}{R}\right)} + \frac{4n}{3} \tanh\left(\frac{nL_x}{R}\right) \right. \\ \left. \times \tanh\left(\frac{nL_y}{R}\right) \tanh\left(\frac{nL_z}{R}\right) \frac{\coth\left(\frac{nL_x}{R}\right) + \coth\left(\frac{nL_y}{R}\right) + \coth\left(\frac{nL_z}{R}\right)}{\tanh\left(\frac{nL_x}{R}\right) + \tanh\left(\frac{nL_y}{R}\right) + \tanh\left(\frac{nL_z}{R}\right)} \right]. \quad (3.43)$$

For equilateral baryons, this result can likewise be written in terms of (quasi-)modular forms of \mathbf{q} and $\sqrt{\mathbf{q}}$:

$$\langle S_{\text{junction}}^{(1)} \rangle = \frac{(d+1)m_j l_s^2}{144L} \ln \mathbf{q} (2E_2(\mathbf{q}) - E_2(\sqrt{\mathbf{q}})) . \quad (3.44)$$

3.2.3 An accidental \mathbb{Z}_2 symmetry

In this section, we discuss an accidental \mathbb{Z}_2 symmetry of baryon junctions in 4-dimensional spacetime (i.e., $d = 4$) that is broken by the junction mass m_j . To see this, we consider a class of line defects living on the confining string worldsheet with the effective action (3.4). The defect \mathcal{D} is defined by coupling the NGB fields across the line manifold \mathcal{M}_1 as follows:

$$\mathcal{D}(\mathcal{M}_1) \equiv \exp \left(i \int_{\mathcal{M}_1} (x_3^- dx_4^+ - x_4^- dx_3^+) \right) = \exp \left(i S_{\text{defect}}^{(0)} \right) , \quad (3.45)$$

where x_i^- denotes the field profile on the left-hand side of \mathcal{M}_1 , while x_i^+ denotes the profile on the right-hand side. See also Figure 3.2. This construction is analogous to the S-duality defects (2.27) in the Maxwell theory. The insertion of the defect \mathcal{D} preserves the transverse rotation group $SO(2)$ and modifies the equations of motion for the NGB fields. It follows from the variational principle that the fields on the two sides of the defect are matched according to

$$(\partial_t x_3^-, \partial_\sigma x_3^-, \partial_t x_4^-, \partial_\sigma x_4^-) = (\partial_\sigma x_4^+, \partial_t x_4^+, -\partial_\sigma x_3^+, -\partial_t x_3^+) . \quad (3.46)$$

For the probe baryon configurations shown in Figure 3.1, we can similarly define defects \mathcal{D} on the confining string worldsheets using variables y_i^\pm and z_i^\pm , respectively.

Up to order 0, the baryon effective action (3.17) is governed by the quadratic kinetic term (3.19) and the junction condition (3.21). One readily verifies that the worldsheet stress-energy tensor is continuous across \mathcal{D} at this order. Equation (3.45) therefore defines a topological defect line in the free theory, which generates a \mathbb{Z}_2 global symmetry on the worldsheet. In particular, the symmetry transformation rule for local operators is given by

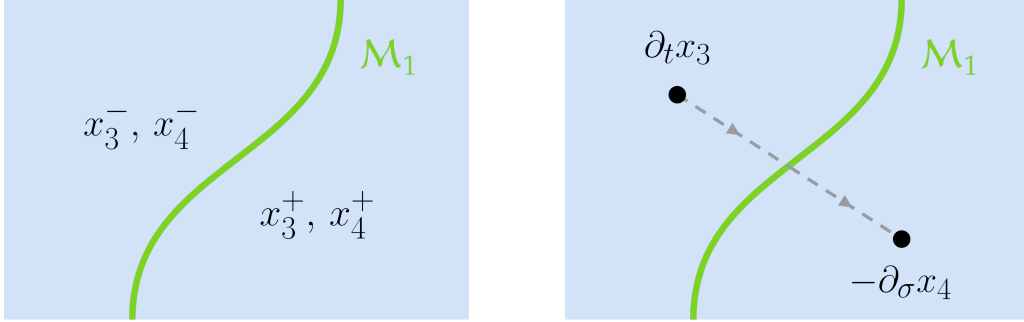


Figure 3.2: Topological defect line \mathcal{D} on the confining string worldsheet. Left: the NGB field profiles are taken to be discontinuous across the line \mathcal{M}_1 , and the defect action is given by the bilinear coupling between x_i^- and x_i^+ . Right: local operators transform according to equation (3.46) upon crossing the defect line. The \mathbb{Z}_2 symmetry transformation rule can be schematically written as $(\partial_t x_3, \partial_\sigma x_3) \xrightarrow{\mathcal{D}} (-\partial_\sigma x_4, -\partial_t x_4) \xrightarrow{\mathcal{D}} (\partial_t x_3, \partial_\sigma x_3)$.

(3.46).⁴

Notably, the baryon junction condition (3.21) preserves the \mathbb{Z}_2 symmetry generated by the topological defect line \mathcal{D} .⁵ The key observation is as follows: the linear combinations of NGB fields $\xi_3^{[1]}$, $\xi_4^{[2]}$, and $\xi_4^{[3]}$ satisfy Dirichlet boundary conditions at the junction, while the other combinations $\xi_3^{[2]}$, $\xi_3^{[3]}$, and $\xi_4^{[1]}$ satisfy Neumann boundary conditions. The \mathbb{Z}_2 symmetry (3.45) exchanges Dirichlet and Neumann conditions and acts by a $\pi/2$ rotation on the spatial indices transverse to the confining string, therefore leaving the junction condition invariant. In the free theory limit, the baryon junction worldline can be merged with the defect \mathcal{D} across the three connected worldsheets as in Figure 3.3. The \mathbb{Z}_2 symmetry acts on operators localized at the baryon junction through the topological intersection of the junction worldline with the line defects.

We now examine whether the \mathbb{Z}_2 symmetry generated by the defect \mathcal{D} persists in the full effective theory (3.17). On the confining string worldsheets, we note that the quartic interaction in equation (3.22) is invariant under the \mathbb{Z}_2 transformation (3.46). The leading

⁴Local vertex operators (e.g., $\exp(ik_i x_i)$) are mapped to semi-local twist operators under this \mathbb{Z}_2 symmetry. These twist operators are characterized by the field monodromy $x_i \rightarrow x_i + \text{const}$ around the operator insertion.

⁵For effective string theories in d -dimensional spacetime, we can analogously define a line defect that preserves the transverse rotation group $SO(d-2)$ as follows:

$$\mathcal{D}'(\mathcal{M}_1) \equiv \exp\left(i \int_{\mathcal{M}_1} x_i^- dx_i^+\right), \quad \text{where } 3 \leq i \leq d.$$

The baryon junction condition (3.21), however, is not invariant under the symmetry generated by \mathcal{D}' .

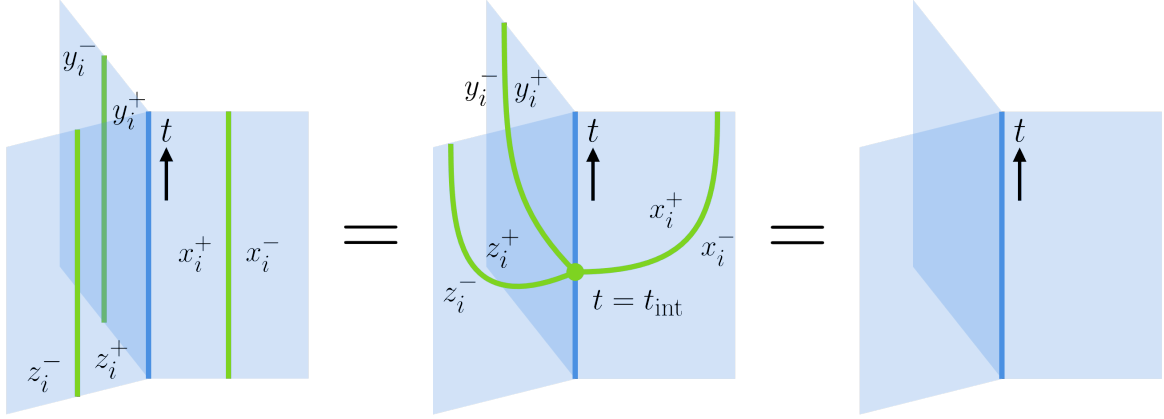


Figure 3.3: Merging the topological defect lines with the baryon junction worldline.

symmetry-breaking interaction on the worldsheets arises at order 4 and is controlled by the Polyakov–Kleinert rigidity term.

On the other hand, the baryon junction worldline preserves the \mathbb{Z}_2 symmetry if its intersection with defect \mathcal{D} remains topological. We first note that coupling the worldsheets on the two sides of the defect using (3.45) requires the longitudinal displacements δX_2 , δY_2 , and δZ_2 in (3.26) to be continuous across the defect line. This leads to the following consistency condition at the intersection point $t = t_{\text{int}}$ (see Figure 3.3):

$$\text{gluing condition : } x_3^+ = x_3^-, y_3^+ = y_3^-, \text{ and } z_3^+ = z_3^- \text{ at } (t, \sigma) = (t_{\text{int}}, 0), \quad (3.47)$$

which can be implemented using Lagrange multipliers at the intersection point.

We consider the worldline stress-energy tensor \hat{T} as in (2.14). More explicitly, it is defined by the local divergence of the worldsheet stress-energy tensors $T_{\alpha\beta}[x_i]$, $T_{\alpha\beta}[y_i]$, and $T_{\alpha\beta}[z_i]$ as follows:

$$\partial^\alpha T_{\alpha t}[x_i] + \partial^\alpha T_{\alpha t}[y_i] + \partial^\alpha T_{\alpha t}[z_i] = -\delta(\sigma)\partial_t \hat{T}. \quad (3.48)$$

The operator \hat{T} represents the energy stored at the baryon junction, which vanishes at order 0. In the full effective theory, \hat{T} receives corrections from the actions (3.25), (3.28), (3.29), and other higher-order terms. For example, the contribution from longitudinal displacements on the X -string follows from (3.27) and takes the form

$$\hat{T} \supset \sum_{n \in \mathbb{N}} (-\delta X_2)^{n+1} \partial_\sigma^n \left(\frac{1}{l_s^2} + \frac{1}{2} ((\partial_t x_i)^2 + (\partial_\sigma x_i)^2) + O(\partial^4) \right). \quad (3.49)$$

Using the transformation rule (3.46) and the condition (3.47), we find that the corrections to the stress-energy tensor \hat{T} in (3.49) are continuous across the intersection point $t = t_{\text{int}}$ up to order 2. The discontinuity at $t = t_{\text{int}}$ arises from the worldline kinetic term (3.25) and

is given by

$$\begin{aligned} \hat{T}^+ - \hat{T}^- = \frac{m_j l_s^2}{18} & \left[(\partial_t x_4^+ + \partial_t y_4^+ + \partial_t z_4^+)^2 - (\partial_\sigma x_3^+ + \partial_\sigma y_3^+ + \partial_\sigma z_3^+)^2 \right. \\ & + (\partial_t x_3^+ + \partial_t y_3^+ - 2\partial_t z_3^+)^2 - (\partial_\sigma x_4^+ + \partial_\sigma y_4^+ - 2\partial_\sigma z_4^+)^2 \\ & \left. + 3(\partial_t x_3^+ - \partial_t y_3^+)^2 - 3(\partial_\sigma x_4^+ - \partial_\sigma y_4^+)^2 \right] + O(\partial^4) , \end{aligned} \quad (3.50)$$

where \hat{T}^+ and \hat{T}^- denote the stress-energy tensor evaluated on the two sides of the intersection point. The discontinuity (3.50) quantifies the obstruction to moving the intersection point topologically along the baryon junction worldline, thereby signaling the \mathbb{Z}_2 symmetry breaking.

We conclude that the baryon junction mass m_j is the leading parameter that breaks the \mathbb{Z}_2 symmetry (3.45) in the 4-dimensional effective string theory. Unlike the boundary parameters in (3.7) and (3.9), the baryon junction mass can be defined without reference to external probes (e.g., static quarks) and is therefore intrinsic to the underlying UV theory. Conversely, if the \mathbb{Z}_2 symmetry is exactly realized in the UV theory, it imposes strong constraints on the baryon junction mass, forcing $m_j = 0$.

3.3 Open-closed duality of baryon junctions

In this section, we establish the open-closed duality for the junctions of confining strings. To set the stage, it is useful to recall the dual channels of a finite open string reviewed in Section 3.1.3. The open-closed duality identifies the thermal partition function of a probe meson (3.10) with the two-point correlation function of Polyakov loop operators (3.14). We assume that the Polyakov operators (i.e., the quark endpoints of the confining strings) can be decomposed into massive particles in $(d-1)$ -dimensional space. By matching the partition function (3.11) with (3.15) via modular transformations, we fix the decomposition coefficients up to leading orders as in equation (3.16).

We now turn to the probe baryon configuration in Figure 3.1. In the open channel, the baryon partition function Z_{baryon} takes the form

$$\text{open channel : } Z_{\text{baryon}} = \sum_{E_{\text{baryon}}} e^{-\beta E_{\text{baryon}}} , \quad (3.51)$$

where E_{baryon} denotes the energy eigenvalues of the baryon states. The open-channel partition function was partially computed in Section 3.2.2, with $\beta = 2\pi R$. In this section, we continue that calculation and evaluate the order 2 nonlinear corrections.

With three external quarks, we argue that the closed channel of the baryon partition

function is given by the three-point function of Polyakov operators:

$$\text{closed channel : } Z_{\text{baryon}} = \langle \Omega(X^\perp) \Omega(Y^\perp) \Omega(Z^\perp) \rangle, \quad (3.52)$$

where X^\perp , Y^\perp , and Z^\perp denote positions in $(d-1)$ -dimensional space. We adopt the convention

$$X^\perp = (L_x, 0, \dots), \quad Y^\perp = \left(-\frac{1}{2}L_y, \frac{\sqrt{3}}{2}L_y, \dots\right), \quad \text{and} \quad Z^\perp = \left(-\frac{1}{2}L_z, -\frac{\sqrt{3}}{2}L_z, \dots\right), \quad (3.53)$$

where we have omitted the $(d-3)$ directions perpendicular to the string plane, and the Fermat-Weber point of the $X^\perp Y^\perp Z^\perp$ triangle is at the origin. In this section, we show that the three-point function (3.52) is dominated by the tree-level s -wave scattering of the massive particles. Using the open-closed duality, we further determine the leading contributions to the coupling constants governing these scattering processes.

3.3.1 S -wave scattering and selection rules

Higher-point functions of the Polyakov loop operators are determined by the potential $V(\Phi_a, \dots)$ in the effective action (3.13). For trivalent baryon junctions in Figure 3.1, we have assumed that the underlying d -dimensional gauge theory is endowed with a \mathbb{Z}_3 1-form symmetry, either exact in the UV or emergent in the IR. Upon dimensional reduction, this 1-form symmetry descends to a \mathbb{Z}_3 0-form acting on the complex scalar fields Φ_a in $(d-1)$ -dimensional space. We note that the \mathbb{Z}_3 -symmetric potential $V(\Phi_a, \Phi_b, \dots)$ admits cubic interaction vertices of the form:

$$\begin{aligned} V(\Phi_a, \Phi_b, \dots) \supset \frac{1}{2} \left(\frac{3}{2\pi} \right)^{\frac{d-1}{2}} (\sqrt{\pi} l_s)^{\frac{d-4}{2}} \sum_{a,b,c} \sqrt{E_a^{\text{closed}} E_b^{\text{closed}} E_c^{\text{closed}}} \\ \times \left[C_{abc}^{(0)} \Phi_a \Phi_b \Phi_c + C_{abc}^{(2)} \partial_\nu \Phi_a \partial_\nu \Phi_b \Phi_c + (\text{c.c.}) + O(\partial^4) \right], \end{aligned} \quad (3.54)$$

where $C_{abc}^{(n)}$ denote the order n cubic coupling constants, fully symmetric in the massive mode indices a, b, c . The various prefactors in equation (3.54) are chosen so that $C_{abc}^{(0)}$ are dimensionless and geometric factors are canceled, as we will see below.

At tree-level in the perturbation theory, these interaction vertices determine scattering amplitudes between massive particles in $(d-1)$ -dimensional space. See also Figure 3.4. In particular, the coupling constants $C_{abc}^{(0)}$ are associated with the s -wave scattering. Likewise, $C_{abc}^{(2)}$ correspond to the p -wave scattering, while higher-spin scatterings (e.g. d -wave) arise at order $O(\partial^4)$ in the potential (3.54). We find that the following interaction vertices become

total derivatives upon using the equations of motion:

$$2 \sum_{a,b,c} C_{abc}^{(2)} \partial_\nu \Phi_a \partial_\nu \Phi_b \Phi_c = \sum_{a,b,c} C_{abc}^{(2)} \left(\partial_\nu (\partial_\nu \Phi_a \Phi_b \Phi_c) - (\partial_\nu^2 \Phi_a) \Phi_b \Phi_c \right). \quad (3.55)$$

As far as local kinetic terms are concerned, the coupling constants $C_{abc}^{(2)}$ can be removed by redefining $C_{abc}^{(0)}$ and the higher-spin terms. We therefore find that the tree-level amplitudes in the three-point function $\langle \Phi_a \Phi_b \Phi_c \rangle$ are determined entirely by s -wave scatterings up to order 3.

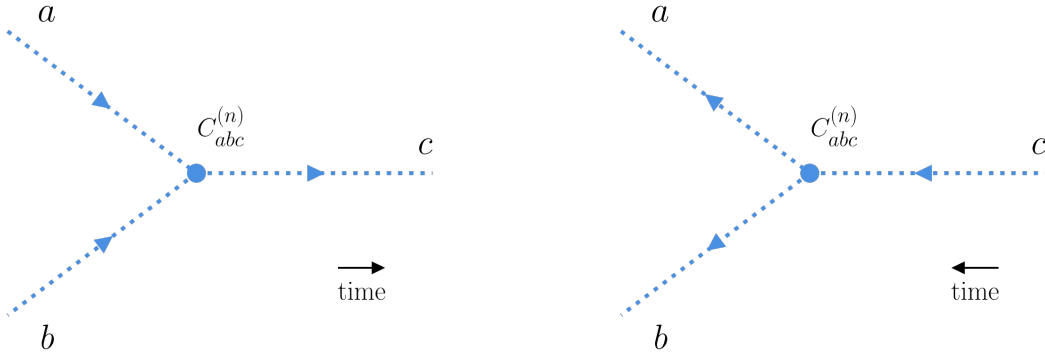


Figure 3.4: Tree-level scattering amplitudes of massive modes in the closed channel. Interpreting one direction of the d -dimensional space as time, the cubic interaction vertices in equation (3.54) describe the $2 \rightarrow 1$ fusion process (Left) and the $1 \rightarrow 2$ decay process (Right). The external legs in this figure are generally off-shell, since all modes in the closed channel have approximately the same mass (3.5).

As in Section 3.1.3, we argue that the loop contributions in the three-point function (3.52) are exponentially suppressed. The partition function up to the order 3 is thereby given by the tree-level Feynman integral

$$Z_{\text{baryon}} = \sum_{a,b,c} \int d^{d-1} W^\perp l_s^{1-d} C_{abc}^{(0)} v_a v_b v_c \left(\frac{(E_a^{\text{closed}})^{\frac{d-1}{2}} l_s^{d-2}}{\sqrt{\pi} (2L_{wx})^{\frac{d-3}{2}}} K_{\frac{d-3}{2}} (E_a^{\text{closed}} L_{wx}) \right) \times \left(\frac{(E_b^{\text{closed}})^{\frac{d-1}{2}} l_s^{d-2}}{\sqrt{\pi} (2L_{wy})^{\frac{d-3}{2}}} K_{\frac{d-3}{2}} (E_b^{\text{closed}} L_{wy}) \right) \left(\frac{(E_c^{\text{closed}})^{\frac{d-1}{2}} l_s^{d-2}}{\sqrt{\pi} (2L_{wz})^{\frac{d-3}{2}}} K_{\frac{d-3}{2}} (E_c^{\text{closed}} L_{wz}) \right), \quad (3.56)$$

where $L_{wx} = |X^\perp - W^\perp|$, $L_{wy} = |Y^\perp - W^\perp|$, and $L_{wz} = |Z^\perp - W^\perp|$. In equation (3.56), we have employed the decomposition (3.12) of the Polyakov operators and used the massive propagator (3.14) derived from the effective action (3.13).

The Feynman integral (3.56) is heavily dominated by its saddle point contribution. For

each set of closed string states, the saddle point is given by the $(d-1)$ -dimensional vector $W^\perp = (W_1, W_2, \dots)$ that maximizes the integrand of (3.56). Finding such a vector reduces to the Fermat-Weber problem, which we solve perturbatively in powers of $R^{-1} \sim \beta^{-1}$. Denoting the energy levels of the closed string states in (3.5) by n_a , n_b , and n_c , we find that

$$W_{\text{saddle}}^\perp = \frac{L_s^2}{3\pi R^2} (2n_a - n_b - n_c, \sqrt{3}(n_b - n_c), 0, \dots) + O(R^{-3}) . \quad (3.57)$$

Near this saddle point, equation (3.56) reduces to a Gaussian integral at the leading order. It is convenient to introduce the following dual modular parameters:

$$\tilde{\mathbf{q}}_x \equiv e^{-\frac{2L_x}{R}} , \quad \tilde{\mathbf{q}}_y \equiv e^{-\frac{2L_y}{R}} , \quad \text{and} \quad \tilde{\mathbf{q}}_z \equiv e^{-\frac{2L_z}{R}} , \quad (3.58)$$

so that the partition function (3.56) takes the form [6]

$$\begin{aligned} Z_{\text{baryon}} = & \left(\frac{3\pi R}{L_x + L_y + L_z} \right)^{d-\frac{5}{2}} \left(\frac{(L_x + L_y + L_z)^2}{3(L_x L_y + L_y L_z + L_z L_x)} \right)^{\frac{d}{2}-2} \\ & \times \frac{e^{-2\pi R(L_x + L_y + L_z)/l_s^2}}{2^{\frac{d-1}{2}} (\tilde{\mathbf{q}}_x \tilde{\mathbf{q}}_y \tilde{\mathbf{q}}_z)^{\frac{d-2}{24}}} \sum_{a,b,c} \left(C_{abc}^{(0)} + O(\partial^2) \right) v_a v_b v_c \tilde{\mathbf{q}}_x^{n_a} \tilde{\mathbf{q}}_y^{n_b} \tilde{\mathbf{q}}_z^{n_c} . \end{aligned} \quad (3.59)$$

The open-closed duality of the baryon junctions identifies the two representations (3.30) and (3.59) of the partition function. This allows us to fix the coupling constants $C_{abc}^{(0)}$ by consistency conditions, even though the underlying confining gauge theory is strongly coupled. Indeed, the open channel terms in equations (3.34) and (3.43) admit expansions in $\tilde{\mathbf{q}}_x$, $\tilde{\mathbf{q}}_y$, and $\tilde{\mathbf{q}}_z$ using the modular transformation. Putting together $Z_{\text{baryon}}^{(0)}$, $\langle S_{\text{junction}}^{(1)} \rangle$, and the classical contribution (3.32) to the partition function, we find the four coupling constants involving the closed string states $\mathbf{0}$ and $\mathbf{1}$:

$$\begin{aligned} C_{\mathbf{000}}^{(0)} &= e^{-2\pi m_j R} \left[1 + \frac{(d+1)m_j l_s^2}{36R} + O(R^{-2}) \right] , \\ C_{\mathbf{001}}^{(0)} &= \frac{e^{-2\pi m_j R}}{3\sqrt{d-2}} \left[(d-4) + \frac{(d+1)(d+20)m_j l_s^2}{36R} + O(R^{-2}) \right] , \\ C_{\mathbf{011}}^{(0)} &= \frac{e^{-2\pi m_j R}}{9(d-2)} \left[(d^2 - 4d + 8) + \frac{(d^3 + 45d^2 - 236d - 88)m_j l_s^2}{36R} + O(R^{-2}) \right] , \\ C_{\mathbf{111}}^{(0)} &= \frac{e^{-2\pi m_j R}}{27(d-2)^{\frac{3}{2}}} \left[(d-4)(d^2 + 6d - 19) \right. \\ & \quad \left. + \frac{(d^4 + 73d^3 - 544d^2 + 2360d - 3360)m_j l_s^2}{36R} + O(R^{-2}) \right] . \end{aligned} \quad (3.60)$$

These coupling constants in (3.60) depend on the effective string parameters l_s and m_j , as well as on the radius R of Polyakov loops. They are independent of the operator positions (i.e., L_x , L_y , and L_z), as expected from the locality of the interaction vertices in (3.54).

Notably, the \mathbb{Z}_2 symmetry (3.45) constrains the interaction vertices in the effective potential $V(\Phi_a, \Phi_b, \dots)$ and implies selection rules for scattering processes. For example, the closed string ground state $\mathbf{0}$ is even under the \mathbb{Z}_2 transformation, while the excited state $\mathbf{1}$ is odd. By the \mathbb{Z}_2 symmetry, the coupling constants in (3.54) must satisfy

$$C_{\mathbf{001}}^{(0)} = C_{\mathbf{111}}^{(0)} = 0, \quad (3.61)$$

in agreement with the explicit results (3.60) with $d = 4$ and $m_j = 0$. In general, we expect the \mathbb{Z}_2 symmetry to be accidental, with the baryon junction acquiring a nonzero mass $m_j \sim l_s^{-1}$. The s -wave scattering processes in 4 dimensions are associated with different scales, corresponding to the \mathbb{Z}_2 symmetry-preserving (SP) and symmetry-breaking (SB) channels:

$$\Lambda_{s\text{-wave}}^{\text{SP}} \sim R l_s^{-2} e^{-\frac{4\pi}{3} m_j R}, \quad \text{and} \quad \Lambda_{s\text{-wave}}^{\text{SB}} \sim m_j^{\frac{2}{3}} R^{\frac{1}{3}} l_s^{-\frac{2}{3}} e^{-\frac{4\pi}{3} m_j R}. \quad (3.62)$$

Around the saddle point (3.57), we can incorporate non-Gaussian corrections to the Feynman integral (3.56) through a perturbative expansion. This is carried out in [7]. In particular, we find that the s -wave scattering amplitude corresponding to the equilateral baryon reads

$$\begin{aligned} Z_{\text{baryon}} = & \left(\frac{\pi R}{L} \right)^{d-\frac{5}{2}} \frac{e^{-6\pi R L / l_s^2}}{2^{\frac{d-1}{2}} \tilde{\mathbf{q}}^{\frac{d-2}{8}}} \sum_{a,b,c} C_{abc}^{(0)} v_a v_b v_c \tilde{\mathbf{q}}^{n_a+n_b+n_c} \left\{ 1 - \frac{l_s^2}{6\pi R^2} \left[\frac{4d^2 - 32d + 59}{4 \ln \tilde{\mathbf{q}}} \right. \right. \\ & + \frac{(2d-5)}{8} (d-2 - 8(n_a + n_b + n_c)) + \left(\frac{(d-2)^2}{64} - \frac{d-2}{4} (n_a + n_b + n_c) \right. \\ & \left. \left. + 6(n_a^2 + n_b^2 + n_c^2) - (n_a + n_b + n_c)^2 \right) \ln \tilde{\mathbf{q}} \right] + O(\partial^4) \left. \right\}, \quad (3.63) \end{aligned}$$

where we have $\tilde{\mathbf{q}}_x = \tilde{\mathbf{q}}_y = \tilde{\mathbf{q}}_z = \tilde{\mathbf{q}}$. The locality of the interaction vertices in (3.54) requires the coupling constants $C_{abc}^{(0)}$ to be independent of the confining string length $L \sim \ln \tilde{\mathbf{q}}$. For the open-closed duality to be consistent, the terms scaling as $(\ln \tilde{\mathbf{q}})^1$ and $(\ln \tilde{\mathbf{q}})^{-1}$ in equation (3.63) must match exactly with those obtained from the open-channel calculation at order 2. In the next section, we will show that this is indeed the case.

3.3.2 Nonlinear corrections to the partition function

As shown in Figure 3.5, the order 2 nonlinear corrections to the partition function (3.30) are evaluated by loop diagrams either on confining string worldsheets or localized on the baryon junction worldline. The loop integrals in $\langle S_{\text{displacement}}^{(2)} \rangle$, $\langle S_{\text{strings}}^{(2)} \rangle$, $\langle (S_{\text{junction}}^{(1)})^2 \rangle$, and

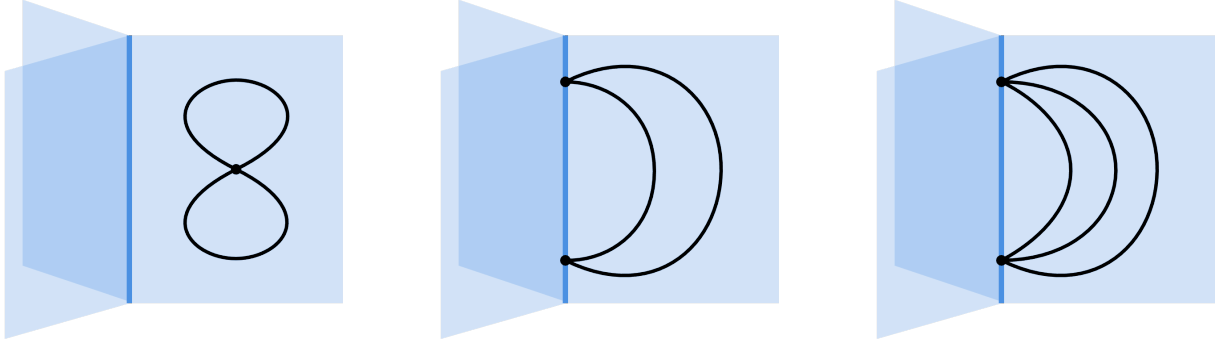


Figure 3.5: Worldsheet loop diagrams. The black lines denote the propagators of the NGB fields x_i , y_i , and z_i . See appendix in [7] for the explicit forms of these propagators. Left: $\langle S_{\text{strings}}^{(2)} \rangle$ is given by the 2-loop diagrams on the confining string worldsheets; Middle: $\langle (S_{\text{junction}}^{(1)})^2 \rangle$ is given by the 1-loop diagrams on the baryon junction worldline; Right: $\langle (S_{\text{displacement}}^{(1)})^2 \rangle$ is given by the 2-loop diagrams on the baryon junction worldline.

$\langle (S_{\text{displacement}}^{(1)})^2 \rangle$ are generally UV divergent. In [7], we adopt the zeta-function regularization and extract the finite contribution from these loop integrals. Below, we present the results for equilateral baryons and comment on their implications for open-closed duality.

We start with the quartic interaction (3.29) at the baryon junction arising from longitudinal displacements. Under zeta-function regularization, we find

$$\langle S_{\text{displacement}}^{(2)} \rangle = 0 . \quad (3.64)$$

The quartic interaction (3.22) on the confining string worldsheets follows from the Nambu-Goto action. Using zeta-function regularization once again, we obtain $\langle S_{\text{strings}}^{(2)} \rangle$ in terms of the Eisenstein series

$$\begin{aligned} \langle S_{\text{strings}}^{(2)} \rangle = \frac{\pi l_s^2}{13824L^2} (\ln \mathbf{q}) & \left[2(d+1)E_4(\sqrt{\mathbf{q}}) + 4(d-4)(d-10)((E_2(\mathbf{q}))^2 \right. \\ & + 24(d-4)E_4(\mathbf{q}) + (d^2 - 4d - 1)(E_2(\sqrt{\mathbf{q}}))^2 \\ & \left. + 4(d-1)(d-4)E_2(\sqrt{\mathbf{q}})E_2(\mathbf{q}) \right] . \end{aligned} \quad (3.65)$$

Here, the result is expressed in terms of $\mathbf{q} = \exp(-2\pi^2 R/L)$. In the open channel, equation (3.65) represents subleading corrections to the probe baryon energy levels E_{baryon} . After being weighted by the Boltzmann factor $\exp(-\beta E_{\text{baryon}})$, these corrections scale with positive powers of $\ln \mathbf{q} \sim \beta$. Alternatively, we can recast (3.65) in terms of the dual variable $\tilde{\mathbf{q}} =$

$\exp(-2L/R)$ using the modular transformation. We find that

$$\begin{aligned}
\langle S_{\text{strings}}^{(2)} \rangle &= \frac{(4d^2 - 28d + 47)l_s^2}{24\pi R^2(\ln \tilde{\mathbf{q}})} \\
&+ \frac{l_s^2}{144\pi R^2} \left[(d-4)(2d-11)E_2(\tilde{\mathbf{q}}) + 2(2d^2 - 9d + 3)E_2(\tilde{\mathbf{q}}^2) \right] \\
&+ \frac{l_s^2}{3456\pi R^2} (\ln \tilde{\mathbf{q}}) \left[8(d+1)E_4(\tilde{\mathbf{q}}^2) + 4(d^2 - 4d - 1)(E_2(\tilde{\mathbf{q}}^2))^2 \right. \\
&\quad \left. + 6(d-4)E_4(\tilde{\mathbf{q}}) + (d-4)(d-10)(E_2(\tilde{\mathbf{q}}))^2 \right. \\
&\quad \left. + 4(d-1)(d-4)E_2(\tilde{\mathbf{q}})E_2(\tilde{\mathbf{q}}^2) \right], \tag{3.66}
\end{aligned}$$

where it splits into terms that scale as $(\ln \tilde{\mathbf{q}})^{-1}$, $(\ln \tilde{\mathbf{q}})^0$ and $(\ln \tilde{\mathbf{q}})^1$. As we will show shortly, the $(\ln \tilde{\mathbf{q}})^0$ term in (3.65) encodes corrections to the local interaction vertices $C_{abc}^{(0)}$ in the closed channel, whereas the $(\ln \tilde{\mathbf{q}})^{-1}$ and $(\ln \tilde{\mathbf{q}})^1$ terms follow from the tree-level Feynman integral (3.56).

The kinetic action of the baryon junction (3.25) generates the following nonlinear corrections at order 2:

$$\begin{aligned}
\langle (S_{\text{junction}}^{(1)})^2 \rangle &= \frac{(d+5)m_j^2 l_s^4}{216L^2} (\ln \mathbf{q}) \left[2E_2(\mathbf{q}) - E_2(\sqrt{\mathbf{q}}) \right] \\
&+ \frac{m_j^2 l_s^4}{20736L^2} (\ln \mathbf{q})^2 \left[2(d+5)E_4(\sqrt{\mathbf{q}}) + (d^2 - 9)(E_2(\sqrt{\mathbf{q}}))^2 \right. \\
&\quad \left. - 8(d+5)E_4(\mathbf{q}) - 4(d+1)^2 E_2(\sqrt{\mathbf{q}})E_2(\mathbf{q}) \right. \\
&\quad \left. + 4(d^2 + 4d + 11)(E_2(\mathbf{q}))^2 \right]. \tag{3.67}
\end{aligned}$$

As in (3.65), (3.67) represents subleading corrections to the probe baryon energy levels, with the corresponding terms scaling as $\ln \mathbf{q} \sim \beta$ and $(\ln \mathbf{q})^2 \sim \beta^2$. In the dual variable $\tilde{\mathbf{q}}$, we find

$$\begin{aligned}
\langle (S_{\text{junction}}^{(1)})^2 \rangle &= \frac{m_j^2 l_s^4}{1296R^2} \left[8(d+5)E_4(\tilde{\mathbf{q}}^2) - 2(d+5)E_4(\tilde{\mathbf{q}}) - 4(d+1)^2 E_2(\tilde{\mathbf{q}})E_2(\tilde{\mathbf{q}}^2) \right. \\
&\quad \left. + (d^2 + 4d + 11)(E_2(\tilde{\mathbf{q}}))^2 + 4(d^2 - 9)(E_2(\tilde{\mathbf{q}}^2))^2 \right], \tag{3.68}
\end{aligned}$$

so that it scales as $(\ln \tilde{\mathbf{q}})^0$, indicating that the baryon junction mass m_j affects only the local interaction vertices in the effective action (3.13).

Finally, the longitudinal displacements (3.28) gives rise to the nonlinear correction

$$\langle (S_{\text{displacement}}^{(1)})^2 \rangle = \frac{\pi l_s^2}{1728L^2} (\ln \mathbf{q}) \left[(E_2(\sqrt{\mathbf{q}}))^2 + 4(d-4)(E_2(\mathbf{q}))^2 - E_4(\sqrt{\mathbf{q}}) - 4(d-4)E_4(\mathbf{q}) \right]. \quad (3.69)$$

Unlike the corrections from the world line kinetics (i.e., $\langle S_{\text{junction}}^{(1)} \rangle$ and $\langle (S_{\text{junction}}^{(1)})^2 \rangle$), (3.69) contains contributions scaling as $(\ln \tilde{\mathbf{q}})^{-1}$, $(\ln \tilde{\mathbf{q}})^0$ and $(\ln \tilde{\mathbf{q}})^1$ when written in terms of the variable $\tilde{\mathbf{q}}$:

$$\langle (S_{\text{displacement}}^{(1)})^2 \rangle = \frac{(d-3)l_s^2}{3\pi R^2 (\ln \tilde{\mathbf{q}})} + \frac{l_s^2}{18\pi R^2} \left[(d-4)E_2(\tilde{\mathbf{q}}) + 2E_2(\tilde{\mathbf{q}}^2) \right] + \frac{l_s^2}{432\pi R^2} (\ln \tilde{\mathbf{q}}) \times \left[4(E_2(\tilde{\mathbf{q}}^2))^2 + (d-4)(E_2(\tilde{\mathbf{q}}))^2 - (d-4)E_4(\tilde{\mathbf{q}}) - 4E_4(\tilde{\mathbf{q}}^2) \right]. \quad (3.70)$$

As a side remark, our analysis yields predictions for the baryon spectrum that can be tested in lattice simulations. In particular, we consider the ground state energy of an equilateral baryon (3.40). From the open-channel interpretation and results in (3.41), (3.44), (3.64), (3.65), (3.67), and (3.69), we find that

$$E_{\text{GS}} = \frac{3L}{l_s^2} + m_j - \frac{(d-3)\pi}{16L} - \frac{(d+1)\pi m_j l_s^2}{144L^2} + \frac{(d+5)\pi m_j^2 l_s^4}{432L^3} - \frac{(d-3)^2 \pi^2 l_s^2}{1536L^3} + O(L^{-4}). \quad (3.71)$$

Notably, the quantum corrections in (3.71) are fixed by the two classical parameters (i.e., the string tension l_s^{-2} and the junction mass m_j) up to the next-to-next-to-leading order. This is a consequence of the Poincaré symmetry and diffeomorphism invariance on the confining string worldsheet.

On the other hand, by matching the closed-channel interpretation (3.63) with the results (3.64), (3.66), (3.68), and (3.70), we determine the two cubic coupling constants $C_{\mathbf{000}}^{(0)}$ and $C_{\mathbf{001}}^{(0)}$. We find that

$$C_{\mathbf{000}}^{(0)} = e^{-2\pi m_j R} \left[1 + \frac{(d+1)m_j l_s^2}{36R} + \frac{5(d-2)l_s^2}{144\pi R^2} + \frac{(d+1)^2 m_j^2 l_s^4}{2592R^2} + O(R^{-3}) \right],$$

$$C_{\mathbf{001}}^{(0)} = \frac{e^{-2\pi m_j R}}{3\sqrt{d-2}} \left[(d-4) + \frac{(d+1)(d+20)m_j l_s^2}{36R} + \frac{(d-4)(5d-178)l_s^2}{144\pi R^2} + \frac{(d^3 + 46d^2 - 487d - 2836)m_j^2 l_s^4}{2592R^2} + O(R^{-3}) \right]. \quad (3.72)$$

which are independent of $L \sim \ln \tilde{\mathbf{q}}$. In particular, we note that $C_{\mathbf{001}}^{(0)} = O(R^{-3})$ when $d = 4$ and $m_j = 0$. This agrees with the selection rule (3.61) that follows from the \mathbb{Z}_2 symmetry (3.45) of the low-energy effective theory.

Chapter 4

Defects in Atomic Quantum Gases

While defects in relativistic quantum field theories exhibit rich and intriguing physics, as we have discussed extensively in Chapters 2 and 3, experimental setups often involve nonrelativistic systems that are Galilean invariant. In particular, atomic quantum gases provide versatile platforms for realizing and probing many-body phenomena in controllable settings. Prominent examples of these nonrelativistic systems include Bose–Einstein condensates confined in traps and ultracold Fermi gases with tunable interactions. For reviews of this broad and active field of research, see, e.g., [161–164].

The framework of RG flow extends naturally to nonrelativistic quantum gases. At long distances, the dynamics of atomic degrees of freedom are described by quantum fields with couplings that generally run under scale transformations. Fixed points of such RG flows are commonly referred to as nonrelativistic CFTs. The Jackiw–Pi models [165–168] furnish an important class of examples. These models describe the dynamics of abelian and non-abelian anyons in 2-dimensional space and exhibit emergent nonrelativistic conformal symmetry. We refer the reader to [169–175] for representative works on formal aspects of nonrelativistic CFTs, and to [176] for a modern review.

In this chapter, we discuss universal aspects of defects in atomic quantum gases using the formalism developed in [8]. We also study a concrete example with direct experimental relevance, drawn from [9]. The sections are organized as follows. Section 4.1 provides a pedagogical review of Galilean symmetry and the extended Schrödinger symmetry. In Section 4.2, we study the long-distance dynamics of point-like impurities immersed in dilute quantum gases. In particular, we apply DCFT methods to conformal defects in free and unitary Fermi gases. Finally, in Section 4.3, we study the effective theory of superfluids that emerge from quantum gases at large particle density. We analyze the giant vortex, a macroscopic defect recently observed in superfluid experiments [177].

Before concluding this preface, we highlight a change in convention: throughout this chapter, we use d to denote the dimension of the space. This is clearly more convenient for nonrelativistic systems, where time and space play distinct roles. For reasons that will become clear shortly, we will also refer to nonrelativistic CFTs as Schrödinger field theories

in what follows.

4.1 Galilean field theories

Just as the dynamics of relativistic field theories are governed by Poincaré symmetry, the nonrelativistic systems are subject to the Galilean symmetry. In d -dimensional space, the simply connected part of the Galilean group is generated by spatial translations P_μ , $\mathfrak{so}(d)$ spatial rotations $J_{\mu_1\mu_2}$, Galilean boosts B_μ , and time translation H . Both the translations and boosts transform as vectors under the rotation, with the corresponding commutation relations

$$\begin{aligned} [J_{\mu_1\mu_2}, J_{\mu_1\mu_2}] &= i(\delta_{\mu_1\mu_3}J_{\mu_2\mu_4} - \delta_{\mu_2\mu_3}J_{\mu_1\mu_4} + \delta_{\mu_1\mu_4}J_{\mu_3\mu_2} - \delta_{\mu_2\mu_4}J_{\mu_3\mu_1}) ; \\ [J_{\mu_1\mu_2}, P_{\mu_3}] &= i(\delta_{\mu_1\mu_3}P_{\mu_2} - \delta_{\mu_2\mu_3}P_{\mu_1}) ; \\ [J_{\mu_1\mu_2}, B_{\mu_3}] &= i(\delta_{\mu_1\mu_3}B_{\mu_2} - \delta_{\mu_2\mu_3}B_{\mu_1}) . \end{aligned} \tag{4.1}$$

Time translations are generated by the Hamiltonian H , which commutes with spatial translations and rotations. Galilean boosts, however, act as $x_\mu \rightarrow x_\mu + v_\mu t$ and therefore involve the time coordinate. This leads to the commutation relation

$$[H, B_\mu] = -iP_\mu . \tag{4.2}$$

With all other commutators vanishing, (4.1) and (4.2) define the Galilean algebra acting on spacetime coordinates.

The Galilean algebra can be extended to the Bargmann algebra by introducing a central element in the commutation relation between spatial translations and Galilean boosts:

$$[B_{\mu_1}, P_{\mu_2}] = i\delta_{\mu_1\mu_2}M . \tag{4.3}$$

The central charge M has the physical interpretation of nonrelativistic mass and generates the $U(1)$ particle number symmetry. The fact that Galilean invariant systems are associated with a $U(1)$ symmetry might be odd at first sight. Denoting the speed of light by c , one finds that anti-particles decouple from the spectrum in the $c \rightarrow \infty$ limit of relativistic systems. The Hilbert space consequently decomposes into superselection sectors of fixed particle number, giving rise to the $U(1)$ symmetry.

As a simple example of a Galilean field theory, we consider the action of a free complex scalar field

$$S_{\text{free}} = \int dt d^d x \left(i\phi^\dagger \partial_t \phi - \frac{|\partial_\mu \phi|^2}{2m} \right) , \tag{4.4}$$

where the parameter m is defined by $[M, \phi^\dagger] = m\phi^\dagger$. This theory also has an enhanced scaling symmetry, which we discuss below.

4.1.1 Schrödinger symmetry

We now consider the analogue of conformal symmetry in nonrelativistic systems. The Schrödinger algebra $\mathfrak{sch}(d)$ is defined by extending the Bargmann algebra in d -dimensional space with dilation D and special conformal transformation C . Notably, the dispersion relation of the free model (4.4) has dynamical critical exponent $z = 2$.¹ We thus consider scaling transformations that act differently on the spatial and temporal directions. In particular, generators of the Galilean transformations are of the weight

$$[D, P_\mu] = iP_\mu, \quad [D, H] = 2iH, \quad [D, B_\mu] = -iB_\mu. \quad (4.5)$$

When acting on local operators, H and P_μ raise their scaling dimensions by 2 and 1, while B_μ reduces scaling dimensions by 1. The special conformal transformation C completes the Schrödinger algebra through the additional nontrivial commutation relations

$$[D, C] = -2iC, \quad [H, C] = -iD, \quad [C, P_\mu] = iB_\mu, \quad (4.6)$$

so that it reduces scaling dimensions by 2 when acting on local operators.

Dynamics of Schrödinger field theories are strongly constrained by the $\mathfrak{sch}(d)$ symmetry [169, 170, 173]. In particular, we consider the two-point functions of an operator \mathcal{O} that transform as a scalar under $\mathfrak{so}(d)$. The nonrelativistic mass $m(\mathcal{O})$ and the scaling dimension $\Delta(\mathcal{O})$ of the operator is given by the commutation relations

$$\begin{aligned} [M, \mathcal{O}] &= m(\mathcal{O})\mathcal{O}, \\ [D, \mathcal{O}] &= i(2t\partial_t + x^\mu\partial_\mu + \Delta(\mathcal{O}))\mathcal{O}. \end{aligned} \quad (4.7)$$

Parallel to the conformal descendants in relativistic theories, we can define descendants of \mathcal{O} by recursively acting on it with P_μ and H . On the other hand, a primary operator with nonzero mass² satisfies $[B_\mu, \mathcal{O}] = [C, \mathcal{O}] = 0$, where

$$\begin{aligned} [B_\mu, \mathcal{O}] &= (-it\partial_\mu + x_\mu m(\mathcal{O}))\mathcal{O}, \\ [C, \mathcal{O}] &= \left(-itx^\mu\partial_\mu - it^2\partial_t - it\Delta(\mathcal{O}) + \frac{|x|^2}{2}m(\mathcal{O}) \right)\mathcal{O}. \end{aligned} \quad (4.8)$$

It is convenient to introduce the Wick rotation of the time coordinate $t \rightarrow -i\tau$, so that the convergence of the correlation functions becomes rapidly apparent. Let us now consider the two-point function $\langle \mathcal{O}\mathcal{O}^\dagger \rangle$. Due to the absence of antiparticles in the spectrum, operators

¹In Lifshitz theories [178–182], the dispersion relation generally takes the form $\omega \propto |k|^z$, where ω is the frequency and $|k|$ is the spatial wavenumber.

²The notion of a primary operator is ambiguous when $m(\mathcal{O}) = 0$, since P_μ and B_μ commute in these cases. To avoid confusion, we reserve the term bulk/defect primaries only for operators with nonzero charge under the particle-number symmetry.

in Schrödinger field theories can be normally ordered without encountering singularities [174, 175]. It follows that, for a non-identity operator, either $\mathcal{O}|0\rangle = 0$ or $\mathcal{O}^\dagger|0\rangle = 0$, where $|0\rangle$ denotes the vacuum. We will assume $\mathcal{O}|0\rangle = 0$ with $m(\mathcal{O}^\dagger) = -m(\mathcal{O}) > 0$, so that the two-point function $\langle \mathcal{O}(\tau, x)\mathcal{O}^\dagger(\tilde{\tau}, \tilde{x}) \rangle \propto \Theta(\tau - \tilde{\tau})$ yields a Euclidean time ordering.

The explicit functional form of $\langle \mathcal{O}\mathcal{O}^\dagger \rangle$ is also constrained by the translation and rotation symmetries of $\mathfrak{sch}(d)$ in a straightforward way. For primary operators, it is further fixed up to an overall constant by the conditions from (4.8), such that

$$\langle \mathcal{O}(\tau, x)\mathcal{O}^\dagger(\tilde{\tau}, \tilde{x}) \rangle = C_{\mathcal{O}\mathcal{O}^\dagger} \frac{\Theta(\tau - \tilde{\tau})}{|\tau - \tilde{\tau}|^{\Delta(\mathcal{O})}} \exp\left(-m(\mathcal{O}^\dagger) \frac{|x - \tilde{x}|^2}{2|\tau - \tilde{\tau}|}\right). \quad (4.9)$$

By contrast, three-point and higher-point functions in Schrödinger field theories depend on crossratios, and their functional forms can not be uniquely determined from the symmetry algebra $\mathfrak{sch}(d)$.

Another key aspect of Schrödinger field theories is the state/operator correspondence. We introduce the oscillator frame [173]:

$$t_{\text{osc}} = \frac{1}{\omega} \arctan(\omega t), \quad (x_{\text{osc}})_\mu = \frac{x_\mu}{\sqrt{1 + \omega^2 t^2}}, \quad (4.10)$$

where ω denotes the harmonic frequency. Time translations in this frame are generated by

$$H_{\text{osc}} = H + \omega^2 C. \quad (4.11)$$

Importantly, the operator H_{osc} takes the form of the quantum mechanical Hamiltonian for particles in a harmonic trap. We consider the state

$$|\mathcal{O}^\dagger\rangle_{\text{osc}} \equiv e^{-H/\omega} \mathcal{O}^\dagger(t=0, x=0) |0\rangle, \quad \text{s.t.} \quad H_{\text{osc}} |\mathcal{O}^\dagger\rangle_{\text{osc}} = \omega \Delta(\mathcal{O}) |\mathcal{O}^\dagger\rangle_{\text{osc}}. \quad (4.12)$$

Here, the scaling dimension of the operator \mathcal{O} is interpreted as the energy of the quantum state $|\mathcal{O}^\dagger\rangle_{\text{osc}}$ in units of the trap frequency ω . Moreover, we consider the two-point function

$$\Psi_{\mathcal{O}}(\tau_{\text{osc}}, x_{\text{osc}}) \equiv \langle 0 | \mathcal{O}(\tau_{\text{osc}}, x_{\text{osc}}) |\mathcal{O}^\dagger\rangle_{\text{osc}} \propto \exp\left(-\omega \Delta(\mathcal{O}) \tau_{\text{osc}} - \omega m(\mathcal{O}^\dagger) \frac{|x_{\text{osc}}|^2}{2}\right), \quad (4.13)$$

where the Wick-rotation is $t_{\text{osc}} \rightarrow -i\tau_{\text{osc}}$. This is precisely the Hartree-Fock wave function of a many-body bound state in the harmonic trap. We therefore see that (4.12) and (4.13) establish the nonrelativistic state/operator correspondence.

4.1.2 Unitary Fermi gases

As noted previously, the free model (4.4) provides a simple example of a Schrödinger field theory. In this section, we introduce an interacting model with broad experimental applica-

tions; see [164, 183–185] and many references therein.

Unitary Fermi gases are systems of fermionic atoms with short-range attractive interactions tuned near the an s -wave Feshbach resonance [186–188]. For a dilute ultracold Fermi gas, we denote by k_F the Fermi momentum, which sets the typical interatomic distance, and by a_s the s -wave scattering length, which characterizes the interaction strength. In 3-dimensional space, this system has two perturbative regimes: the Bardeen–Cooper–Schrieffer limit, where $a_s < 0$ and $|a_s k_F| \ll 1$, and the Bose–Einstein condensate limit, where $a_s > 0$ and $|a_s k_F| \ll 1$. In the cross-over regime, where $|a_s| \gg k_F^{-1}$, the s -wave scattering length exceeds the interatomic distance. In this limit, the system approaches the unitarity bound, and the $\mathfrak{sch}(3)$ Schrödinger symmetry emerges [170, 171].

Unitary Fermi gases are strongly coupled in 3-dimensional space, which makes their dynamics particularly challenging to analyze. Nevertheless, they become perturbatively accessible when the spatial dimension $d \gtrsim 2$ or $d \lesssim 4$.

When $d \gtrsim 2$, unitary Fermi gases admit a perturbative Gross-Neveu type description. Let us now consider the case of a single-flavor Fermi gas. We represent the two spin components of the fermionic atoms by Grassmann fields ψ_\uparrow and ψ_\downarrow . At zero particle density, the interacting Fermi gas is described by the action

$$S_{\text{Fermi}} = \int dt d^d x \left(\sum_{\varsigma=\uparrow,\downarrow} \psi_\varsigma^\dagger \left(i\partial_t + \frac{\partial_\mu^2}{2m} \right) \psi_\varsigma + \frac{m}{\lambda} \Lambda^{d-2} \Phi^\dagger \Phi - (\Phi^\dagger \psi_\downarrow \psi_\uparrow + \text{h.c.}) \right), \quad (4.14)$$

where Λ sets a UV scale, λ is the coupling constant, and Φ denotes an auxiliary scalar field. We also note that the equation of motion identifies $\Phi^\dagger = \lambda_b \psi_\uparrow^\dagger \psi_\downarrow^\dagger$ as a composite two-body operator. Crucially, the RG flow associated with the coupling λ can be determined by considering loop Feynman diagrams in the two-body sector and is therefore 1-loop exact [171]. The corresponding beta function reads

$$-\beta(\lambda) = -\bar{\epsilon}\lambda - \frac{\lambda^2}{2\pi} + O(\bar{\epsilon}^3), \quad \text{where } \bar{\epsilon} \equiv d - 2 \ll 1. \quad (4.15)$$

Here we have omitted geometric factors that affect only the $O(\bar{\epsilon}^3)$ terms, while keeping all orders in λ . This beta function admits a stable trivial fixed point and a multicritical interacting fixed point with $\lambda_{\text{fixed}} = -2\pi\bar{\epsilon} + O(\bar{\epsilon}^2)$. We summarize that the scaling dimensions of the one-body and two-body operators at each fixed point as follows

$$\begin{aligned} \text{Free Fermi gas} : \quad & \lambda = 0, \quad \Delta(\psi_\varsigma) = \frac{d}{2}, \quad \Delta(\Phi) = d; \\ \text{Unitary Fermi gas} : \quad & \lambda = \lambda_{\text{fixed}} < 0, \quad \Delta(\psi_\varsigma) = \frac{d}{2}, \quad \Delta(\Phi) = 2. \end{aligned} \quad (4.16)$$

For the one-body operator ψ_ς , a non-renormalization theorem following from particle-number symmetry states that its scaling dimension is the same at the trivial and interacting fixed

points [175]. Moreover, at the interacting fixed point, the 1-loop exactness of the RG flow gives the exact result $\Delta(\Phi) = 2$.

When $d \lesssim 4$, the two-body operator Φ in the unitary Fermi gas approaches the scalar unitarity bound $\Delta \geq d/2$ [174]. The field Φ may therefore be regarded as a free scalar, up to perturbative corrections. Indeed, the interacting Fermi gas in this case is described by the action ³

$$S_{\text{Fermi}} = \int dt d^d x \left(\sum_{\varsigma=\uparrow,\downarrow} \psi_{\varsigma}^{\dagger} \left(i\partial_t + \frac{\partial_{\mu}^2}{2m} \right) \psi_{\varsigma} + \Phi^{\dagger} \left(i\partial_t + \frac{\partial_{\mu}^2}{4m} \right) \Phi - \frac{\Lambda^{\frac{4-d}{2}}}{m} (g\Phi^{\dagger}\psi_{\downarrow}\psi_{\uparrow} + \text{h.c.}) \right), \quad (4.17)$$

where g is a Yukawa-type coupling constant. As in (4.15), the beta function associated with the 1-loop exact RG flow of g reads

$$-\beta(|g|^2) = \epsilon|g|^2 - \frac{|g|^4}{8\pi^2} + O(\epsilon^3), \quad \text{where } \epsilon = 4 - d \ll 1. \quad (4.18)$$

This gives a stable interacting fixed point with $|g|_{\text{fixed}} = 8\pi^2\epsilon + O(\epsilon^2)$, corresponding to the unitary Fermi gas. At first sight, it may seem confusing that the unitary Fermi gas appears multicritical in (4.15), whereas it appears stable in (4.18). This is resolved by noting that the model (4.17) flows to the free Fermi gas under the relevant deformation

$$\delta S_{\text{Fermi}} = -\mu \int dt d^d x \Phi^{\dagger} \Phi, \quad (4.19)$$

where μ denotes the chemical potential for the particle represented by the field Φ .

4.2 Conformal defects in Schrödinger field theories

To understand the dynamics of a heavy defect immersed in atomic quantum gases, we now develop the DCFT formalism for Schrödinger field theories. In particular, we focus on defects that are point-like in space and extended along the time direction. Physically, these defects can model impurity atoms pinned by optical lattices and coupled locally to the ambient bath. See [189–191] for a limited selection of references on this broad research area.

The microscopic details of the defect and the ambient quantum gas vary from one experimental setup to another. Our goal is to determine what universalities, if any, emerge at long distances. We first note that the maximal conformal subalgebra preserved by a point-like

³To avoid double counting loop diagrams in the two-body sector, we introduce the counterterm

$$\delta S_{\text{Fermi}} = - \int dt d^d x \left(\Phi^{\dagger} \left(i\partial_t + \frac{\partial_{\mu}^2}{4m} \right) \Phi \right).$$

The resulting Feynman rules from (4.17) then agree with those from (4.14).

impurity is

$$\mathfrak{so}(2, 1) \times \mathfrak{so}(d) \subset \mathfrak{sch}(d) . \quad (4.20)$$

This is precisely the same conformal algebra (2.1) of line defects in relativistic CFTs. We therefore adopt the same conventions as in Section 2.1 and denote a defect primary of transverse spin s by $\hat{\mathcal{O}}^s$. Additionally, we assume that the defect preserves the particle number symmetry $U(1)$, thereby excluding local sources or sinks of atoms.

4.2.1 Bulk-to-defect OPE

We begin by setting our conventions. Without loss of generality, we take the defect to be located at $x_\mu = 0$. We also perform the Wick rotation to the time coordinate, so that $t \rightarrow -i\tau$. We normalize the defect operator $\hat{\mathcal{O}}^s$ such that its two-point function takes the form

$$\langle \hat{\mathcal{O}}^s(\tau) \hat{\mathcal{O}}^{s\dagger}(\tilde{\tau}) \rangle = \frac{\Theta(\tau - \tilde{\tau})}{|\tau - \tilde{\tau}|^{\Delta(\hat{\mathcal{O}}^s)}} , \quad (4.21)$$

where the Euclidean time ordering follows from the $U(1)$ particle number symmetry.

The Schrödinger symmetry imposes strong constraints on the bulk-to-defect two-point function $\langle \mathcal{O} \hat{\mathcal{O}}^{s\dagger} \rangle$. The argument closely parallels the derivation of the relativistic result (2.6). By the particle number symmetry, $\langle \mathcal{O} \hat{\mathcal{O}}^{s\dagger} \rangle = 0$ unless $m(\mathcal{O}) = m(\hat{\mathcal{O}}^s)$, which we assume from now on. Using Ward identities following from (4.8), we further fix the two-point function of primary operators up to an overall coefficient:

$$\langle \mathcal{O}(\tau, x) \hat{\mathcal{O}}^{s\dagger}(\tilde{\tau}) \rangle = C_{\mathcal{O}}^{\hat{\mathcal{O}}^s} \frac{\Theta(\tau - \tilde{\tau}) Y_s(x_\mu/|x|)}{|\tau - \tilde{\tau}|^{\Delta(\hat{\mathcal{O}}^s)} |x|^{\Delta(\mathcal{O}) - \Delta(\hat{\mathcal{O}}^s)}} \exp\left(-\frac{m(\mathcal{O}^\dagger)|x|^2}{2|\tau - \tilde{\tau}|}\right) . \quad (4.22)$$

Here, $C_{\mathcal{O}}^{\hat{\mathcal{O}}^s}$ is the corresponding bulk-to-defect OPE coefficient. The two-point function (4.22) implies that, as the bulk scalar operator \mathcal{O} approaches the defect at $x_\mu = 0$, it admits the following decomposition

$$\mathcal{O}(\tau, x) = \sum_{\hat{\mathcal{O}}^s} \frac{Y_s(x_\mu/|x|)}{|x|^{\Delta(\mathcal{O}) - \Delta(\hat{\mathcal{O}}^s)}} C_{\mathcal{O}}^{\hat{\mathcal{O}}^s} \sum_{n \geq 0} \frac{\left(-\frac{m(\mathcal{O}^\dagger)}{2}|x|^2 \partial_\tau\right)^n}{n! (\Delta(\hat{\mathcal{O}}^s))_n} \hat{\mathcal{O}}^s(\tau) . \quad (4.23)$$

A careful treatment of the convergence of the operator equation (4.23), as well as the associated crossing equation, lies beyond the scope of our discussion. We refer the reader to [173, 175] for relevant studies.

Under the state/operator correspondence, the defect operator $\hat{\mathcal{O}}^s$ is mapped to an energy eigenstate in a harmonic trap deformed by delta-function potentials at the center. This can be seen as follows. Since the defect preserves the $\mathfrak{so}(2, 1)$ conformal algebra, we can construct

defect states in the oscillator frame (4.10), in direct analogy with (4.12), as follows:

$$|\hat{\mathcal{O}}^{s\dagger}\rangle_{\text{osc}} \equiv e^{-H/\omega} \hat{\mathcal{O}}^{s\dagger}(t=0) |0\rangle, \quad \text{s.t.} \quad H_{\text{osc}} |\hat{\mathcal{O}}^{s\dagger}\rangle_{\text{osc}} = \omega \Delta(\hat{\mathcal{O}}^s) |\hat{\mathcal{O}}^{s\dagger}\rangle_{\text{osc}}. \quad (4.24)$$

The scaling dimensions of defect operators therefore correspond to energy levels measured in units of the harmonic frequency ω , as in the case of bulk operators.

In the oscillator frame, the two-point function of primary operators (4.22) takes the form

$$\begin{aligned} \Psi_{\hat{\mathcal{O}}^s}(\tau_{\text{osc}}, x_{\text{osc}}) &\equiv \langle 0 | \mathcal{O}(\tau_{\text{osc}}, x_{\text{osc}}) | \hat{\mathcal{O}}^s \rangle_{\text{osc}} \\ &\propto \frac{Y_s(x_\mu/|x|)}{|x_{\text{osc}}|^{\Delta(\mathcal{O}) - \Delta(\hat{\mathcal{O}}^s)}} \exp\left(-\omega \Delta(\hat{\mathcal{O}}^s) \tau_{\text{osc}} - \omega m (\mathcal{O}^\dagger) \frac{|x_{\text{osc}}|^2}{2}\right). \end{aligned} \quad (4.25)$$

This is precisely the Hartree-Fock wave function of a bound state with angular momentum s and falloff $|x_{\text{osc}}|^{\Delta(\hat{\mathcal{O}}^s) - \Delta(\mathcal{O})}$ near the trap center. What about the defect descendant operators $\partial_\tau^n \hat{\mathcal{O}}^s$? Under the state/operator correspondence, these operators are mapped to excitations of the breathing modes [192, 193]. The creation (+) and annihilation (-) operators for these modes in the oscillator frame are given by

$$L_{\text{osc}}^\pm \equiv \frac{1}{2\omega} H - \frac{\omega}{2} C \pm iD. \quad (4.26)$$

4.2.2 One-body operators and s -wave resonance

We now discuss general properties of defect operators with unit charge under the $U(1)$ particle number symmetry. For concreteness, we present the argument in the Fermi gas model (4.14):

$$S_{\text{Fermi}} = \int d\tau d^d x \left(\sum_{\varsigma=\uparrow,\downarrow} \psi_\varsigma^\dagger \left(\partial_\tau - \frac{\partial_\mu^2}{2m} \right) \psi_\varsigma + \frac{\lambda}{m} \Lambda^{2-d} \psi_\uparrow^\dagger \psi_\downarrow^\dagger \psi_\downarrow \psi_\uparrow \right). \quad (4.27)$$

It follows from the absence of anti-particles that correlation functions of one-body operators, such as $\langle \psi_\varsigma \psi_\varsigma^\dagger \rangle$, are independent of the bulk coupling λ . We can thus work either in the free Fermi gas with $\lambda = 0$, in the unitary Fermi gas with $\lambda = \lambda_{\text{fixed}} < 0$, or in more complicated models with additional matter fields. In the absence of defects, we find

$$\begin{aligned} \langle \psi_\varsigma(\tau, x) \psi_\varsigma^\dagger(\tilde{\tau}, \tilde{x}) \rangle &= \delta_{\varsigma\tilde{\varsigma}} G(\tau - \tilde{\tau}, x - \tilde{x}; m), \\ \text{where } G(\tau, x; m) &\equiv \Theta(\tau) \left(\frac{m}{2\pi\tau} \right)^{d/2} \exp\left(-\frac{m|x|^2}{2\tau}\right). \end{aligned} \quad (4.28)$$

A simple example of the defect preserving the $SU(2)$ spin rotation symmetry is given by

$$S_{\text{impurity}} = \frac{\hat{\lambda}}{m} \Lambda^{2-d} \int_{x=0} d\tau (\psi_{\uparrow}^{\dagger} \psi_{\uparrow} + \psi_{\downarrow}^{\dagger} \psi_{\downarrow}) , \quad (4.29)$$

which can be viewed as a local spike in the chemical potential, or equivalently as the two-body interaction between the fermionic atoms and the heavy impurity. More generally, one may include other interaction vertices or additional degrees of freedom localized on the defect. For the one-body sector, however, it suffices to consider the bilinear deformation in (4.29).

We denote the defect primaries with nonrelativistic mass m by $\psi_{\zeta}^{s\dagger}$ and consider the bulk-to-defect two-point function $\langle \psi_{\zeta} \psi_{\zeta}^{s\dagger} \rangle$. As for correlation functions of bulk one-body operators, applying the equation of motion to the ψ_{ζ} field yields

$$\left(\partial_{\tau} - \frac{\partial_{\mu}^2}{2m} \right) \langle \psi_{\zeta}(\tau, x) \psi_{\zeta}^{s\dagger}(\tilde{\tau}) \rangle \propto C_{\psi_{\zeta} \psi_{\zeta}^s} (\Delta(\psi_{\zeta}^s) + \frac{d}{2} + s - 2) (\Delta(\psi_{\zeta}^s) - \frac{d}{2} - s) = 0 , \quad (4.30)$$

where we have used (4.22). We therefore conclude that defect primaries with nonzero OPE coefficients must have either $\Delta(\hat{\psi}_{\zeta}^s) = \frac{d}{2} + s$ or $\Delta(\hat{\psi}_{\zeta}^s) = 2 - \frac{d}{2} - s$. This argument runs in close parallel to the analysis of DCFTs in relativistic free theories [3, 45, 56]. In nonrelativistic theories, however, the $U(1)$ particle number symmetry allows us to extend the argument to interacting cases.

We refer to defect RG fixed points with $\Delta(\hat{\psi}_{\zeta}^0) = 2 - \frac{d}{2}$ and $C_{\psi_{\zeta} \psi_{\zeta}^0} \neq 0$ as s -wave resonances. As in Section 2.4, the unitarity of the $\mathfrak{so}(2, 1)$ conformal algebra requires $\Delta(\hat{\psi}_{\zeta}^s) \geq 0$. We thus find that s -wave resonances only exist when the spatial dimension $d \leq 4$. In the model (4.29), the s -wave resonance fixed point is obtained by fine-tuning the coupling $\hat{\lambda}$ associated with the defect bilinear deformation to criticality. In this case, the bulk two-point function $\langle \psi_{\zeta} \psi_{\zeta}^{s\dagger} \rangle$ in the presence of a resonant conformal defect at $x_{\mu} = 0$ is given by

$$\langle \psi_{\zeta}(\tau, x) \psi_{\zeta}^{s\dagger}(\tilde{\tau}, \tilde{x}) \rangle = \delta_{\zeta \tilde{\zeta}} \left(G(\tau - \tilde{\tau}, x - \tilde{x}; m) + \delta G(\tau - \tilde{\tau}, x, \tilde{x}; m) \right) , \quad \text{where} \quad (4.31)$$

$$\delta G(\tau, x, \tilde{x}; m) = -\Theta(\tau) \frac{m \sin\left(\frac{d\pi}{2}\right) \Gamma\left(\frac{d}{2}\right)}{\pi^{\frac{d}{2}+1} \tau (|x| |\tilde{x}|)^{\frac{d}{2}-1}} K_{1-\frac{d}{2}}\left(m|x||\tilde{x}|/\tau\right) \exp\left(-\frac{m}{2\tau}(|x|^2 + |\tilde{x}|^2)\right) .$$

Our analysis of one-body operators applies to a broad class of conformal defects in Schrödinger field theories with local interactions. An important class of exceptions is provided by Schrödinger field theories with inverse-square nonlocal potentials [194–196]. Such potentials modify the equation of motion (4.30); we leave these exceptional cases for future work.

4.2.3 Defects in free and unitary Fermi gases

While the bulk interaction can be neglected for the dynamics of one-body operators, this is no longer true for many-body operators. In this section, we analyze the two-body operators in the defect model (4.29).

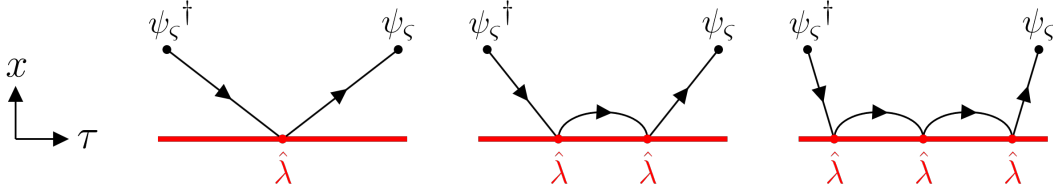


Figure 4.1: Ladder diagrams induced by the defect bilinear deformation. The red line denotes the defect extending in the time direction, while the directed black lines represent the free-field propagators in (4.28).

We begin by considering the defect immersed in a free Fermi gas. The RG flow of the defect coupling $\hat{\lambda}$ associated with the bilinear deformation (4.29) is determined by the loop diagrams in Figure 4.1. Importantly, these loop contributions form a recursive set of ladder diagrams as a consequence of the $U(1)$ particle-number symmetry. This indicates the one-loop exactness of the defect RG flow, and we find the beta function

$$-\beta(\hat{\lambda}) = -\bar{\epsilon}\hat{\lambda} - \frac{\hat{\lambda}^2}{\pi} + O(\bar{\epsilon}^3) \ , \quad \text{where } \bar{\epsilon} \equiv d - 2 \ll 1 \ . \quad (4.32)$$

As in (4.15), we have omitted geometric factors at $O(\bar{\epsilon}^3)$, while keeping all orders in $\hat{\lambda}$. The beta function (4.32) admits a stable trivial fixed point and a multicritical fixed point with $\hat{\lambda}_{\text{fixed}} = -\pi\bar{\epsilon} + O(\bar{\epsilon}^2)$. The latter fixed point, with $\hat{\lambda} = \hat{\lambda}_{\text{fixed}} < 0$, is precisely the s -wave resonance, for which the bulk two-point function is given by (4.31).

Let us consider the defect primaries appearing in the OPE (4.23) of the two-body operator $\Phi \propto \psi_\downarrow\psi_\uparrow$. For the free Fermi gas, the theory remains Gaussian with the defect bilinear deformation. Denoting these two-body defect primaries by $\hat{\Phi}^s$, we find the scaling dimensions

$$\begin{aligned} \text{Free Fermi gas} : \quad \Delta(\hat{\Phi}^0) &= 2\Delta(\hat{\psi}_\zeta^0) = 4 - d \ ; \\ \Delta(\hat{\Phi}^{s \geq 1}) &= \Delta(\hat{\psi}_\zeta^s) + \Delta(\hat{\psi}_\zeta^0) = 2 + s \ . \end{aligned} \quad (4.33)$$

Under the state/operator correspondence, this implies that the two-body wave function is given by the Slater determinant of the corresponding one-body wave functions. The energy of the two-body state is therefore simply the sum of the one-body energies. We also note that $\Delta(\hat{\Phi}^{s \geq 1})$ gives the energy of the spinning two-body ground state, where one particle is bound to the impurity and the other rotates around it.

We next consider the defect immersed in a unitary Fermi gas. Since the defect RG flow (4.32) can be determined from one-body operators, it is independent of bulk interactions and consequently remains one-loop exact in the unitary Fermi gas. In what follows, we focus on the s -wave resonance with the critical defect coupling $\hat{\lambda} = \hat{\lambda}_{\text{fixed}} < 0$.

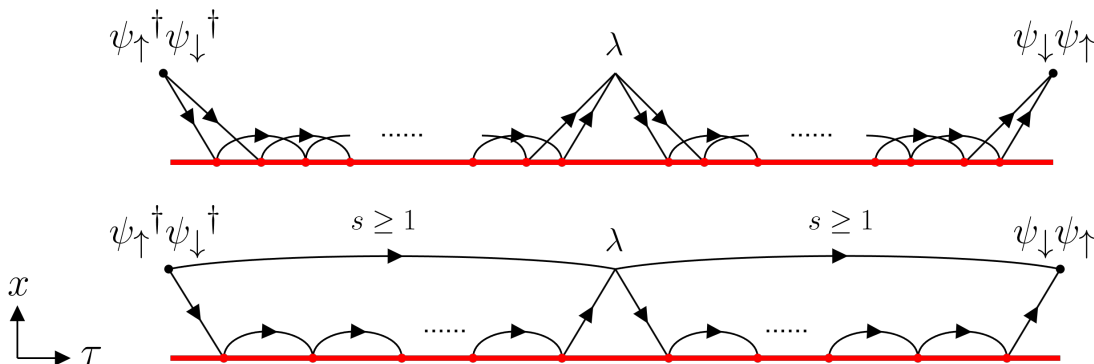


Figure 4.2: Leading Feynman diagrams contributing to the anomalous dimension of the defect two-body operator for $d \gtrsim 2$. Here and in Figure 4.3, we include the infinite ladder diagrams induced by the defect bilinear deformation.

As we reviewed in Section 4.1, the interaction between fermionic atoms becomes perturbative when the spatial dimension $d \gtrsim 2$ or $d \lesssim 4$. We first use the description (4.14), where $\bar{\epsilon} = d - 2 \ll 1$ and the bulk coupling $\lambda = O(\bar{\epsilon})$ is small. In the presence of the defect, the leading $O(\lambda)$ loop correction to the two-point function $\langle \Phi \Phi^\dagger \rangle$ is given by the Feynman diagrams in Figure 4.2. The corresponding Feynman integrals are collected in the appendices of [8]. In the limit where the operator Φ approaches the defect, we expand the two-point function using the bulk-to-defect OPE (4.23). We identify the perturbed scaling dimensions of the two-body defect primaries as follows

$$\begin{aligned} \text{Unitary Fermi gas at } d = 2 + \bar{\epsilon} : \quad \Delta(\hat{\Phi}^0) &= 2 - 2\bar{\epsilon} + O(\bar{\epsilon}^2) , \\ \Delta(\hat{\Phi}^{s \geq 1}) &= 2 + s - \frac{\bar{\epsilon}}{2^{s-1}} + O(\bar{\epsilon}^2) . \end{aligned} \tag{4.34}$$

Interestingly, we find that corrections to the energy levels of the spinning two-body state are exponentially suppressed at large spin s . This is because these corrections are controlled by the wave-function overlap between the particle bound to the impurity and the particle rotating around it, which becomes exponentially small at large s .

When $\epsilon = 4 - d \ll 1$, we instead use the description (4.17), where the bulk coupling satisfies $|g|^2 = O(\epsilon)$. The scaling dimensions of the two-body defect primaries can be computed using the same approach as in (4.34), with the $O(|g|^2)$ loop Feynman diagrams shown in Figure 4.3. We also refer the reader to the appendices of [8] for a detailed treatment of

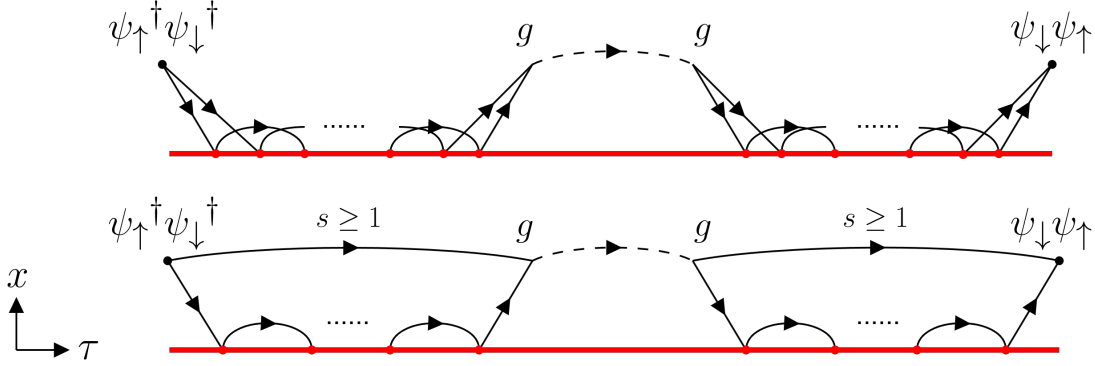


Figure 4.3: Leading Feynman diagrams contributing to the anomalous dimension of the defect two-body operator for $d \lesssim 4$.

the associated Feynman integrals. We find

$$\begin{aligned} \text{Unitary Fermi gas at } d = 4 - \epsilon : \quad \Delta(\hat{\Phi}^0) &= \frac{19}{3}\epsilon + O(\epsilon^2) , \\ \Delta(\hat{\Phi}^{s \geq 1}) &= 2 + s + O(\epsilon^2) . \end{aligned} \quad (4.35)$$

Under the state/operator correspondence, (4.35) implies that the energy levels of spinning two-body states remain unperturbed at $O(\epsilon)$. Qualitatively, this reflects the small wavefunction overlap at large spatial dimensions.

4.3 Giant superfluid vortices

In the previous section, we focused on atomic quantum gases at zero density. Experimental setups, however, typically involve quantum gases at finite particle density confined in traps. For bosonic systems, the $U(1)$ particle-number symmetry is often spontaneously broken at finite density. This occurs, for example, in ^4He and in trapped alkali-metal gases, which enter a superfluid phase at low temperatures. See [162, 197, 198], among many others, for reviews and references.

Vortices appear in the superfluid as the trap rotates. In 2-dimensional space, vortices are point-like defects in the particle condensate that carry angular momentum. As we increase the angular frequency of the trap, they form an Abrikosov lattice [199] and substantially change the superfluid dynamics.

Interestingly, superfluids exhibit new universalities at sufficiently high angular frequencies of the trap. It was predicted theoretically [200, 201] and observed experimentally [177] that a rapidly rotating superfluid forms a dynamical ring, which we investigate in the remainder

of this section.

4.3.1 Rapidly rotating superfluids

We begin by reviewing the low-energy effective theory of Galilean invariant superfluids in 2-dimensional space. Physically, we consider a Bose–Einstein condensate confined in a trap. At low energies, we neglect fluctuations of the condensate density and assume that the only remaining degree of freedom is the phase of the condensate wave function. Denoted by $\varphi \sim \varphi + 2\pi$, this phase is identified with the NGB of the $U(1)$ particle number symmetry.

To the lowest order in derivatives, the effective action of the condensate is written in terms of φ via the combination [202, 203]

$$\mathbf{X} \equiv D_t\varphi - \frac{(D_\mu\varphi)^2}{2m} . \quad (4.36)$$

where m is both the mass of the microscopic constituents and the central extension of the Galilean algebra (4.3). The NGB field φ couples to the background potential $\mathbf{V}(x)$ via the covariant derivative $D_t\varphi = \partial_t\varphi - A_t$ and $D_\mu\varphi = \partial_\mu\varphi - A_\mu$. In the static gauge, $A_t = \mathbf{V}(x)$ and $A_\mu = 0$. Accordingly,

$$\mathbf{X} = \partial_t\varphi - \frac{(\partial_\mu\varphi)^2}{2m} - \mathbf{V}(x) . \quad (4.37)$$

The low-energy effective action of the superfluid is given by a functional of \mathbf{X} with no additional derivatives,

$$S_{\text{superfluid}} = \int dt d^2x \mathbf{P}(\mathbf{X}) . \quad (4.38)$$

Given a classical background for the NGB field, $\mathbf{P}(\mathbf{X}_{\text{cl}})$ is identified with the thermodynamic pressure at chemical potential \mathbf{X}_{cl} . The functional form of $P(X)$ generally depends on the UV details of the superfluid, and it could be complicated even for weakly coupled microscopic models [204]. In particular, for Schrödinger field theories in d -dimensional space,

$$\mathbf{P}(\mathbf{X}) \propto \mathbf{X}^{\frac{d+2}{2}} . \quad (4.39)$$

This is analogous to the effective actions of conformal superfluids [205–208], which capture universalities in the large charge sector of relativistic CFTs. In the following, we will often use the 2-dimensional Schrödinger superfluids with $\mathbf{P}(\mathbf{X}) \propto \mathbf{X}^2$ as examples.

The superfluid action (4.38) yield the equation of motion

$$m\partial_t\mathbf{P}'(\mathbf{X}) - \partial^\mu(\mathbf{P}'(\mathbf{X})\partial_\mu\varphi) = 0 . \quad (4.40)$$

This equation admits classical solutions that take the form

$$\varphi_{\text{cl}} = \mu t \quad \Rightarrow \quad \mathbf{X}_{\text{cl}} = \mu - \mathbf{V}(x) , \quad (4.41)$$

where μ is the chemical potential. The parameter μ controls the total particle number in the trap, with the local particle density given by $\mathbf{P}'(\mathbf{X})$. Note that it is not physically meaningful to allow $\mathbf{P}'(\mathbf{X})$ to attain negative values – this restricts the domain of integration in (4.38) to where $\mathbf{P}'(\mathbf{X}) \geq 0$. We further assume that $\mathbf{P}'(\mathbf{X}) = 0$ for $\mathbf{X} = 0$. Physically, this means that the superfluid is confined to the region where $V(x) \leq \mu$. For finite-size condensates, we require that no particles flow through the boundary of the superfluid. To the leading orders in derivatives, this condition reads [209, 210]

$$\mathbf{P}'(\mathbf{X}) n_\mu^\perp \partial^\mu \varphi = 0 , \quad (4.42)$$

where n_μ^\perp is the unit vector transverse to the boundary.

When the trap is axisymmetric, the equation of motion (4.40) also admits another set of solutions. We introduce polar coordinates $r \geq 0$ and $\theta \sim \theta + 2\pi$, so that the axisymmetric trap $\mathbf{V}(x) = \mathbf{V}(r)$. We consider solutions with a single vortex at the center of the trap:

$$\varphi_{\text{cl}} = \mu t - J\theta \quad \Rightarrow \quad \mathbf{X}_{\text{cl}} = \mu - \frac{J^2}{2mr^2} - \mathbf{V}(r) , \quad (4.43)$$

where the vorticity $J \in \mathbb{Z}$ denotes the angular momentum carried by the superfluid.

The core size of conventional vortices is set by a UV scale of the Bose–Einstein condensate, known as the healing length ξ_h . See [211] and references therein. For small J , the vortex solution in (4.43) has a core size of order $J\xi_h$ and can be analyzed using the method of [212]. The superfluid rotates more rapidly as J increases. Consequently, the vortex core grows until its size becomes comparable to the size of the trap. In the limit $J \gg 1$, the superfluid is concentrated in a narrow annulus between the vortex core and the edge of the trap. We refer to vortices in this limit as giant vortices.

In the presence of a giant vortex, the superfluid system becomes effectively 1-dimensional. Do rapidly rotating superfluids exhibit universal low-energy dynamics? In the remainder of this section, we show that the dynamics of the superfluid circulating around the giant vortex are described by a Warped Conformal Field Theory (WCFT) [213–215], up to perturbative corrections.

4.3.2 Giant vortices in a hard-wall trap

Let us first consider superfluids confined in the region $r \leq R$ with $\mathbf{V}(r) = 0$, i.e., an axisymmetric hard-wall trap. We assume that the core of the giant vortex (4.43) occupies $r \leq (1 - \varepsilon)R$, with the superfluid concentrated in the annular region $(1 - \varepsilon)R \leq r \leq R$. See Figure 4.4. At the interior of the annulus $r = (1 - \varepsilon)R$, we expect the particle density $\mathbf{P}'(\mathbf{X}_{\text{cl}}) = 0$, and accordingly $\mathbf{X}_{\text{cl}} = 0$. It then follows that

$$\mathbf{X}_{\text{cl}} = \frac{J^2}{2m} \left(\frac{1}{(1 - \varepsilon)^2 R^2} - \frac{1}{r^2} \right) . \quad (4.44)$$

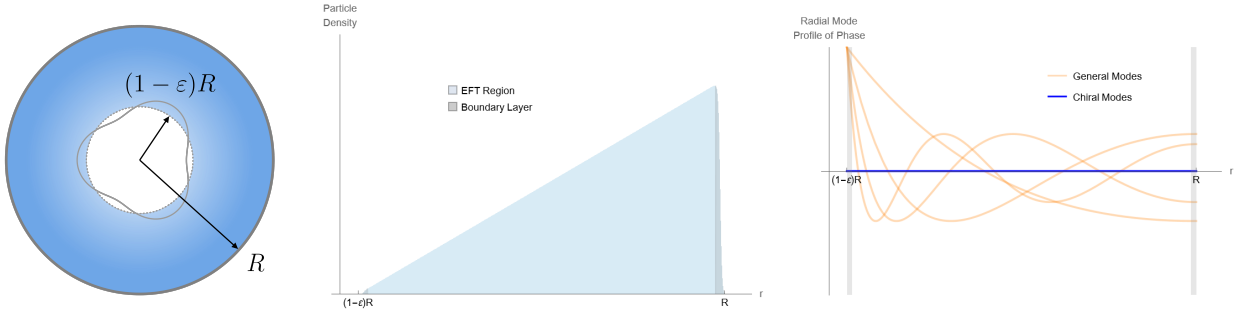


Figure 4.4: Particle density and eigenmode profiles of a giant vortex in a hard-wall trap. The figure shows a giant vortex in Schrödinger superfluids with $\mathbf{P}(\mathbf{X}) \propto \mathbf{X}^2$.

For concreteness, we take the Schrödinger superfluids as an example, with $\mathbf{P}(\mathbf{X}) = a\mathbf{X}^2$. The total particle number confined in the trap is then given by

$$N = \frac{2\pi a J^2}{m} \int_{(1-\varepsilon)R}^R r dr \left(\frac{1}{(1-\varepsilon)^2 R^2} - \frac{1}{r^2} \right) = \frac{\pi a J^2}{m} \left(\frac{1}{(1-\varepsilon)^2} - 1 + 2 \ln(1-\varepsilon) \right). \quad (4.45)$$

Keeping the particle number N fixed, we clearly see that $\varepsilon = O(1/J) \ll 1$ in the giant vortex limit.

We now analyze the spectrum of superfluid excitations in the limit $\varepsilon \ll 1$ while keeping the equation of state $\mathbf{P}(\mathbf{X})$ generic. Specifically, we expand $\varphi = \varphi_{\text{cl}} + \delta\varphi$ and solve for the eigenmodes of the quantum fluctuation $\delta\varphi$. These modes are labelled by the angular wave number $n \in \mathbb{Z}$ and the radial wave number $n' \in \mathbb{N}$, with the ansatz of the mode profile

$$\delta\varphi(t, r, \theta) = e^{-i\omega t + in\theta} \delta\varphi_{\tilde{n}}(r). \quad (4.46)$$

We also introduce the angular velocity of the rotating superfluid near the edge of the hard-wall trap,

$$\Omega = \frac{J}{mR^2}. \quad (4.47)$$

For modes with radial wave number $\tilde{n} \geq 1$, the profile (4.46) depends nontrivially on the coordinate r , and the corresponding eigenfrequencies take the form [9]

$$\omega_{n, \tilde{n}} = \Omega \left(\frac{k_{\tilde{n}}}{\sqrt{\varepsilon}} + n + O(\sqrt{\varepsilon}) \right), \quad (4.48)$$

where $k_{\tilde{n}} > 0$ are determined by the equation of state $\mathbf{P}(\mathbf{X})$. For Schrödinger superfluids, we further find that $k_{\tilde{n}} = j_{1, \tilde{n}}/2$, where $j_{1, \tilde{n}}$ denotes \tilde{n} -th zero of the Bessel function J_1 .

Modes with radial quantum number $\tilde{n} = 0$ have profiles that are independent of the

coordinate r . Their eigenfrequencies are

$$\omega_{n,0} = \Omega \left(n + \sqrt{\varepsilon} \alpha_{\mathbf{P}} |n| + O(\varepsilon) \right). \quad (4.49)$$

Here, the coefficient $\alpha_{\mathbf{P}}$ is given by

$$\alpha_{\mathbf{P}} \equiv \lim_{\varepsilon \rightarrow 0} \sqrt{\frac{\int d^2x \mathbf{P}'(\mathbf{X}_{\text{cl}})}{\mu_{\text{eff}} \int d^2x \mathbf{P}''(\mathbf{X}_{\text{cl}})}} > 0. \quad (4.50)$$

where $\mu_{\text{eff}} = \mu - \frac{J^2}{2mR^2}$ denotes the effective chemical potential. For example, the Schrödinger superfluids with $\mathbf{P}(\mathbf{X}) \propto \mathbf{X}^2$ give $\alpha_{\mathbf{P}} = \sqrt{2}/2$.

Let us now switch to a frame rotating with angular frequency Ω . The Hamiltonian in this frame is given by the differential operator

$$i(\partial_t + \Omega \partial_\theta), \quad (4.51)$$

with $\omega - n\Omega$ denoting the excitation energy of the mode (4.46). Notably, (4.51) takes the same form as the left-moving Virasoro zero mode of a relativistic CFT defined on a circle of circumference $2\pi/\Omega$. In the rotating frame, the modes in (4.48) have energies of the order $\Omega/\sqrt{\varepsilon}$, and therefore become ultramassive in units of Ω when $\varepsilon \ll 1$. By contrast, the modes in (4.49) have approximately zero energies of the order $\sqrt{\varepsilon}\Omega$. This implies that the modes with $\tilde{n} = 0$ can be effectively described by relativistic right-moving chiral waves. We therefore refer to them as chiral modes.

4.3.3 Giant vortices in smooth traps

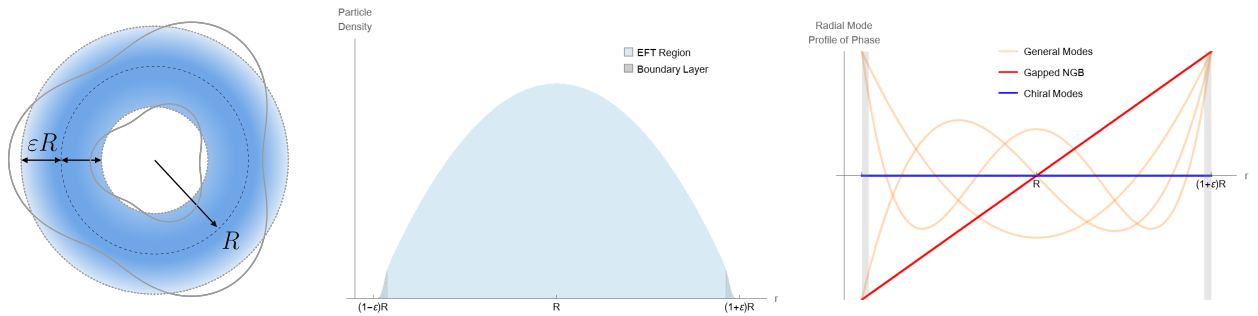


Figure 4.5: Particle density and eigenmode profiles of a giant vortex in smooth traps. The figure shows a giant vortex in Schrödinger superfluids with $\mathbf{P}(\mathbf{X}) \propto \mathbf{X}^2$.

In this section, we generalize the analysis to arbitrary smooth traps $\mathbf{V}(r)$ and formulate the WCFT description of the chiral modes. The superfluid occupies the region where the

particle density $\mathbf{P}'(\mathbf{X}_{\text{cl}}) \geq 0$, which we assume coincides with the region $\mathbf{X}_{\text{cl}} \geq 0$. Let R denote the radius at which \mathbf{X}_{cl} attains its maximum. It is then determined by

$$\frac{J^2}{mR^3} - \mathbf{V}'(R) = 0. \quad (4.52)$$

We also assume that (4.52) admits a unique solution, so that the superfluid concentrates in a single annulus. This condition holds for power-law traps $\mathbf{V}(r) \propto r^v$, which we will use as examples below.

For convenience, we introduce the following parameters

$$\mu_{\text{eff}} = \mu - \frac{J^2}{2mR^2} - \mathbf{V}(R) > 0, \quad \varepsilon = \sqrt{\frac{2m\mu_{\text{eff}}R^2}{3J^2 + R^2\mathbf{V}''(R)}}. \quad (4.53)$$

In particular, ε denotes the width of the superfluid annulus in units of R , which we assume to be small in the giant vortex limit $J \gg 1$. See Figure 4.5. The expansion of \mathbf{X}_{cl} near its maximum then takes the form

$$\mathbf{X}_{\text{cl}} = \mu_{\text{eff}} \left(1 - u^2 + O(\varepsilon) \right), \quad (4.54)$$

where we have introduced a new coordinate u through $r = (1 + \varepsilon u)R$. To the leading order in ε , the superfluid occupies the region $-1 \leq u \leq 1$, and R coincides with the center of the annulus. We also use Ω in (4.47) to denote the angular velocity of the superfluid at $r = R$.

The superfluid excitations of giant vortices in smooth traps can be analyzed in close analogy with the hard-wall trap case. We refer the readers to the appendix in [9] for further details. In the limit $\varepsilon \ll 1$, the dispersion relation involves the factor

$$\beta_{\mathbf{V}} \equiv \sqrt{\frac{m\mu_{\text{eff}}}{2}} \frac{R}{\varepsilon J}, \quad (4.55)$$

which roughly characterizes the steepness of the trap around $r = R$. For example, the power-law trap $\mathbf{V}(r) \propto r^v$ yields $\beta_{\mathbf{V}} = \sqrt{(v+2)/4}$.

For modes with nontrivial dependence in the radial direction, we find the eigenfrequencies

$$\omega_{n,\tilde{n}} = \Omega \left(n + \sqrt{2}\beta_{\mathbf{V}}k_{\tilde{n}} + O(\varepsilon) \right), \quad (4.56)$$

where $\tilde{n} \geq 1$. While $k_{\tilde{n}}$ with $\tilde{n} \geq 2$ are generally determined by the equation of state $\mathbf{P}(\mathbf{X})$ as in (4.48), we note that $k_1 = \sqrt{2}$ is universal. To the leading order in ε , these modes correspond to the extended symmetry generators of a locally harmonic trap [216]. For Schrödinger superfluids, we also find that $k_{\tilde{n}} = \sqrt{\tilde{n}(\tilde{n}+1)}$.

Interestingly, the modes with trivial radial dependence (i.e. $\tilde{n} = 0$) are non-tachyonic only for $\beta_{\mathbf{V}} > 1$. This has a simple physical interpretation: the trap must be steep enough

to balance the centrifugal force. For instance, a power-law trap $\mathbf{V}(r) \propto r^v$ supports stable giant-vortex excitations only for $v > 2$. For the stable modes, we find the eigenfrequencies

$$\omega_{n,0} = \Omega \left(n + \varepsilon \alpha_{\mathbf{P}} \sqrt{2(\beta_{\mathbf{V}}^2 - 1)} |n| + O(\varepsilon^2) \right), \quad (4.57)$$

where $\alpha_{\mathbf{P}}$ is given in (4.50).

The dispersion relation (4.57) implies that certain multi-phonon states are approximately degenerate. This occurs for any two Fock-space states, labeled by excitation numbers n_1^a, n_2^a, \dots and n_1^b, n_2^b, \dots , that satisfy $\sum_i n_i^a = \sum_i n_i^b$ and $\sum_i |n_i^a| = \sum_i |n_i^b|$. Given two such states, we find that the degeneracy is lifted at order $O(\varepsilon^3)$:

$$E(n_i^a) - E(n_i^b) = \Omega \left(\varepsilon^3 \gamma_{\mathbf{P},\mathbf{V}} \left(\sum_i |n_i^a|^3 - \sum_i |n_i^b|^3 \right) + O(\varepsilon^4) \right), \quad (4.58)$$

where $E(n_i^a)$ and $E(n_i^b)$ denote the energies of the corresponding multi-phonon states. Here, the coefficient $\gamma_{\mathbf{P},\mathbf{V}}$ depends on both the equation of state $\mathbf{P}(\mathbf{X})$ and the geometry of the trap $\mathbf{V}(r)$. It is given by

$$\begin{aligned} \gamma_{\mathbf{P},\mathbf{V}} = & - \frac{1}{\alpha_{\mathbf{P}} \sqrt{2(\beta_{\mathbf{V}}^2 - 1)} \int_{-1}^1 du \mathbf{P}''(\mu_{\text{eff}}(1 - u^2))} \\ & \times \int_{-1}^1 du \frac{\mu_{\text{eff}}}{\mathbf{P}'(\mu_{\text{eff}}(1 - u^2))} \left[\int_{-1}^u \frac{d\tilde{u}}{\beta_{\mathbf{V}}} \left(\frac{\beta_{\mathbf{V}}^2}{\mu_{\text{eff}}} \mathbf{P}'(\mu_{\text{eff}}(1 - \tilde{u}^2)) \right. \right. \\ & \left. \left. - \left(\alpha_{\mathbf{P}} \sqrt{\beta_{\mathbf{V}}^2 - 1} + \sqrt{2}\tilde{u} \right)^2 \mathbf{P}''(\mu_{\text{eff}}(1 - \tilde{u}^2)) \right) \right]^2 < 0. \end{aligned} \quad (4.59)$$

Crucially, the sign $\gamma_{\mathbf{P},\mathbf{V}} < 0$ implies that single-phonon states have lower energy than the corresponding multi-phonon states. For Schrödinger superfluids, (4.59) simplifies to

$$\gamma_{\mathbf{P},\mathbf{V}} = - \frac{\beta_{\mathbf{V}}^4 + 64\beta_{\mathbf{V}}^2 - 56}{45\beta_{\mathbf{V}}^2 \sqrt{3(\beta_{\mathbf{V}}^2 - 1)}} < 0. \quad (4.60)$$

Finally, we discuss the effective description for the chiral modes of giant vortices. We introduce the light-cone coordinates

$$z^{\pm} = t \pm \Omega^{-1}\theta, \quad (4.61)$$

so that the dispersion relation (4.57) can be reproduced from the effective action

$$S_{\text{chiral}} \propto \int dz^+ dz^- \left((\partial_+ \varphi)^2 + \frac{\varepsilon^2}{2} \alpha_{\mathbf{P}}^2 (\beta_{\mathbf{V}}^2 - 1) (\partial_+ \varphi - \partial_- \varphi)^2 + O(\varepsilon^3) \right). \quad (4.62)$$

To the leading order in ε , this effective action describes a free WCFT whose conformal symmetry is generated by a right-moving Virasoro algebra and a left-moving $U(1)$ Kac-Moody algebra. Additionally, the leading order action (4.62) also admits a fractonic shift symmetry $\varphi \rightarrow \varphi + \delta\varphi(x^-)$, which leads to infinite ground-state degeneracy in the rotating frame. These degeneracies are lifted by the $O(\varepsilon^2)$ marginal term in (4.62). Moreover, the degeneracies among excited states are lifted by an $O(\varepsilon^4)$ irrelevant term,

$$\int dz^+ dz^- ((\partial_+ - \partial_-)^2 \varphi)^2, \quad (4.63)$$

which corresponds to the correction in (4.58).

Bibliography

- [1] D. Gaiotto, A. Kapustin, N. Seiberg, and B. Willett, *Generalized Global Symmetries*, *JHEP* **02** (2015) 172, [[arXiv:1412.5148](#)].
- [2] D. S. Freed, G. W. Moore, and C. Teleman, *Topological symmetry in quantum field theory*, [arXiv:2209.07471](#).
- [3] S.-H. Shao and S. Zhong, *Where non-invertible symmetries end: twist defects for electromagnetic duality*, *JHEP* **01** (2026) 118, [[arXiv:2509.21279](#)].
- [4] A. Raviv-Moshe and S. Zhong, *Phases of surface defects in Scalar Field Theories*, *JHEP* **08** (2023) 143, [[arXiv:2305.11370](#)].
- [5] M. Barkeshli, C. Feuchis, Z. Komargodski, and S. Zhong, *Disclinations, Dislocations, and Emanant Flux at Dirac Criticality*, *Phys. Rev. X* **16** (2026), no. 1 011017, [[arXiv:2501.13866](#)].
- [6] Z. Komargodski and S. Zhong, *Baryon junction and string interactions*, *Phys. Rev. D* **110** (2024), no. 5 056018, [[arXiv:2405.12005](#)].
- [7] X. Lou and S. Zhong, *Baryon Junction and String Interactions: Part II*, [arXiv:2602.17771](#).
- [8] A. Raviv-Moshe and S. Zhong, *Impurities in Schrödinger field theories and s-wave resonance*, *JHEP* **09** (2025) 134, [[arXiv:2411.04040](#)].
- [9] G. Cuomo, Z. Komargodski, and S. Zhong, *Chiral modes of giant superfluid vortices*, *Phys. Rev. B* **110** (2024), no. 14 144514, [[arXiv:2312.06095](#)].
- [10] K. Jensen and A. O’Bannon, *Constraint on Defect and Boundary Renormalization Group Flows*, *Phys. Rev. Lett.* **116** (2016), no. 9 091601, [[arXiv:1509.02160](#)].
- [11] G. Cuomo, Z. Komargodski, and A. Raviv-Moshe, *Renormalization Group Flows on Line Defects*, *Phys. Rev. Lett.* **128** (2022), no. 2 021603, [[arXiv:2108.01117](#)].

- [12] T. Shachar, R. Sinha, and M. Smolkin, *RG flows on two-dimensional spherical defects*, *SciPost Phys.* **15** (2023), no. 6 240, [[arXiv:2212.08081](#)].
- [13] E. Witten, *Quantum Field Theory and the Jones Polynomial*, *Commun. Math. Phys.* **121** (1989) 351–399.
- [14] S. Elitzur, G. W. Moore, A. Schwimmer, and N. Seiberg, *Remarks on the Canonical Quantization of the Chern-Simons-Witten Theory*, *Nucl. Phys. B* **326** (1989) 108–134.
- [15] X. G. Wen and A. Zee, *A Classification of Abelian quantum Hall states and matrix formulation of topological fluids*, *Phys. Rev. B* **46** (1992) 2290–2301.
- [16] X.-G. Wen, *Theory of the edge states in fractional quantum Hall effects*, *Int. J. Mod. Phys. B* **6** (1992) 1711–1762.
- [17] O. Diatlyk, H. Khanchandani, F. K. Popov, and Y. Wang, *Effective Field Theory of Conformal Boundaries*, *Phys. Rev. Lett.* **133** (2024), no. 26 261601, [[arXiv:2406.01550](#)].
- [18] R. Verresen, U. Borla, A. Vishwanath, S. Moroz, and R. Thorngren, *Higgs Condensates are Symmetry-Protected Topological Phases: I. Discrete Symmetries*, [arXiv:2211.01376](#).
- [19] K. T. K. Chung, R. Flores-Calderón, R. C. Torres, P. Ribeiro, S. Moroz, and P. A. McClarty, *Higgs phases and boundary criticality*, *SciPost Phys.* **19** (2025), no. 4 105, [[arXiv:2404.17001](#)].
- [20] M. Gell-Mann and F. E. Low, *Quantum electrodynamics at small distances*, *Phys. Rev.* **95** (1954) 1300–1312.
- [21] K. G. Wilson, *Renormalization group and critical phenomena. 1. Renormalization group and the Kadanoff scaling picture*, *Phys. Rev. B* **4** (1971) 3174–3183.
- [22] K. G. Wilson, *Renormalization group and critical phenomena. 2. Phase space cell analysis of critical behavior*, *Phys. Rev. B* **4** (1971) 3184–3205.
- [23] D. J. Gross and F. Wilczek, *Ultraviolet Behavior of Nonabelian Gauge Theories*, *Phys. Rev. Lett.* **30** (1973) 1343–1346.
- [24] H. D. Politzer, *Reliable Perturbative Results for Strong Interactions?*, *Phys. Rev. Lett.* **30** (1973) 1346–1349.
- [25] J. Polchinski, *Renormalization and Effective Lagrangians*, *Nucl. Phys. B* **231** (1984) 269–295.

- [26] A. B. Zamolodchikov, *Irreversibility of the Flux of the Renormalization Group in a 2D Field Theory*, *JETP Lett.* **43** (1986) 730–732.
- [27] V. Riva and J. L. Cardy, *Scale and conformal invariance in field theory: A Physical counterexample*, *Phys. Lett. B* **622** (2005) 339–342, [[hep-th/0504197](#)].
- [28] S. El-Showk, Y. Nakayama, and S. Rychkov, *What Maxwell Theory in $D < 4$ teaches us about scale and conformal invariance*, *Nucl. Phys. B* **848** (2011) 578–593, [[arXiv:1101.5385](#)].
- [29] R. Jackiw and S. Y. Pi, *Tutorial on Scale and Conformal Symmetries in Diverse Dimensions*, *J. Phys. A* **44** (2011) 223001, [[arXiv:1101.4886](#)].
- [30] A. Gimenez-Grau, Y. Nakayama, and S. Rychkov, *Scale without conformal invariance in dipolar ferromagnets*, *Phys. Rev. B* **110** (2024), no. 2 024421, [[arXiv:2309.02514](#)].
- [31] D. Simmons-Duffin, *The Conformal Bootstrap*, in *Theoretical Advanced Study Institute in Elementary Particle Physics: New Frontiers in Fields and Strings*, pp. 1–74, 2017. [[arXiv:1602.07982](#)].
- [32] S. Rychkov, *EPFL Lectures on Conformal Field Theory in $D \geq 3$ Dimensions*. SpringerBriefs in Physics. 1, 2016.
- [33] A. M. Polyakov, *Non-Hamiltonian approach to conformal quantum field theory*, *Zh. Eksp. Teor. Fiz.* **66** (1974), no. 1 23–42.
- [34] R. Rattazzi, V. S. Rychkov, E. Tonni, and A. Vichi, *Bounding scalar operator dimensions in 4D CFT*, *JHEP* **12** (2008) 031, [[arXiv:0807.0004](#)].
- [35] S. El-Showk, M. F. Paulos, D. Poland, S. Rychkov, D. Simmons-Duffin, and A. Vichi, *Solving the 3D Ising Model with the Conformal Bootstrap*, *Phys. Rev. D* **86** (2012) 025022, [[arXiv:1203.6064](#)].
- [36] Z. Komargodski and A. Zhiboedov, *Convexity and Liberation at Large Spin*, *JHEP* **11** (2013) 140, [[arXiv:1212.4103](#)].
- [37] A. L. Fitzpatrick, J. Kaplan, D. Poland, and D. Simmons-Duffin, *The Analytic Bootstrap and AdS Superhorizon Locality*, *JHEP* **12** (2013) 004, [[arXiv:1212.3616](#)].
- [38] D. M. McAvity and H. Osborn, *Conformal field theories near a boundary in general dimensions*, *Nucl. Phys. B* **455** (1995) 522–576, [[cond-mat/9505127](#)].
- [39] P. Liendo, L. Rastelli, and B. C. van Rees, *The Bootstrap Program for Boundary CFT_d* , *JHEP* **07** (2013) 113, [[arXiv:1210.4258](#)].

- [40] F. Gliozzi, P. Liendo, M. Meineri, and A. Rago, *Boundary and Interface CFTs from the Conformal Bootstrap*, *JHEP* **05** (2015) 036, [[arXiv:1502.07217](#)]. [Erratum: *JHEP* **12**, 093 (2021)].
- [41] M. Billò, V. Gonçalves, E. Lauria, and M. Meineri, *Defects in conformal field theory*, *JHEP* **04** (2016) 091, [[arXiv:1601.02883](#)].
- [42] E. Lauria, M. Meineri, and E. Trevisani, *Radial coordinates for defect CFTs*, *JHEP* **11** (2018) 148, [[arXiv:1712.07668](#)].
- [43] E. Lauria, M. Meineri, and E. Trevisani, *Spinning operators and defects in conformal field theory*, *JHEP* **08** (2019) 066, [[arXiv:1807.02522](#)].
- [44] P. Liendo, Y. Linke, and V. Schomerus, *A Lorentzian inversion formula for defect CFT*, *JHEP* **08** (2020) 163, [[arXiv:1903.05222](#)].
- [45] E. Lauria, P. Liendo, B. C. Van Rees, and X. Zhao, *Line and surface defects for the free scalar field*, *JHEP* **01** (2021) 060, [[arXiv:2005.02413](#)].
- [46] C. P. Herzog and A. Shrestha, *Two point functions in defect CFTs*, *JHEP* **04** (2021) 226, [[arXiv:2010.04995](#)].
- [47] A. Chalabi, C. P. Herzog, A. O’Bannon, B. Robinson, and J. Sisti, *Weyl anomalies of four dimensional conformal boundaries and defects*, *JHEP* **02** (2022) 166, [[arXiv:2111.14713](#)].
- [48] Y. Nakayama, *Is boundary conformal in CFT?*, *Phys. Rev. D* **87** (2013), no. 4 046005, [[arXiv:1210.6439](#)].
- [49] M. S. Costa, J. Penedones, D. Poland, and S. Rychkov, *Spinning Conformal Correlators*, *JHEP* **11** (2011) 071, [[arXiv:1107.3554](#)].
- [50] D. M. McAvity and H. Osborn, *Energy momentum tensor in conformal field theories near a boundary*, *Nucl. Phys. B* **406** (1993) 655–680, [[hep-th/9302068](#)].
- [51] A. Antinucci, C. Copetti, G. Galati, and G. Rizi, *Topological constraints on defect dynamics*, *Phys. Rev. D* **111** (2025), no. 6 065025, [[arXiv:2412.18652](#)].
- [52] M. A. Metlitski, *Boundary criticality of the $O(N)$ model in $d = 3$ critically revisited*, *SciPost Phys.* **12** (2022), no. 4 131, [[arXiv:2009.05119](#)].
- [53] G. Cuomo, Z. Komargodski, and M. Mezei, *Localized magnetic field in the $O(N)$ model*, *JHEP* **02** (2022) 134, [[arXiv:2112.10634](#)].

- [54] N. Drukker, Z. Kong, and G. Sakkas, *Broken Global Symmetries and Defect Conformal Manifolds*, *Phys. Rev. Lett.* **129** (2022), no. 20 201603, [[arXiv:2203.17157](#)].
- [55] S. Bartlett-Tisdall, D. Ge, and C. P. Herzog, *How to get an interacting conformal line defect for free theories*, [arXiv:2510.02871](#).
- [56] C. P. Herzog and A. Shrestha, *Conformal surface defects in Maxwell theory are trivial*, *JHEP* **08** (2022) 282, [[arXiv:2202.09180](#)].
- [57] L. Fraser-Taliente, C. P. Herzog, and A. Shrestha, *A nonlocal Schwinger model*, *JHEP* **06** (2025) 252, [[arXiv:2412.02514](#)].
- [58] Y. Choi, C. Cordova, P.-S. Hsin, H. T. Lam, and S.-H. Shao, *Non-invertible Condensation, Duality, and Triality Defects in 3+1 Dimensions*, *Commun. Math. Phys.* **402** (2023), no. 1 489–542, [[arXiv:2204.09025](#)].
- [59] Y. Choi, H. T. Lam, and S.-H. Shao, *Noninvertible Time-Reversal Symmetry*, *Phys. Rev. Lett.* **130** (2023), no. 13 131602, [[arXiv:2208.04331](#)].
- [60] P. Niro, K. Roumpedakis, and O. Sela, *Exploring non-invertible symmetries in free theories*, *JHEP* **03** (2023) 005, [[arXiv:2209.11166](#)].
- [61] S. Gukov and E. Witten, *Gauge Theory, Ramification, And The Geometric Langlands Program*, [hep-th/0612073](#).
- [62] S. Gukov and E. Witten, *Rigid Surface Operators*, *Adv. Theor. Math. Phys.* **14** (2010), no. 1 87–178, [[arXiv:0804.1561](#)].
- [63] D. Gaiotto and E. Witten, *S-Duality of Boundary Conditions In $N=4$ Super Yang-Mills Theory*, *Adv. Theor. Math. Phys.* **13** (2009), no. 3 721–896, [[arXiv:0807.3720](#)].
- [64] A. Kapustin and M. Tikhonov, *Abelian duality, walls and boundary conditions in diverse dimensions*, *JHEP* **11** (2009) 006, [[arXiv:0904.0840](#)].
- [65] Y. Choi, C. Cordova, P.-S. Hsin, H. T. Lam, and S.-H. Shao, *Noninvertible duality defects in 3+1 dimensions*, *Phys. Rev. D* **105** (2022), no. 12 125016, [[arXiv:2111.01139](#)].
- [66] C. Cordova and K. Ohmori, *Quantum duality in electromagnetism and the fine structure constant*, *Phys. Rev. D* **109** (2024), no. 10 105019, [[arXiv:2307.12927](#)].
- [67] S. Kim, O. Sela, and Z. Sun, *Higher structure of non-invertible symmetries from Lagrangian descriptions*, [arXiv:2509.20540](#).

- [68] M. Billó, M. Caselle, D. Gaiotto, F. Gliozzi, M. Meineri, and R. Pellegrini, *Line defects in the 3d Ising model*, *JHEP* **07** (2013) 055, [[arXiv:1304.4110](#)].
- [69] D. Gaiotto, D. Mazac, and M. F. Paulos, *Bootstrapping the 3d Ising twist defect*, *JHEP* **03** (2014) 100, [[arXiv:1310.5078](#)].
- [70] S. Giombi, E. Helfenberger, Z. Ji, and H. Khanchandani, *Monodromy defects from hyperbolic space*, *JHEP* **02** (2022) 041, [[arXiv:2102.11815](#)].
- [71] L. Bianchi, A. Chalabi, V. Procházka, B. Robinson, and J. Sisti, *Monodromy defects in free field theories*, *JHEP* **08** (2021) 013, [[arXiv:2104.01220](#)].
- [72] R. Floreanini and R. Jackiw, *Selfdual Fields as Charge Density Solitons*, *Phys. Rev. Lett.* **59** (1987) 1873.
- [73] A. Sen, *Self-dual forms: Action, Hamiltonian and Compactification*, *J. Phys. A* **53** (2020), no. 8 084002, [[arXiv:1903.12196](#)].
- [74] K. Mkrtchyan, *On Covariant Actions for Chiral p -Forms*, *JHEP* **12** (2019) 076, [[arXiv:1908.01789](#)].
- [75] S. Giombi and B. Liu, *Notes on a surface defect in the $O(N)$ model*, *JHEP* **12** (2023) 004, [[arXiv:2305.11402](#)].
- [76] M. Trépanier, *Surface defects in the $O(N)$ model*, *JHEP* **09** (2023) 074, [[arXiv:2305.10486](#)].
- [77] Y. J. Deng, H. W. J. Blote, and M. P. Nightingale, *Surface and bulk transitions in three-dimensional $O(n)$ models*, *Phys. Rev. E* **72** (2005) 016128–016138, [[cond-mat/0504173](#)].
- [78] F. P. Toldin, *Boundary Critical Behavior of the Three-Dimensional Heisenberg Universality Class*, *Phys. Rev. Lett.* **126** (2021), no. 13 135701, [[arXiv:2012.00039](#)].
- [79] J. Padayasi, A. Krishnan, M. A. Metlitski, I. A. Gruzberg, and M. Meineri, *The extraordinary boundary transition in the 3d $O(N)$ model via conformal bootstrap*, *SciPost Phys.* **12** (2022), no. 6 190, [[arXiv:2111.03071](#)].
- [80] Z. Zhou and Y. Zou, *Studying the 3d Ising surface CFTs on the fuzzy sphere*, *SciPost Phys.* **18** (2025), no. 1 031, [[arXiv:2407.15914](#)].
- [81] G. Cuomo, Z. Komargodski, M. Mezei, and A. Raviv-Moshe, *Spin impurities, Wilson lines and semiclassics*, *JHEP* **06** (2022) 112, [[arXiv:2202.00040](#)].

- [82] O. Aharony, G. Cuomo, Z. Komargodski, M. Mezei, and A. Raviv-Moshe, *Phases of Wilson Lines in Conformal Field Theories*, *Phys. Rev. Lett.* **130** (2023), no. 15 151601, [[arXiv:2211.11775](#)].
- [83] K. G. Wilson and J. B. Kogut, *The Renormalization group and the epsilon expansion*, *Phys. Rept.* **12** (1974) 75–199.
- [84] M. A. Shpot, *Boundary conformal field theory at the extraordinary transition: The layer susceptibility to $O(\varepsilon)$* , *JHEP* **01** (2021) 055, [[arXiv:1912.03021](#)].
- [85] P. Dey, T. Hansen, and M. Shpot, *Operator expansions, layer susceptibility and two-point functions in BCFT*, *JHEP* **12** (2020) 051, [[arXiv:2006.11253](#)].
- [86] C. J. C. Burges, D. Z. Freedman, S. Davis, and G. W. Gibbons, *Supersymmetry in Anti-de Sitter Space*, *Annals Phys.* **167** (1986) 285.
- [87] E. D’Hoker and D. Z. Freedman, *Supersymmetric gauge theories and the AdS / CFT correspondence*, in *Theoretical Advanced Study Institute in Elementary Particle Physics (TASI 2001): Strings, Branes and EXTRA Dimensions*, pp. 3–158, 1, 2002. [hep-th/0201253](#).
- [88] C. R. Graham, *Volume and area renormalizations for conformally compact Einstein metrics*, *Rend. Circ. Mat. Palermo S* **63** (2000) 31–42, [[math/9909042](#)].
- [89] D. E. Diaz and H. Dorn, *Partition functions and double-trace deformations in AdS/CFT*, *JHEP* **05** (2007) 046, [[hep-th/0702163](#)].
- [90] S. K. Kehrein, *The Spectrum of critical exponents in ϕ^{**2} in two-dimensions theory in $D = (4-\text{epsilon})$ -dimensions: Resolution of degeneracies and hierarchical structures*, *Nucl. Phys. B* **453** (1995) 777–806, [[hep-th/9507044](#)].
- [91] J. Henriksson, *The critical $O(N)$ CFT: Methods and conformal data*, *Phys. Rept.* **1002** (2023) 1–72, [[arXiv:2201.09520](#)].
- [92] Z. Komargodski and D. Simmons-Duffin, *The Random-Bond Ising Model in 2.01 and 3 Dimensions*, *J. Phys. A* **50** (2017), no. 15 154001, [[arXiv:1603.04444](#)].
- [93] A. Krishnan and M. A. Metlitski, *A plane defect in the 3d $O(N)$ model*, *SciPost Phys.* **15** (2023), no. 3 090, [[arXiv:2301.05728](#)].
- [94] G. Cuomo and S. Zhang, *Spontaneous symmetry breaking on surface defects*, *JHEP* **03** (2024) 022, [[arXiv:2306.00085](#)].
- [95] S. R. Coleman, *There are no Goldstone bosons in two-dimensions*, *Commun. Math. Phys.* **31** (1973) 259–264.

- [96] E. H. Lieb, T. Schultz, and D. Mattis, *Two soluble models of an antiferromagnetic chain*, *Annals Phys.* **16** (1961) 407–466.
- [97] M. Cheng and N. Seiberg, *Lieb-Schultz-Mattis, Luttinger, and 't Hooft - anomaly matching in lattice systems*, *SciPost Phys.* **15** (2023), no. 2 051, [[arXiv:2211.12543](#)].
- [98] N. Seiberg and S.-H. Shao, *Majorana chain and Ising model - (non-invertible) translations, anomalies, and emanant symmetries*, *SciPost Phys.* **16** (2024), no. 3 064, [[arXiv:2307.02534](#)].
- [99] N. Manjunath, V. Calvera, and M. Barkeshli, *Nonperturbative constraints from symmetry and chirality on Majorana zero modes and defect quantum numbers in (2+1) dimensions*, *Phys. Rev. B* **107** (2023), no. 16 165126, [[arXiv:2210.02452](#)].
- [100] S. D. Pace, G. Delfino, H. T. Lam, and Ö. M. Aksoy, *Gauging modulated symmetries: Kramers-Wannier dualities and non-invertible reflections*, *SciPost Phys.* **18** (2025), no. 1 021, [[arXiv:2406.12962](#)].
- [101] X.-L. Qi, Y.-S. Wu, and S.-C. Zhang, *Topological quantization of the spin Hall effect in two-dimensional paramagnetic semiconductors*, *Phys. Rev. B* **74** (2006), no. 8 085308.
- [102] R. Kupferman, M. Moshe, and J. P. Solomon, *Metric description of singular defects in isotropic materials*, *Archive for Rational Mechanics and Analysis* **216** (2015), no. 3 1009–1047.
- [103] G. S. Bali, K. Schilling, and C. Schlichter, *Observing long color flux tubes in $SU(2)$ lattice gauge theory*, *Phys. Rev. D* **51** (1995) 5165–5198, [[hep-lat/9409005](#)].
- [104] G. S. Bali, K. Schilling, and A. Wachter, *Complete $O(v^{**2})$ corrections to the static interquark potential from $SU(3)$ gauge theory*, *Phys. Rev. D* **56** (1997) 2566–2589, [[hep-lat/9703019](#)].
- [105] H. B. Nielsen and P. Olesen, *Vortex Line Models for Dual Strings*, *Nucl. Phys. B* **61** (1973) 45–61.
- [106] S. Mandelstam, *Vortices and Quark Confinement in Nonabelian Gauge Theories*, *Phys. Rept.* **23** (1976) 245–249.
- [107] A. A. Abrikosov, *On the Magnetic Properties of Superconductors of the Second Group*, *Sov. Phys. JETP* **5** (1957) 1174–1182.
- [108] J. S. Schwinger, *Gauge Invariance and Mass. 2.*, *Phys. Rev.* **128** (1962) 2425–2429.

- [109] F. J. Wegner, *Duality in Generalized Ising Models and Phase Transitions Without Local Order Parameters*, *J. Math. Phys.* **12** (1971) 2259–2272.
- [110] A. M. Polyakov, *Quark Confinement and Topology of Gauge Groups*, *Nucl. Phys. B* **120** (1977) 429–458.
- [111] E. H. Fradkin and S. H. Shenker, *Phase Diagrams of Lattice Gauge Theories with Higgs Fields*, *Phys. Rev. D* **19** (1979) 3682–3697.
- [112] N. Seiberg and E. Witten, *Electric - magnetic duality, monopole condensation, and confinement in $N=2$ supersymmetric Yang-Mills theory*, *Nucl. Phys. B* **426** (1994) 19–52, [[hep-th/9407087](#)]. [Erratum: *Nucl.Phys.B* 430, 485–486 (1994)].
- [113] K. Dietz and T. Filk, *On the Renormalization of String Functionals*, *Phys. Rev. D* **27** (1983) 2944.
- [114] J. Polchinski and A. Strominger, *Effective string theory*, *Phys. Rev. Lett.* **67** (1991) 1681–1684.
- [115] M. Luscher and P. Weisz, *String excitation energies in $SU(N)$ gauge theories beyond the free-string approximation*, *JHEP* **07** (2004) 014, [[hep-th/0406205](#)].
- [116] J. M. Drummond, *Universal subleading spectrum of effective string theory*, [[hep-th/0411017](#)].
- [117] H. B. Meyer, *Poincare invariance in effective string theories*, *JHEP* **05** (2006) 066, [[hep-th/0602281](#)].
- [118] O. Aharony and E. Karzbrun, *On the effective action of confining strings*, *JHEP* **06** (2009) 012, [[arXiv:0903.1927](#)].
- [119] O. Aharony and N. Klinghoffer, *Corrections to Nambu-Goto energy levels from the effective string action*, *JHEP* **12** (2010) 058, [[arXiv:1008.2648](#)].
- [120] O. Aharony and M. Field, *On the effective theory of long open strings*, *JHEP* **01** (2011) 065, [[arXiv:1008.2636](#)].
- [121] O. Aharony and M. Dodelson, *Effective String Theory and Nonlinear Lorentz Invariance*, *JHEP* **02** (2012) 008, [[arXiv:1111.5758](#)].
- [122] S. Dubovsky, R. Flauger, and V. Gorbenko, *Effective String Theory Revisited*, *JHEP* **09** (2012) 044, [[arXiv:1203.1054](#)].
- [123] M. Meineri, *Lorentz completion of effective string action*, *PoS ConfinementX* (2012) 041, [[arXiv:1301.3437](#)].

- [124] O. Aharony and Z. Komargodski, *The Effective Theory of Long Strings*, *JHEP* **05** (2013) 118, [[arXiv:1302.6257](#)].
- [125] N. Brambilla, M. Groher, H. E. Martinez, and A. Vairo, *Effective string theory and the long-range relativistic corrections to the quark-antiquark potential*, *Phys. Rev. D* **90** (2014), no. 11 114032, [[arXiv:1407.7761](#)].
- [126] S. Hellerman, S. Maeda, J. Maltz, and I. Swanson, *Effective String Theory Simplified*, *JHEP* **09** (2014) 183, [[arXiv:1405.6197](#)].
- [127] B. B. Brandt and M. Meineri, *Effective string description of confining flux tubes*, *Int. J. Mod. Phys. A* **31** (2016), no. 22 1643001, [[arXiv:1603.06969](#)].
- [128] S. Hellerman and S. Maeda, *On Vertex Operators in Effective String Theory*, [arXiv:1701.06406](#).
- [129] J. Elias Miró, A. L. Guerrieri, A. Hebbar, J. Penedones, and P. Vieira, *Flux Tube S-matrix Bootstrap*, *Phys. Rev. Lett.* **123** (2019), no. 22 221602, [[arXiv:1906.08098](#)].
- [130] J. Elias Miró and A. Guerrieri, *Dual EFT bootstrap: QCD flux tubes*, *JHEP* **10** (2021) 126, [[arXiv:2106.07957](#)].
- [131] M. Caselle, *Effective String Description of the Confining Flux Tube at Finite Temperature*, *Universe* **7** (2021), no. 6 170, [[arXiv:2104.10486](#)].
- [132] J. Albert and A. Homrich, *Imprints of asymptotic freedom on confining strings*, [arXiv:2602.15097](#).
- [133] J. Polchinski and Y. Cai, *Consistency of Open Superstring Theories*, *Nucl. Phys. B* **296** (1988) 91–128.
- [134] J. L. Cardy, *Boundary Conditions, Fusion Rules and the Verlinde Formula*, *Nucl. Phys. B* **324** (1989) 581–596.
- [135] T. T. Takahashi, H. Matsufuru, Y. Nemoto, and H. Suganuma, *The Three quark potential in the SU(3) lattice QCD*, *Phys. Rev. Lett.* **86** (2001) 18–21, [[hep-lat/0006005](#)].
- [136] T. T. Takahashi, H. Suganuma, Y. Nemoto, and H. Matsufuru, *Detailed analysis of the three quark potential in SU(3) lattice QCD*, *Phys. Rev. D* **65** (2002) 114509, [[hep-lat/0204011](#)].
- [137] F. Bissey, F.-G. Cao, A. Kitson, B. G. Lasscock, D. B. Leinweber, A. I. Signal, A. G. Williams, and J. M. Zanotti, *Gluon field distribution in baryons*, *Nucl. Phys. B Proc. Suppl.* **141** (2005) 22–25, [[hep-lat/0501004](#)].

- [138] F. Bissey, F.-G. Cao, A. R. Kitson, A. I. Signal, D. B. Leinweber, B. G. Lasscock, and A. G. Williams, *Gluon flux-tube distribution and linear confinement in baryons*, *Phys. Rev. D* **76** (2007) 114512, [[hep-lat/0606016](#)].
- [139] I. Low and A. V. Manohar, *Spontaneously broken space-time symmetries and Goldstone's theorem*, *Phys. Rev. Lett.* **88** (2002) 101602, [[hep-th/0110285](#)].
- [140] R. Auzzi, S. Bolognesi, J. Evslin, K. Konishi, and A. Yung, *NonAbelian superconductors: Vortices and confinement in $N=2$ SQCD*, *Nucl. Phys. B* **673** (2003) 187–216, [[hep-th/0307287](#)].
- [141] A. Hanany and D. Tong, *Vortex strings and four-dimensional gauge dynamics*, *JHEP* **04** (2004) 066, [[hep-th/0403158](#)].
- [142] M. Edalati and D. Tong, *Heterotic Vortex Strings*, *JHEP* **05** (2007) 005, [[hep-th/0703045](#)].
- [143] P. Cooper, S. Dubovsky, V. Gorbenko, A. Mohsen, and S. Storace, *Looking for Integrability on the Worldsheet of Confining Strings*, *JHEP* **04** (2015) 127, [[arXiv:1411.0703](#)].
- [144] A. Athenodorou, B. Bringoltz, and M. Teper, *Closed flux tubes and their string description in $D=3+1$ $SU(N)$ gauge theories*, *JHEP* **02** (2011) 030, [[arXiv:1007.4720](#)].
- [145] A. Athenodorou, B. Bringoltz, and M. Teper, *Closed flux tubes and their string description in $D=2+1$ $SU(N)$ gauge theories*, *JHEP* **05** (2011) 042, [[arXiv:1103.5854](#)].
- [146] M. Caselle, L. Castagnini, A. Feo, F. Gliozzi, and M. Panero, *Thermodynamics of $SU(N)$ Yang-Mills theories in $2+1$ dimensions I - The confining phase*, *JHEP* **06** (2011) 142, [[arXiv:1105.0359](#)].
- [147] T. Solberg and M. Yutushui, *The action of long strings in supersymmetric field theories*, *JHEP* **02** (2019) 037, [[arXiv:1811.00325](#)].
- [148] Y. Nambu, *Duality and Hadrodynamics*, pp. 280–301.
- [149] T. Goto, *Relativistic quantum mechanics of one-dimensional mechanical continuum and subsidiary condition of dual resonance model*, *Prog. Theor. Phys.* **46** (1971) 1560–1569.
- [150] A. M. Polyakov, *Fine Structure of Strings*, *Nucl. Phys. B* **268** (1986) 406–412.

- [151] H. Kleinert, *The Membrane Properties of Condensing Strings*, *Phys. Lett. B* **174** (1986) 335–338.
- [152] J. F. Arvis, *The Exact $q\bar{q}$ Potential in Nambu String Theory*, *Phys. Lett. B* **127** (1983) 106–108.
- [153] P. Giudice, F. Gliozzi, and S. Lottini, *The Confining string beyond the free-string approximation in the gauge dual of percolation*, *JHEP* **03** (2009) 104, [[arXiv:0901.0748](#)].
- [154] O. Jahn and P. de Forcrand, *Baryons and confining strings*, *Nucl. Phys. B Proc. Suppl.* **129** (2004) 700–702, [[hep-lat/0309115](#)].
- [155] M. Pfeuffer, G. S. Bali, and M. Panero, *Fluctuations of the baryonic flux-tube junction from effective string theory*, *Phys. Rev. D* **79** (2009) 025022, [[arXiv:0810.1649](#)].
- [156] A. S. Bakry, X. Chen, and P.-M. Zhang, *Y-stringlike behavior of a static baryon at finite temperature*, *Phys. Rev. D* **91** (2015) 114506, [[arXiv:1412.3568](#)].
- [157] P. Lakatos and L. Losonczi, *Self-inversive polynomials whose zeros are on the unit circle*, *Publ. Math. Debrecen* **65** (2004), no. 3-4 409–420.
- [158] Y. Imamura, *On string junctions in supersymmetric gauge theories*, *Prog. Theor. Phys.* **112** (2004) 1061–1086, [[hep-th/0410138](#)].
- [159] Y. Koma and M. Koma, *Precise determination of the three-quark potential in $SU(3)$ lattice gauge theory*, *Phys. Rev. D* **95** (2017), no. 9 094513, [[arXiv:1703.06247](#)].
- [160] M. Caselle, N. Magnoli, D. Panfalone, and L. Verzichelli, *The Mass of the Baryon Junction: a lattice computation in 2 +1 dimensions*, [arXiv:2508.00608](#).
- [161] M. Lewenstein, A. Sanpera, V. Ahufinger, B. Damski, A. S. De, and U. Sen, *Ultracold atomic gases in optical lattices: mimicking condensed matter physics and beyond*, *Adv. Phys.* **56** (2007), no. 2 243–379, [[cond-mat/0606771](#)].
- [162] C. J. Pethick and H. Smith, *Bose–Einstein condensation in dilute gases*. Cambridge university press, 2008.
- [163] I. Bloch, J. Dalibard, and W. Zwerger, *Many-body physics with ultracold gases*, *Rev. Mod. Phys.* **80** (2008) 885–964, [[arXiv:0704.3011](#)].
- [164] S. Giorgini, L. P. Pitaevskii, and S. Stringari, *Theory of ultracold atomic Fermi gases*, *Rev. Mod. Phys.* **80** (2008) 1215–1274, [[arXiv:0706.3360](#)].
- [165] R. Jackiw and S.-Y. Pi, *Classical and quantal nonrelativistic Chern-Simons theory*, *Phys. Rev. D* **42** (1990) 3500. [Erratum: *Phys.Rev.D* 48, 3929 (1993)].

- [166] R. Jackiw and S. Y. Pi, *Soliton Solutions to the Gauged Nonlinear Schrödinger Equation on the Plane*, *Phys. Rev. Lett.* **64** (1990) 2969–2972.
- [167] N. Doroud, D. Tong, and C. Turner, *On Superconformal Anyons*, *JHEP* **01** (2016) 138, [[arXiv:1511.01491](#)].
- [168] N. Doroud, D. Tong, and C. Turner, *The Conformal Spectrum of Non-Abelian Anyons*, *SciPost Phys.* **4** (2018), no. 4 022, [[arXiv:1611.05848](#)].
- [169] M. Henkel, *On the two point correlation function in dynamical scaling and Schrödinger invariance*, *Int. J. Mod. Phys. C* **3** (1992) 1011, [[hep-th/9210102](#)].
- [170] Y. Nishida and D. T. Son, *Nonrelativistic conformal field theories*, *Phys. Rev. D* **76** (2007) 086004, [[arXiv:0706.3746](#)].
- [171] P. Nikolic and S. Sachdev, *Renormalization-group fixed points, universal phase diagram, and $1/N$ expansion for quantum liquids with interactions near the unitarity limit*, *Phys. Rev. A* **75** (2007) 033608, [[cond-mat/0609106](#)].
- [172] Y. Nishida and D. T. Son, *Unitary Fermi gas, epsilon expansion, and nonrelativistic conformal field theories*, *Lect. Notes Phys.* **836** (2012) 233–275, [[arXiv:1004.3597](#)].
- [173] W. D. Goldberger, Z. U. Khandker, and S. Prabhu, *OPE convergence in non-relativistic conformal field theories*, *JHEP* **12** (2015) 048, [[arXiv:1412.8507](#)].
- [174] S. Pal, *Unitarity and universality in nonrelativistic conformal field theory*, *Phys. Rev. D* **97** (2018), no. 10 105031, [[arXiv:1802.02262](#)].
- [175] M. Boisvert, S. H. Fadda, J. Kulp, and R. M. Yazdi, *Revisiting Schrödinger CFTs: Factorization, Massless Particles, and a Path to the Bootstrap*, [[arXiv:2510.26872](#)].
- [176] S. Baiguera, *Aspects of non-relativistic quantum field theories*, *Eur. Phys. J. C* **84** (2024), no. 3 268, [[arXiv:2311.00027](#)].
- [177] Y. Guo, R. Dubessy, M. d. G. de Herve, A. Kumar, T. Badr, A. Perrin, L. Longchambon, and H. Perrin, *Supersonic rotation of a superfluid: A long-lived dynamical ring*, *Physical review letters* **124** (2020), no. 2 025301.
- [178] R. M. Hornreich, M. Luban, and S. Shtrikman, *Critical Behavior at the Onset of $k \rightarrow$ -Space Instability on the λ Line*, *Phys. Rev. Lett.* **35** (1975) 1678–1681.
- [179] E. Ardonne, P. Fendley, and E. Fradkin, *Topological order and conformal quantum critical points*, *Annals Phys.* **310** (2004) 493–551, [[cond-mat/0311466](#)].
- [180] S. Kachru, X. Liu, and M. Mulligan, *Gravity duals of Lifshitz-like fixed points*, *Phys. Rev. D* **78** (2008) 106005, [[arXiv:0808.1725](#)].

- [181] B. Chen and Q.-G. Huang, *Field Theory at a Lifshitz Point*, *Phys. Lett. B* **683** (2010) 108–113, [[arXiv:0904.4565](#)].
- [182] P. Horava, *Quantum Gravity at a Lifshitz Point*, *Phys. Rev. D* **79** (2009) 084008, [[arXiv:0901.3775](#)].
- [183] K. O'hara, S. Hemmer, M. Gehm, S. Granade, and J. Thomas, *Observation of a strongly interacting degenerate fermi gas of atoms*, *Science* **298** (2002), no. 5601 2179–2182.
- [184] J. E. Thomas, J. Kinast, and A. Turlapov, *Virial Theorem and Universality in a Unitary Fermi Gas*, *Phys. Rev. Lett.* **95** (2005) 120402, [[cond-mat/0503620](#)].
- [185] S. Nascimbène, N. Navon, K. J. Jiang, F. Chevy, and C. Salomon, *Exploring the thermodynamics of a universal Fermi gas*, *Nature* **463** (2010), no. 7284 1057–1060, [[arXiv:0911.0747](#)].
- [186] E. Tiesinga, B. J. Verhaar, and H. T. C. Stoof, *Threshold and resonance phenomena in ultracold ground-state collisions*, *Phys. Rev. A* **47** (1993) 4114–4122.
- [187] E. Timmermans, P. Tommasini, M. Hussein, and A. Kerman, *Feshbach resonances in atomic bose–einstein condensates*, *Physics Reports* **315** (1999), no. 1-3 199–230.
- [188] C. Chin, R. Grimm, P. Julienne, and E. Tiesinga, *Feshbach resonances in ultracold gases*, *Rev. Mod. Phys.* **82** (2010), no. 2 1225–1286.
- [189] M. Knap, A. Shashi, Y. Nishida, A. Imambekov, D. A. Abanin, and E. Demler, *Time-dependent impurity in ultracold fermions: Orthogonality catastrophe and beyond*, *Physical Review X* **2** (2012), no. 4 041020.
- [190] N. Spethmann, F. Kindermann, S. John, C. Weber, D. Meschede, and A. Widera, *Dynamics of single neutral impurity atoms immersed in an ultracold gas*, *Physical review letters* **109** (2012), no. 23 235301.
- [191] J. Bauer, C. Salomon, and E. Demler, *Realizing a kondo-correlated state with ultracold atoms*, *Physical review letters* **111** (2013), no. 21 215304.
- [192] F. Werner and Y. Castin, *The Unitary three-body problem in a trap*, *Phys. Rev. Lett.* **97** (2006) 150401, [[cond-mat/0507399](#)].
- [193] F. Werner and Y. Castin, *The Unitary gas in an isotropic harmonic trap: Symmetry properties and applications*, *Phys. Rev. A* **74** (2006) 053604, [[cond-mat/0607821](#)].
- [194] V. de Alfaro, S. Fubini, and G. Furlan, *Conformal Invariance in Quantum Mechanics*, *Nuovo Cim. A* **34** (1976) 569.

- [195] D. B. Kaplan, J.-W. Lee, D. T. Son, and M. A. Stephanov, *Conformality Lost*, *Phys. Rev. D* **80** (2009) 125005, [[arXiv:0905.4752](#)].
- [196] S. Moroz and R. Schmidt, *Nonrelativistic inverse square potential, scale anomaly, and complex extension*, *Annals Phys.* **325** (2010) 491–513, [[arXiv:0909.3477](#)].
- [197] A. L. Fetter and A. A. Svidzinsky, *Vortices in a trapped dilute bose-einstein condensate*, *Journal of Physics: condensed matter* **13** (2001), no. 12 R135–R194.
- [198] A. Schmitt, *Introduction to Superfluidity: Field-theoretical approach and applications*, vol. 888. 2015.
- [199] J. R. Abo-Shaeer, C. Raman, J. M. Vogels, and W. Ketterle, *Observation of vortex lattices in bose-einstein condensates*, *Science* **292** (2001), no. 5516 476–479.
- [200] U. R. Fischer and G. Baym, *Vortex states of rapidly rotating dilute bose-einstein condensates*, *Physical review letters* **90** (2003), no. 14 140402.
- [201] A. Aftalion and I. Danaïla, *Giant vortices in combined harmonic and quartic traps*, *Physical Review A—Atomic, Molecular, and Optical Physics* **69** (2004), no. 3 033608.
- [202] D. T. Son, *Low-energy quantum effective action for relativistic superfluids*, [hep-ph/0204199](#).
- [203] D. T. Son and M. Wingate, *General coordinate invariance and conformal invariance in nonrelativistic physics: Unitary Fermi gas*, *Annals Phys.* **321** (2006) 197–224, [[cond-mat/0509786](#)].
- [204] A. Nicolis, A. Podo, and L. Santoni, *The connection between nonzero density and spontaneous symmetry breaking for interacting scalars*, *JHEP* **09** (2023) 200, [[arXiv:2305.08896](#)].
- [205] S. Hellerman, D. Orlando, S. Reffert, and M. Watanabe, *On the CFT Operator Spectrum at Large Global Charge*, *JHEP* **12** (2015) 071, [[arXiv:1505.01537](#)].
- [206] A. Monin, D. Pirtskhalava, R. Rattazzi, and F. K. Seibold, *Semiclassics, Goldstone Bosons and CFT data*, *JHEP* **06** (2017) 011, [[arXiv:1611.02912](#)].
- [207] G. Cuomo, A. de la Fuente, A. Monin, D. Pirtskhalava, and R. Rattazzi, *Rotating superfluids and spinning charged operators in conformal field theory*, *Phys. Rev. D* **97** (2018), no. 4 045012, [[arXiv:1711.02108](#)].
- [208] G. Cuomo and Z. Komargodski, *Giant Vortices and the Regge Limit*, *JHEP* **01** (2023) 006, [[arXiv:2210.15694](#)].

- [209] S. Hellerman and I. Swanson, *Droplet-Edge Operators in Nonrelativistic Conformal Field Theories*, [arXiv:2010.07967](#).
- [210] G. Cuomo, M. Mezei, and A. Raviv-Moshe, *Boundary conformal field theory at large charge*, *JHEP* **10** (2021) 143, [[arXiv:2108.06579](#)].
- [211] F. Dalfovo, S. Giorgini, L. P. Pitaevskii, and S. Stringari, *Theory of Bose-Einstein condensation in trapped gases*, *Rev. Mod. Phys.* **71** (1999) 463–512, [[cond-mat/9806038](#)].
- [212] B. Horn, A. Nicolis, and R. Penco, *Effective string theory for vortex lines in fluids and superfluids*, *JHEP* **10** (2015) 153, [[arXiv:1507.05635](#)].
- [213] D. M. Hofman and A. Strominger, *Chiral Scale and Conformal Invariance in 2D Quantum Field Theory*, *Phys. Rev. Lett.* **107** (2011) 161601, [[arXiv:1107.2917](#)].
- [214] S. Detournay, T. Hartman, and D. M. Hofman, *Warped Conformal Field Theory*, *Phys. Rev. D* **86** (2012) 124018, [[arXiv:1210.0539](#)].
- [215] K. Jensen, *Locality and anomalies in warped conformal field theory*, *JHEP* **12** (2017) 111, [[arXiv:1710.11626](#)].
- [216] G. W. Gibbons and C. N. Pope, *Kohn’s Theorem, Larmor’s Equivalence Principle and the Newton-Hooke Group*, *Annals Phys.* **326** (2011) 1760–1774, [[arXiv:1010.2455](#)].